The Dynamics of Dwarf Spheroidal Galaxies.

J. C. Hargreaves

Corpus Christi College

and

Institute of Astronomy, Cambridge

A dissertation submitted to the University of Cambridge
in accordance with the regulations for admission to the degree of
Doctor of Philosophy

Abstract

This thesis presents the results from the analysis of spectra from stars in three dwarf spheroidal galaxies, and analyses the velocity distribution caused by binary star orbits by means of a Monte-Carlo simulation.

High quality spectra have been obtained for seventy four K giants, with twenty two stars in Sextans, thirty five stars in Ursa Minor and seventeen stars in Draco. There are multi-epoch measurements for eighteen stars in Sextans and Ursa Minor, two of which show signs of variability. All three galaxies were investigated for signs of rotation around the major and minor axes, with the only significant detection being around the major axis of Ursa Minor. This is $-4.7\pm^{2.0}_{2.2}$ km s^{-1} per 100 pc from the axis. Velocity dispersions were derived for all three galaxies using the maximum likelihood method to correctly weight the different velocities according to their assigned error. These were $7.0\pm^{1.3}_{1.0}$ km s^{-1}, $6.7\pm^{0.9}_{0.8}$ km s^{-1} and $10.5\pm^{2.2}_{1.7}$ km s^{-1}for Sextans, Ursa Minor and Draco respectively. The value quoted here for Ursa Minor was calculated after the effect of rotation had been subtracted from the velocity distribution. The possibilities for anisotropy in the velocity dispersion, tidal disruption by the Galaxy and the relevance of binary stars are discussed for each galaxy. The calculation of the mass-to-light ratios presumes these three factors to be negligible. The results for the core mass-to-light ratio calculations are $124\pm^{85}_{60}$ $M_\odot/L_{\odot,V}$, $59\pm^{41}_{25}$ $M_\odot/L_{\odot,V}$ and $166\pm^{289}_{107}$ $M_\odot/L_{\odot,V}$ for Sextans, Ursa Minor and Draco respectively, implying that large quantities of dark matter are present in these galaxies.

The questions arising from the detection of two stars of variable velocity in the multi-epoch data are further explored by a Monte-Carlo simulation. The simulation uses period, ellipticity and secondary mass distributions similar to those found for solar mass stars in the solar neighbourhood. With these distributions the velocity dispersion caused by the binary stars alone is small compared to the velocity dispersions which have been measured for dwarf spheroidal galaxies. The number of binary stars that have been identified by the observations presented in this thesis, and by other observers, are consistent with the predictions of the simulation. The distributions of the orbital parameters need to be very different from those found in the solar neighbourhood for the orbital velocities of binary stars to be contributing significantly to the velocity dispersions measured for dwarf spheroidal galaxies.

Declaration

This dissertation is the outcome of my own work, except where explicit reference has been made to the work of others.

I hereby declare that this dissertation is not substantially the same as any that I have submitted for a degree or diploma or other qualification at any other University, and no part of it has been or is submitted for any such degree, diploma or any other qualification.

Chapters 2 and 3 have already been published, before the discovery of the Sagittarius dSph galaxy:

Chapter 2 as MNRAS, 269, 957–974 (1994);

Chapter 3 as MNRAS, 271, 693–705 (1994).

This means that there is some repetition of information. The papers are included here in the form in which they were published, the only changes being the following: in Chapter 2 the limits on the rotation have, for consistency with Chapters 3 and 4, been calculated using the bootstrapping method rather the simple least squares fit as in the original paper; Chapter 2 is referenced in Chapter 3 as such rather than in the form "Hargreaves et al. (1994)"; and other references which were in preparation at the time of first publication have been updated, where possible.

The dissertation does not exceed 60,000 words.

J C Hargreaves

Julia Hargreaves

March 1995

Acknowledgements

Many thanks to Gerry Gilmore for all the inspiration and encouragement, to Mike Irwin for his attention to detail and Dave Carter for assistance with the data crunching. I am also grateful to Robert Cannon for the introduction to the basics of Fortran, and James Annan for lots of conversations about binary stars.

Many people have contributed to my stay in Cambridge being a positive experience. Among these I must particularly mention Jacqui, Genet and Deb, the other three of the oarsome foursome, for much ninja rowing, friendship, and lycra, and for showing CCCBC that women aren't useless girlies who break things; Rob Judd for never failing friendship; Jenny McDonald for making my life feel simple; all at CUTTC for lots of high speed ping pong; and Mark Pryce for the exciting retreats and eye-opening trips to the inner-city.

I am very grateful to J for the rent free accomodation during the last six months of impoverished fourthyeardom, and for all the mountain adventures. Thanks also to Mandi for the food, Coryn for never giving up his xterm and Priya for being far more with it than any other astronomer, except perhaps Helene.

Thank you to Mumz and Popz for all the support and encouragement during all the years of edgumufication.

Finally thanks to Tabitha the Toshiba for doing her thing, to Red Rum for being excptionally fast and to Milton, Gunsynd and poor stolen Desie for all their years of service.

Contents

Chapter 1

Introduction

1.1 Dwarf Spheroidal Galaxies

When the work described in this thesis was started, there were eight dwarf spheroidal (dSph) galaxies known to be in orbit around the Milky Way Galaxy. Of these, Ursa Minor is the closest to the Galaxy centre, at 64 kpc, whereas the furthest away, and therefore least studied at the level of individual stellar velocities, are Leo I and Leo II, at 198 and 207 kpc respectively. Ursa Minor is distinguished by the existence of clumps in the contour map of its luminosity (Olszewski & Aaronson 1985), and by being the only dSph in which any significant rotation has been discovered (Section 3.3.2). Carina, Draco, Leo II, Sextans and Ursa Minor have luminosities ranging between M_v of -8.3 and -9.0, but Fornax is the brightest of the eight with $M_v = -13$. This luminosity range, equivalent to $10^5 - 10^7$ $L_\odot$, is typical of that for globular clusters, but the core radii of dSph galaxies are one to two orders of magnitude larger for the same luminosity.

As well as being the brightest of the eight, Fornax is also the only one which contains globular clusters. It is not, however, necessarily the largest, as the tidal radius of Sextans has been measured as 3100 ± 1030 pc and that of Fornax as 2080 ± 180 pc. The core radius measured for Sextans by fitting a King profile is also large when compared to the other dSphs of similar luminosity. This leads to Sextans, in particular, having a low central surface brightness. In general the dSph galaxies contain a mixture of old and intermediate population stars and show no evidence of gas or recent star formation. Irwin & Hatzidimitriou (1993, 1995), were the source for the values quoted above.

No stellar system smaller than a dSph galaxy has been found that must contain large quantities of dark matter. Globular clusters appear to have a mass-to-light ratio of 2 or 3 $M_\odot/L_\odot$. This value is obtained by applying various simple models (usually Illingworth's method and King's method of core fitting (Section 2.4.1, and Binney & Tremaine (1987) for more details)). These models calculate the mass from the velocities obtained from the stellar observations. When these same models are applied to dSph galaxies, for which the samples of stars with measured velocities are much smaller, the mass-to-light ratios are between 6 and 250 (Irwin & Hatzidimitriou 1995), and at face value imply that all the dSph galaxies are of similar mass but contain a large range of luminous matter.

The smallest scale on which large quantities of dark matter exist can place constraints on the form of dark matter, since cold (or dissipative) dark matter can

cluster on short scales while relativistic matter (eg neutrinos) cannot. In Cold Dark Matter cosmology, objects of about the mass of dSph galaxies, as calculated by the methods mentioned above, should be the first systems in the universe to form, and they should have merged together to form larger galaxies. In this scenario dSph galaxies would be expected to have large dark matter halos, so the apparent high central density found in these galaxies is not explained by this theory.

A mass-to-light ratio of 250 for a dSph galaxy does seem inconsistent with the general trend of mass-to-light ratio compared to size in the rest of the universe; for example, the value for the Milky Way Galaxy is only about 30, measured out to 80 kpc, and that for the Local Group is closer to 100 (Gilmore 1990). This and the wide range of measurements for the mass-to-light ratios of the different dSph galaxies leads to a question over whether the stellar kinematics are quite such simple indicators of the mass of these galaxies as is assumed by the simple models employed to date.

The first measurements of the velocities of stars in dSph galaxies were made by Aaronson (1983). He measured velocities for three Carbon stars in Draco by cross-correlating the spectra obtained from the Draco stars with those for two Galactic stars for which the velocity was already well known. The spectra were obtained using the MMT, taking integrations of more than 30 minutes for these $V \sim 17$ magnitude stars. He claimed an error of close to 1 $\mathrm{km\,s^{-1}}$ for each integration.

He calculated the standard deviation of the velocities thereby obtaining a measure of the velocity dispersion of Draco. The value was 11.2 $\mathrm{km\,s^{-1}}$, and greater than 6.5 $\mathrm{km\,s^{-1}}$ at the 95 % confidence level. He used 6.5 $\mathrm{km\,s^{-1}}$ in his calculations so as to obtain a minimum value for the mass-to-light ratio. He used the Hodge (1971) King Model fit to the brightness profile, with Illingworth's method (outlined in Section 2.4.1) to obtain a mass-to-light ratio for Draco of 31, and suggested the possibility that dSph galaxies could contain large amounts of dark matter.

Since that time more measurements have been made of velocities of stars in Draco and the other dSphs. Carbon stars were originally chosen for study as they are then brightest stars in dSph galaxies, situated at the tip of the giant branch. However, Aaronson's repeat measurements of Carbon stars in Draco and Ursa Minor revealed three out of five to have velocity variations which were noticed over the course of a few years; he suggested two of the stars were binary stars

and that the other's variation was caused by atmospheric jitter. Other studies of Carbon stars (McClure 1984) have suggested that the sort of Carbon stars found in Draco, Ursa Minor and Sculptor have a high binary fraction, so that Carbon stars are now seen as a poor choice for these sorts of observations. In addition, there are only a few Carbon stars in some of the dSph galaxies (none has been found in Sextans) so it became necessary to look a little further down the giant branch to the slightly fainter K-giants.

The early samples used to calculate the velocity dispersions were small (with fewer than 10 stars) or had large measuring errors (of about 5 $\mathrm{km\,s^{-1}}$ on each velocity), and the results obtained were all close to 10 $\mathrm{km\,s^{-1}}$. This lead to a suspicion that an error underestimate could be contributing a large fraction of this apparent dispersion. Godwin & Lynden-Bell (1987) used repeat measurements of the same stars in Carina to calculate an error underestimate of a factor of two between the velocities from three independent sets of data.

By 1991, the only dSph galaxy for which there were reliable measurements by different observational setups was Fornax, for which the mass-to-light ratio was calculated to be about 5 (Paltoglou & Freeman 1987, Mateo et al. 1991). Only Aaronson & Olszewski (1987) had made measurements for stars in Draco and Ursa Minor, their samples containing about 15 stars per galaxy. These two galaxies were also of great interest, being the closest to the Galaxy and having the highest apparent mass-to-light ratios of all the dSphs. There were no measurements of the velocities of stars in the recently discovered Sextans dSph galaxy (Irwin et al. 1990). The observations presented in this thesis are of individual spectra of stars in Sextans, Ursa Minor and Draco with a measuring error of about 2 $\mathrm{km\,s^{-1}}$ per observation.

1.2 Work Covered in this Thesis

This thesis contains a study of the dynamics of the dSph galaxies, using data from the Sextans, Ursa Minor and Draco dwarfs and a computer model which estimates the effect of binary stars on the kinematics.

Chapter 2 contains the results for Sextans, and as this was the first paper to be published it is also the one that contains the details of the data reduction procedure, as well as a description of King's Method of core fitting for deriving

the core mass-to-light ratio, and Illingworth's method for the global mass-to-light ratio. The appendices to this chapter contain the explanation of the maximum likelihood method for weighting the velocity dispersion according to the error on each velocity, explaining the flaws in the method used previously.

Chapter 3 contains the results for Ursa Minor and does not repeat the description of the analysis procedures used as they were identical to those used for Sextans. The implications of the discovery of rotation round the major axis are discussed here.

Chapter 4 contains the results for the Draco data.

Chapter 5 summarises the results from Chapters 2, 3 and 4, discusses the conclusions which can be drawn, and the questions which are still unanswered.

Chapter 6 contains the calculations regarding the importance of binary stars. First the simulations made previous to this work are more fully described. Then a description of the essential details of the programme and in what ways it differs from previous simulations is made. Then the results of the calculations are discussed in light of observations of binary stars in dSph galaxies.

References

Aaronson, M., 1983, AJ, 266, L11.

Aaronson, M. & Olszewski, E., 1987, Kormendy, J., & Knapp, G.R., eds, in Dark Matter in the Universe, Proc. IAU Symp. 117, 153. Reidel.

Binney, J.J. & Tremaine, S., 1987, Galactic Dynamics, 236. Princeton University Press, Princeton.

Gilmore, G., 1990, Lynden-Bell, D., & Gilmore, G. eds, in Baryonic Dark Matter, 137. Kluwer, Dordrecht.

Godwin, P.J. & Lynden-Bell, D., 1987, MNRAS, 229, 7P

Hodge, P.W., 1971, ARAA, 9, 35.

Irwin, M.J., Bunclark, P.S., Bridgeland, M.T., McMahon, R.G., 1990, MNRAS, 244, 16P.

Irwin M.J. & Hatzidimitriou D., 1993, Brodie, J., ed, in Proc. ASP Symp vol 48, 322.

Irwin M.J. & Hatzidimitriou D., 1995 (in preparation).

Mateo, M., Olszewski, E., Welch, D.L., Fischer, P. & Kinkel, W., 1991, AJ, 102, 914.

McClure, R.D., 1984, ApJ Letters, 280, L31.

Olszewski, E.W. & Aaronson, M., 1985, AJ, 90, 2221.

Paltoglou, G., Freeman, K. C., 1987, in de Zeeuw, T. ed, Structure and dynamics of elliptical galaxies, Proc. IAU Symp. 127, 447

Chapter 2

The Sextans Dwarf Spheroidal Galaxy

Abstract

We have observed twenty six giant stars in the Sextans dwarf spheroidal galaxy and have obtained high quality spectra for twenty two of these. We have multi-epoch spectra for nine stars from which two possible binary stars have been found. The velocity dispersion of the sample calculated by a maximum likelihood method is $7.0 \pm^{1.3}_{1.0}$ km s^{-1} and the mean velocity is 224.4 ± 1.6 km s^{-1}. There is no sign of rotation about any axis within the errors of the measurements, the formally derived value around the minor axis being $-0.3 \pm^{0.4}_{0.3}$ km s^{-1} at 100 pc from the axis. It is possible that binary stars may be making a significant contribution to the velocity distribution or that Sextans may be being tidally disrupted. If further work eliminates both these possibilities then, assuming isotropy in the velocity dispersion and dynamical equilibrium, the core mass-to-light ratio is $124 \pm^{85}_{60}$ $M_\odot/L_{\odot,V}$ and the total mass-to-light ratio is $121 \pm^{84}_{58}$ $M_\odot/L_{\odot,V}$, implying the presence of large quantities of dark matter.

2.1 Introduction

This paper presents the results of the first multi-epoch observations and the most accurate velocity measurements for stars in the Sextans dSph galaxy. These are used to calculate a velocity dispersion and mean velocity for Sextans.

The Sextans dSph galaxy is the most recently discovered (Irwin et al. 1990) and least studied of the eight of its kind known to be in orbit around the Milky Way Galaxy. In general these galaxies contain a mixture of old and intermediate population stars and show no evidence of gas or recent star formation. They have similar total luminosity to most globular clusters ($10^5 - 10^7$ $L_\odot$) but their core radii are around an order of magnitude larger for the same luminosity.

Study of the kinematics of stars in both globular clusters and dSph galaxies by application of various simple models has been used to produce measurements for the mass-to-light ratios of these systems. The answers for globular clusters are around 2 or 3 $M_\odot/L_\odot$, whereas those for the different dSph galaxies vary between 6 and 250 (Irwin & Hatzidimitriou 1995), and at face value imply that all the dSph galaxies are of similar mass but contain different proportions of luminous

matter.

It is important to find the smallest scale on which large quantities of dark matter exist because it places constraints on what form that dark matter might take; for example cold (or dissipative) dark matter can cluster on arbitrarily short scales while relativistic matter (eg neutrinos) cannot. Therefore, since dSph galaxies are the next largest scale objects after globular clusters they are also the next largest scale on which to look for dark matter. However a mass-to-light ratio of 250 for a dSph galaxy does seem inconsistent with the general trend of mass-to-light ratio compared to size in the rest of the universe; for example, the value for the Milky Way Galaxy is only about 30, measured out to 80 kpc, and that for the Local Group is closer to 100. This and the wide range of measurements for the mass-to-light ratios of the different dSph galaxies leads to a question over whether the stellar kinematics are quite such simple indicators of the mass of these galaxies as is assumed by the simple models employed to date.

The rest of this paper is divided into several sections. First, the observations at the WHT and the reduction procedure are described. Next, the errors on the observations are discussed. Then the velocity dispersion calculation is described, the mass-to-light ratio theory explained and a value for the mass-to-light ratio obtained. Finally, other possible contributions to the velocity dispersion are discussed.

2.2 Observations, Data Reduction and Error Analysis

2.2.1 Observations

The periods of observations were the nights of 4th–7th May 1991, 27th–29th December 1991, 7th–9th and 26th–27th April 1992. All the observations were made using the William Herschel Telescope in La Palma.

The spectral range observed was 8300–8750 Å, which is the region containing the prominent calcium triplet absorption lines. We used the red arm of ISIS, the R1200R grating, a slit width of one arcsecond with the slit aligned with the parallactic angle and an EEV 1280x1180 CCD as detector. The CCD was

Table 2.1: Coordinates of the Sextans stars. The centre of the Sextans dSph galaxy is at $10^h\ 10.5^m$, $-01°\ 22'$.

Star	RA 1950	DEC 1950	
1	10 09 52.1	-01 07 35	
2	10 10 8.9	-01 30 36	*
3	10 09 47.6	-01 36 58	
4	10 10 34.6	-01 21 07	
5	10 10 8.6	-01 18 01	*
6	10 10 33.9	-01 23 00	*
7	10 11 17.9	-01 30 19	*
8	10 10 38.6	-01 28 09	*
9	10 11 24.3	-01 29 51	*
10	10 11 7.3	-01 18 47	*
11	10 09 53.2	-01 23 39	*
12	10 10 27.8	-01 36 30	*
13	10 10 39.5	-01 27 16	*
14	10 10 32.9	-01 13 08	*
15	10 10 35.3	-01 29 58	
16	10 10 45.7	-01 16 21	*
17	10 10 33.0	-01 30 00	*
22	10 09 32.3	-01 22 55	
23	10 11 33.2	-01 27 47	
32	10 11 21.9	-01 02 10	
37	10 08 39.0	-01 34 01	
38	10 09 14.3	-01 38 39	
44	10 10 32.0	-01 24 21	*
45	10 10 49.8	-01 07 35	
46	10 09 18.3	-01 39 53	
48	10 09 49.1	-01 32 11	*

Note. The asterisks indicate those stars which have also been observed by Suntzeff et al.

Table 2.2: Coordinates of the radial velocity standard stars.

Star	RA 1950	DEC 1950
HD908061	10 29 35.3	28 36 34
HD92588	10 40 7.4	-01 42 45
HD132737	14 59 38.3	27 10 55
HD107328	12 20 4.2	03 20 35

windowed to 400 pixels, which is about 2 arcmin, in the spatial direction. The resulting dispersion was about 0.35 Å per pixel, and the resolution measured from sky and arc lines was twice this. Arc lamp frames were taken before and after each stellar exposure, using a CuNe lamp for the May 1991 run and CuAr and CuNe lamps for the others.

The stars observed were giant branch stars ranging in brightness from 17 to 19 magnitudes in the R band. Forty seven Sextans candidates were observed, of which twenty six turned out to be members. Six of these stars were already known to be members from the AAT observations of Da Costa et al. (1991). Twenty four of the Sextans members were observed more than once and twenty two at more than one epoch. Good spectra were obtained for twenty two stars with nine of these having reasonable spectra at more than one epoch. Two of these nine stars may be velocity variables.

Additionally four bright radial velocity standard stars (RV stars) were observed with integration times of only 5 seconds, one or two on each night of each run. These spectra provided an estimate of the random and systematic errors for high signal-to-noise, short exposure spectra. The random part of this error gave an estimate of the minimum random error for the Sextans data, though it appears that the RV stars may have greater systematic error due to slit centering problems. The RV stars were also used as a check on the data reduction procedure because their actual velocities were already known, and as a base to obtain the absolute mean velocity of Sextans. The coordinates of all the Sextans and RV stars observed are shown in Tables 2.1 and 2.2: Table 2.3 records the coordinates of the Sextans candidates that were discovered not to be members of the galaxy.

Table 2.3: Coordinates of non-members discovered.

Star	RA	DEC
	1950	1950
21	10 11 19.8	-01 08 09
24	10 08 56.5	-01 18 27
25	10 11 33.6	-01 30 00
26	10 09 22.6	-01 44 27
27	10 08 54.3	-01 39 31
28	10 09 33.8	-01 04 00
29	10 09 31.5	-01 11 37
30	10 09 16.5	-01 16 18
31	10 11 37.4	-01 04 58
33	10 11 8.4	-01 02 17
34	10 09 21.4	-01 38 01
35	10 09 26.3	-01 36 45
36	10 09 16.1	-01 15 17
39	10 08 59.6	-01 35 23
40	10 10 15.4	-01 09 06
41	10 09 17.5	-01 28 49
42	10 11 53.1	-01 14 18
43	10 09 48.2	-01 44 34
44	10 10 32.0	-01 24 21
47	10 11 45.6	-01 25 05
50	10 09 26.2	-01 13 27

2.2.2 Data Reduction

Preliminary processing of the CCD frames to remove bias and cosmic ray events was done, mostly at the telescope, using FIGARO routines. Cosmic rays were identified as local events of amplitude greater than four sigma over local signal. Each was removed by interpolation only in the spatial direction, with independent interpolation in each CCD column. This process minimizes creation of correlated noise on scales comparable to a wavelength resolution element. Regions of strong sky lines affected by cosmic rays were excluded from use later in the reduction procedure.

The spectra from the May 1991 run were analysed independently using FIGARO and IRAF routines. Once we were satisfied that the two procedures produced equally good results, the rest of the data were reduced with IRAF, it being the faster and more flexible system. The procedure used is described in detail below.

Wavelength Calibration

The NOAO.TWODSPEC.LONGSLIT programs IDENTIFY, REIDENTIFY, FITCOORDS and TRANSFORM were used to wavelength calibrate the spectra by identification of the arc spectral lines, calculation of two dimensional fits to the arc spectra and transformation of these fits to appropriate stellar spectra respectively.

IDENTIFY found sixteen lines for the May 1991 CuNe arcs and twelve lines for the other CuAr + CuNe arc lamp spectra; REIDENTIFY made three piece spline fits along the wavelength axis every ten lines of the CCD. The rms residuals about the fits were about 0.01 pixels which corresponds to 0.12 $\mathrm{km\,s^{-1}}$.

Arc line fits from one or more spectra can be combined by FITCOORDS into one two dimensional chebyshev polynomial fit. In our case we combined the wavelength fit for the arc spectra on either side of the stellar spectrum in question unless the telescope had been moved a considerable distance in between the two arc lamp exposures. For example, if the previous star had been an RV star then one arc would have been taken at this star's co-ordinates and the next at Sextans' co-ordinates so only one arc would be used for each of these two stars. As the stellar spectrum took up just thirty lines near the centre of the CCD, most of the image was occupied only by sky spectrum and it was possible to extract this alone. The order of the fit was chosen by cross-correlating extracted sky spectra

from the images of several different stars and that order which gave closest to zero shift for all the sky spectra examined was used for the whole of that run. In the wavelength direction the fits were of third order for the May 1991 and Dec 1991 runs and fourth order for the April 1992 data. In the spatial direction all the data were fitted best by third order. The rms residuals about these fits were about 0.04 pixels corresponding to 0.48 km s^{-1}. The TRANSFORM program interpolated the fits produced by FITCOORDS onto the stellar spectra using spline fits. Thus wavelength calibrated spectra were produced.

Sky Subtraction

Sky subtraction was completed by the NOAO.TWODSPEC.LONGSLIT. BACKGROUND program. This calculated a second order chebyshev polynomial fit to each column of the image using an iterative procedure which excluded extreme pixels from the fit and interpolated across the 30 columns containing the stellar spectrum. This fitted background level was then subtracted from each column leaving a sky subtracted image. Figure 2.1 shows a typical spectrum from a Sextans member before and after sky subtraction.

The most intense sky line is at 8430 Å and its residual after sky subtraction from a high signal-to-noise spectrum is about 3.5 %. The data were rebinned to 8460–8700 Å, which contains the calcium triplet but little else to prevent any unavoidable sky contamination affecting the cross-correlation. If too few lines of sky spectrum were used in the sky subtraction calculation (this could happen if the two dimensional images were trimmed too much in the spatial direction), the interpolation across the section containing the stellar spectrum was inadequate and poor results were obtained, though this produced no systematic velocity shift. As shown by Figure 2.2, which is a comparison of template and sky spectra, there are sky emission lines close to each calcium absorption line. The low signal-to-noise spectra were sufficiently poor that, even after sky subtraction, they produced very uncertain velocities. Even in some higher quality spectra one or two of the calcium absorption lines could be badly affected, producing a very non-Gaussian look to the cross-correlation peak. Methods of dealing with such effects are discussed in the next section.

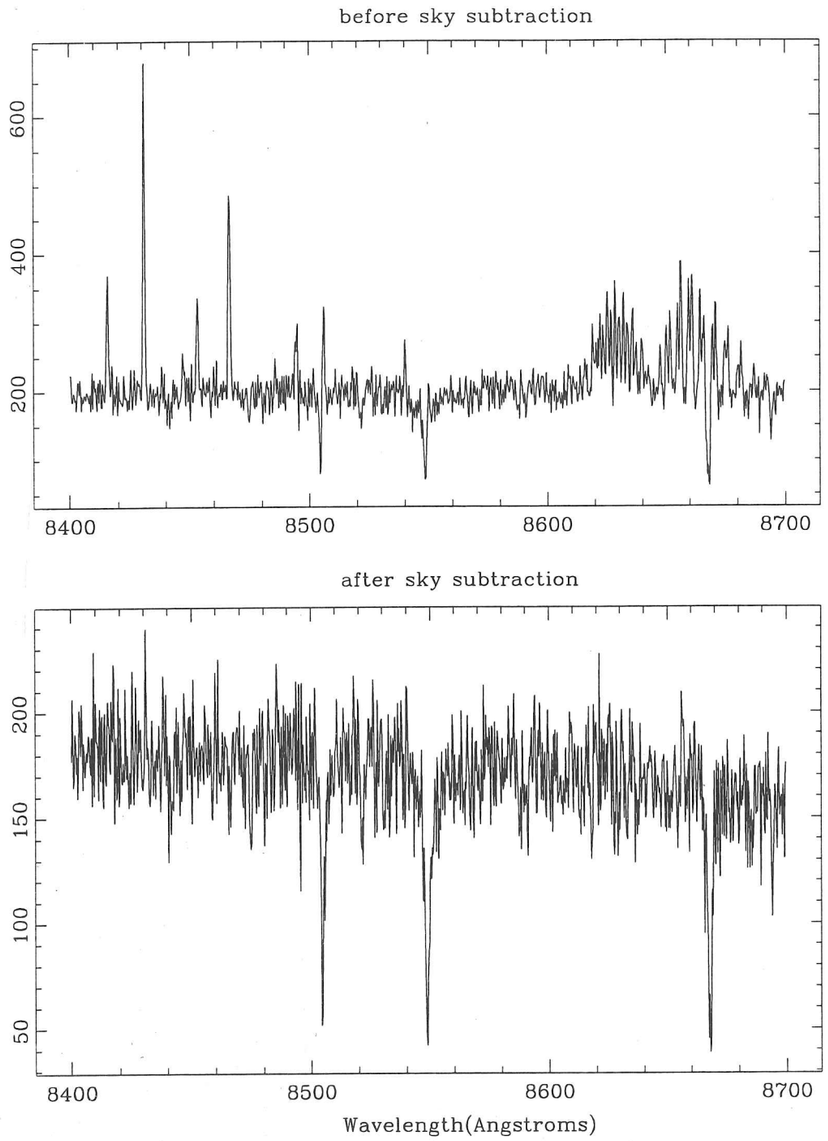

Figure 2.1: Comparison of a spectrum before and after sky subtraction.

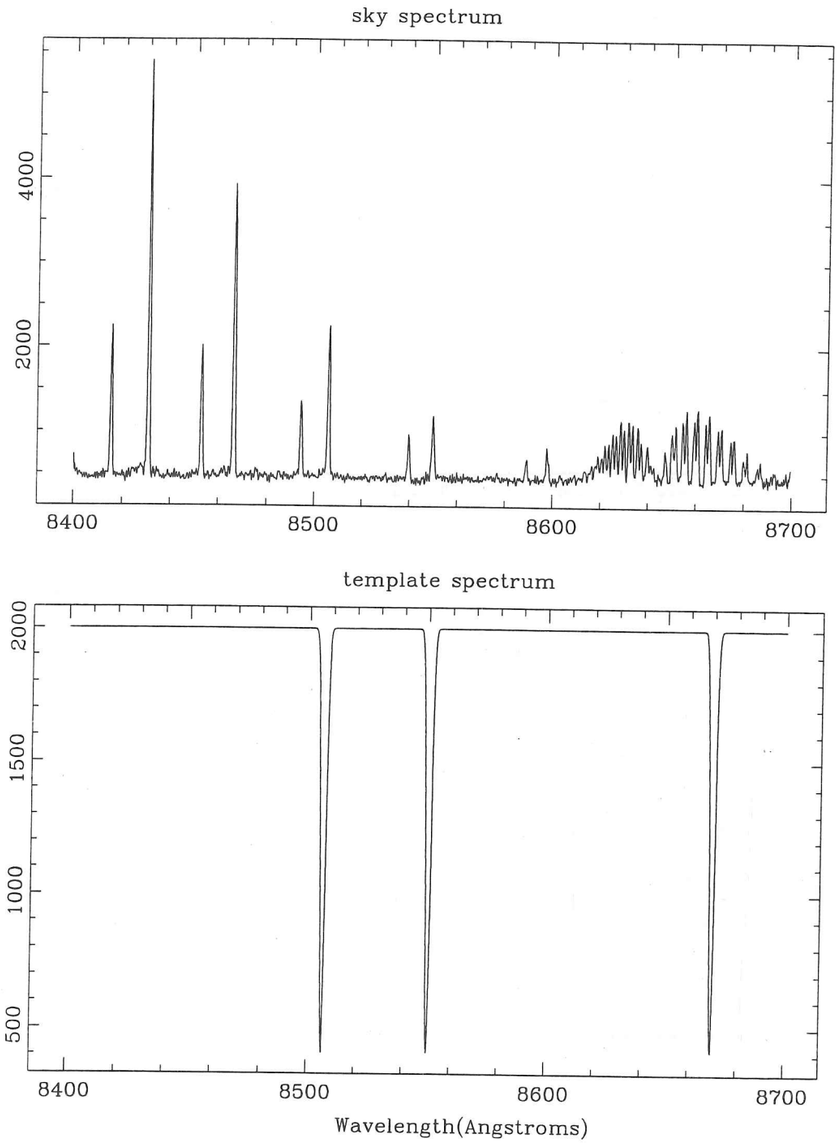

Figure 2.2: Comparison of sky spectrum and template spectrum. The existence of sky lines close to each absorption line in the template shows how crucial it was to have good sky subtraction. The middle template line has a weaker coincident sky line which explains why this line was generally the highest quality line in the reduced spectra.

Cross-correlation

The NOAO.TWODSPEC.APEXTRACT.APEDIT program was used to optimally extract one dimensional spectra by summing the pixels in each column within a defined aperture at each wavelength. There is a fault in the cross-correlation program FXCOR which means it is necessary to bypass the parts of the code involved in rebinning, or meaningless results are obtained. Therefore both the template and stellar spectra should be identically binned before cross-correlation is performed. The NOAO.ONEDSPEC.DISPCOR program was used to do this, rebinning the stellar spectra and the template logarithmically to 1024 bins in the wavelength range of 8460–8700 Å.

The template was created by the NOAO.ARTDATA.MK1DSPEC program and consisted of the three Calcium absorption lines with a one Gaussian width of 1 Å (Full width at half maximum of 1.18 Å). This artificial spectrum was found to be a far more reliable template than either a summation of Sextans spectra or the spectrum of an RV star, because only in this template was there no other information, apart from the absorption lines, for the stellar spectra to correlate with. For example, use of a template formed by summing Sextans spectra could result in systematic velocity shifts caused by beating in velocity space between residual sky lines in the template and in the star of interest. The accuracy of the template was tested by cross-correlating single lines in the template spectrum against their counterparts in the RV stars. Shifts of about 0.5 $\mathrm{km\,s^{-1}}$ between the different lines were observed.

All the stellar spectra were cross-correlated against the same template by the RV.FXCOR program. Initially this program subtracts any continuum from the spectra and then the correlation is performed. A Gaussian was fitted to the highest peak in the cross-correlation function and the centre of this Gaussian was taken to be the shift between the template and stellar spectra. This Gaussian fitting procedure performs much the same task as any filtering of the spectra, producing a smooth fit to a somewhat irregular correlation peak: it was unnecessary to filter the spectra prior to the correlation as this would in no way increase the accuracy of the fit. FXCOR calculates the measured velocity shift and then the heliocentric velocity relative to the template, given sufficient information in the image headers. If the Gaussian fit was poor then the fits to individual lines were checked, and if only one or two lines were contributing to the poor quality, the cross-correlation

was done omitting the region containing those lines.

FXCOR produces a Tonry and Davis R value (Tonry & Davis 1979) for each correlation, and it was this parameter that was used to quantify the quality of the correlation. The noise in a stellar spectrum can distort the cross-correlation peak, causing the measured centre of the peak to be displaced from the actual velocity shift between the star and template. The R value is the ratio of the height of the cross-correlation peak at the velocity shift to the root mean square of the antisymmetric component. The resulting error in the velocity shift is related to the R value, the displacement of the correlation peak being proportional to $1/(1+R)$. Spectra producing sufficiently low quality correlations were discounted by the means discussed in the next section.

It was sometimes possible to combine spectra of the same star with low R values to produce one spectrum of higher quality; the heliocentric shift between spectra taken at different times was calculated using the values output from the FXCOR program, the spectra were shifted by the correct amount using the IMAGES.IMSHIFT program, then both spectra were rebinned to a slightly smaller wavelength range (as was the template), the spectra were added together by IMAGES.IMARITH and correlated in the same way as the other spectra.

Stellar spectra that on correlation with the template produced R values less than about 5 were found to produce very different velocities for each of the three calcium absorption lines. For these very low signal-to-noise spectra differences of more than 10 km s^{-1} between lines were not uncommon. There was too much sky noise in these spectra for any meaningful result to be obtained and although selecting out sky lines may have increased the R value there was no objective way of using these spectra alone. Two spectra of the same star with this low an R value were not combined together although meaningful results could be obtained from one of these spectra combined with another spectrum of higher quality.

2.2.3 Errors in the Velocities

The error on the Sextans data was calculated using the stars for which there were repeat measurements of the velocity. An error distribution was created from the differences of the velocities obtained from individual observations for a star compared with the mean velocity of that star. The Gaussian one sigma width

Table 2.4: The Velocities and Tonry and Davis R values for the Sextans Observations. (The columns are explained in the table footnotes and the text.)

Star	Date	V_t km s^{-1}	R		$\overline{V}_{ex}$ km s^{-1}	ΔV_{ex} km s^{-1}	$\overline{V}_{7.5}$ km s^{-1}	$\Delta V_{7.5}$ km s^{-1}
1	M91 c	-0.4	6.4	*		-1.4	—	—
	M91	-0.1	12.0			-1.7		2.0
	M91	-3.0	26.9			-1.2		-0.9
	D91	-2.0	17.0			-0.2		0.1
	A92-1 c	3.7	5.8	*	-1.8	5.4	—	—
	A92-1	-2.7	21.7			-1.0	-2.1	-0.7
	A92-1	-1.9	10.7			-0.1		0.2
	A92-2	-2.2	8.5			-0.5		0.2
	comb	-3.6	8.5	—	—	—		-0.5
2	M91	-0.5	9.1			-0.3		1.3
	M91	-1.8	10.9			-1.6		-0.0
	M91	0.4	10.5			0.6	-1.8	2.2
	D91	-9.8	11.4	*	-0.2	-9.6		-8.0
	A92-1	1.0	11.7			1.2		2.8
	A92-1	-0.2	9.4			0.1		1.7
	A92-2	-3.8	6.0	*		-3.6	—	—
3	M91 c	-4.3	7.5			-5.6	—	—
	M91	-2.4	9.1			-3.8		-2.2
	A92-1 c	9.2	7.0	*	1.4	7.8	—	—
	A92-1	-2.8	12.7			-4.2	-0.2	-2.6
	A92-1	0.7	13.3			-0.7		0.9
	A92-2	2.0	9.3			0.7		2.3
	comb	1.4	9.8	—	—	—		1.6
4	M91	-10.9	9.5	*		-2.3		-1.6
	A92-1	-8.8	11.0		-8.6	-0.2	-9.3	0.5
	A92-1	-8.3	11.9			0.3		1.0
	A92-2	-32.8	3.4	*		-24.2	—	—
5	M91	-1.8	10.3			-0.5	-1.4	-0.5
	D91	-0.9	11.2		-1.4	0.45		0.5
	A92-2	-20.4	5.8	*		-19.0	—	—

Table 2.4 continued...

Star	Date	V_t km s^{-1}	R		$\overline{V}_{ex}$ km s^{-1}	ΔV_{ex} km s^{-1}	$\overline{V}_{7.5}$ km s^{-1}	$\Delta V_{7.5}$ km s^{-1}
6	M91	10.2	9.0		7.8	2.4	7.8	2.4
	M91	5.3	8.7			-2.4		-2.4
	A92-1	-5.5	12.4			0.8		0.8
	A92-1	-6.2	8.4		-6.3	0.08	-6.3	0.1
	A92-2	-7.2	9.1			-0.9		-0.9
7	M91	10.6	11.2	*		-2.2		-1.5
	M91	13.3	8.4			0.5	12.0	1.2
	D91	12.3	9.8		12.8	-0.5		0.3
	A92-2	4.9	5.6	*		-7.9	—	—
	A92-2	-37.7	1.8	*		-50.5	—	—
8	M91	11.8	8.2		2.5	9.3	11.8	
	A92-2	-6.7	7.4			-9.3	—	—
9	M91 c	0.5	6.8		-5.7	6.2	—	—
	A92-1 c	-11.8	4.1			-6.2	—	—
	comb	-10.7	9.3		—	—	-10.7	
10	M91	-5.0	4.7		-7.5	2.5	—	—
	D91	-10.0	9.4			-2.5	-10.0	
11	M91	15.8	7.7		15.8		15.8	
12	M91	-13.9	4.2			3.0	—	—
	D91	-17.1	4.8		-16.9	-0.2	—	—
	A92-1	-19.8	3.6			-2.9	—	—
13	M91	22.8	3.7		20.9	1.9	—	—
	D91	19.0	4.4			-1.9	—	—
14	M91	-6.5	4.2		-6.1	-0.4	—	—
	D91	-5.7	11.2			0.4	-5.7	
15	M91	-22.7	1.8			-1.9	—	—
	M91	-44.8	1.8		-20.8	-24.0	—	—
	D91	-18.8	5.6			1.9	—	—
16	D91 c	2.1	5.9		-6.4	8.5	—	—
	D91 c	-14.8	4.1			-8.5	—	—
	comb	4.6	7.7	—	—	—	4.6	

Table 2.4 continued...

Star	Date	V_t km s^{-1}	R		$\overline{V}_{ex}$ km s^{-1}	ΔV_{ex} km s^{-1}	$\overline{V}_{7.5}$ km s^{-1}	$\Delta V_{7.5}$ km s^{-1}
17	D91 c	-9.3	2.4		-0.0	9.2	—	—
	D91 c	9.2	6.8			-9.2	—	—
	comb	-2.4	8.8	—	—	—	-2.4	—
22	D91	-5.4	9.8		-5.4		-5.4	—
23	D91	9.5	7.4		5.5	4.0	—	—
	A92-2	1.4	9.92			-4.0	1.4	
32	D91	-7.3	12.0		-6.4	-1.0		-1.0
	A92-2	-5.4	12.7			1.0	-6.4	1.0
37	A92-1	0.3	11.4		-0.4	0.7		0.7
	A92-2	-1.1	11.9			-0.7	-0.4	-0.7
38	A92-1	-1.9	7.3		-3.9	2.0	—	—
	A92-2	-5.9	10.3			-2.0	-5.9	
44	A92-1	2.2	8.7		0.8	1.5		1.5
	A92-2	-0.7	8.2			-1.5	0.8	-1.5
45	A92-1	-12.4	4.8		-11.1	-1.2	—	—
	A92-2	-9.9	8.5			1.2	-9.9	—
46	A92-1 c	-0.8	5.5		-4.2	3.5	—	—
	A92-2 c	-7.7	7.1			-3.5	—	—
	comb	2.2	7.7	—		—	2.2	—
48	A92-1	-12.6	3.4		-11.2	-1.4	—	—
	A92-2	-9.9	3.6			1.4	—	—

Notes. Date: M91, D91, A92-1, A92-2 are abbreviations for the May1991, December 1991, and April 1992 runs, A92-1 being the run at the start of April and A92-2 the one at the end.

V_t: This is the heliocentrically corrected velocity with respect to the template.

R is the Tonry & Davis R value.

$\overline{V}_{ex}$: This is the average for each star of all the values of V_t excluding those that caused a change in the mean of more than 2.5 standard deviations.

Star 6 is probably a binary so two averages at the different observing times were calculated in order that the data from this star could still be used in the analysis of the errors.

$\overline{V}_{7.5}$: This is the average velocity for a star where data which produced a correlation with R <7.5 are not included, and $\Delta V_{7.5} = (V_t - \overline{V}_{7.5})$.

The observations not included at the cutoff are marked by a dash.

of this distribution was taken to be the error on an individual observation. The procedure for finding this value is described in more detail below. There were three sources of error in the results. These were random error caused by low signal-to-noise data which is parameterised by the R value, systematic error caused by instrumental drift and imperfect centering in the slit, and real velocity variations. Further investigation of the errors was conducted by finding the error distribution for the RV stars. This distribution was less Gaussian in shape with a small central core and wide wings. These data are of much higher signal-to-noise, so the width of the central core was seen as an estimate of the minimum random errors of our experiment. The wings to the distribution, which were not apparent in the Sextans error distribution, were probably caused by slit centering problems. This effect is greater in the RV star data because of the short exposure times. Undetected real velocity variations of the stars caused by their being binary stars would have the effect of broadening the velocity distribution of the system. All three issues are discussed below.

The Error Calculation for Sextans

The reduction procedure described in the previous section produced the velocities and R values shown in Table 2.4. The R value was the best indicator of the quality of the spectra, better than the number of counts or air mass which were also inspected. According to theory described in Section 2.2.2, the inaccuracy in the position of the centre of the correlation peak rises sharply with decreasing R value. Therefore, if there is some value of R at which the accuracy is deemed to be acceptable, all the results which produced higher R values should be of even better accuracy. So a cutoff value for R whereby all spectra producing lower values were disregarded was obtained by the following method.

The difference between the velocity obtained for each observation and some mean value was required to give an idea of the accuracy of each measurement, and this could then be compared with the R value for each observation. Therefore an average velocity was calculated for each star. We shall refer to the straight forward average for each star as $\overline{V}$, and the deviation of each observed velocity from the mean for the star as ΔV. An alternative velocity is shown as $\overline{V}_{ex}$ in Table 2.4. Any velocity that differed from the mean (calculated excluding that velocity) by 2.5 or more times the standard deviation of the other velocities was

Table 2.5: ΔV_{ex} from table 2.4. binned into values of R

R	1.5–	2.5–	3.5–	4.5–	5.5–	6.5–	7.5–	8.5–	9.5–	10.5–	11.5–	12.5+
ΔV_{ex}	-50.5	-24.2	3.0	2.5	-1.4	7.8	-5.6	-0.5	-2.3	-0.1	-1.7	-4.2
	-1.9	-1.4	-2.9	-2.5	5.4	9.3	0.1	-0.3	-0.5	-1.6	1.2	-0.7
	-24.0	1.4	1.9	-1.2	-3.6	-9.3	1.5	0.1	-0.5	0.6	0.8	-1.2
	9.2		-1.9	1.2	-19.0	2.0	-1.8	-3.8		-9.6	-1.0	-0.2
	-9.2		-0.4	3.5	-7.9	-2.0	0.5	0.7		-0.2	1.0	1.0
			0.4	-3.5	1.9	4.0		2.4		-0.7	0.3	
			8.5	-0.2		-4.0		-2.4		0.5		
			-8.5					-0.9		-2.2		
			6.2							0.7		
Mean	-15.3	-8.1	0.7	-0.0	-4.1	1.1	-1.0	-0.6	-1.1	-1.4	0.1	-1.5
St.Dev.	23.1	14.0	5.0	2.6	8.6	6.6	2.8	1.9	1.1	3.2	1.2	1.6

Notes. Each correlation produces a velocity and a value of the Tonry and Davis R value.
The velocities here are the same as ΔV_{ex} in table 2.1.
Mean and St.Dev. are the mean value and standard deviation for each column.

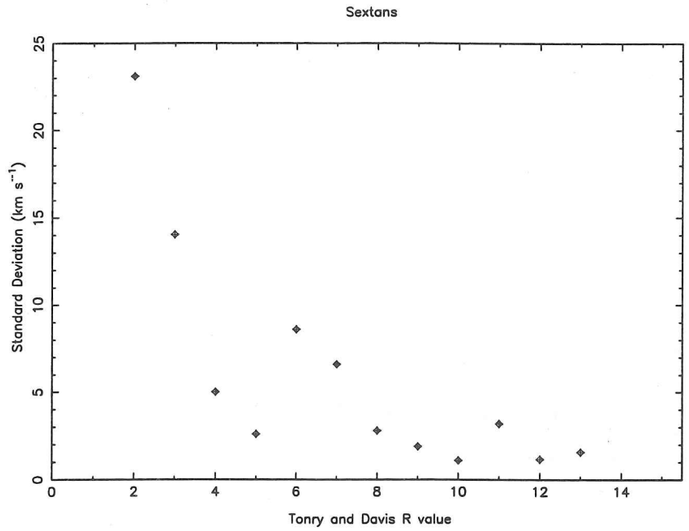

Figure 2.3: The standard deviations from Table 2.4 compared with the Tonry and Davis R value: the steep increase in the standard deviation with decreasing R at low R is as expected for an accuracy verses R diagram. The deduced cutoff value for R is between 7 and 8.

left out of this calculation. Those observations excluded from the average are marked in the table by asterisks. The deviations of the individual velocities from this mean are shown by ΔV_{ex} in the table, and are more extreme for the more deviant velocities than the values of ΔV for the same observations. Star 6 had velocities measured on two different observing runs whose averages differed by 14 km s^{-1}, so this star was therefore assumed to be variable and was not included in the velocity dispersion calculations. It was also possible that star 8 was variable, although with only one observation at each of two observing runs and generally lower quality spectra this was not as likely so this star was still included in the analysis. The relative probabilities of these stars being variable is considered later in the part of Section 2.4.2 which discusses the relevance of binary stars. The values of ΔV_{ex} were grouped according to the appropriate value of R as shown in Table 2.5. When there were only two spectra of a star, both velocities were put in the bin corresponding to the lower R value. Each band of R had unit width, and the mean and standard deviation of the values of ΔV_{ex} in each band were

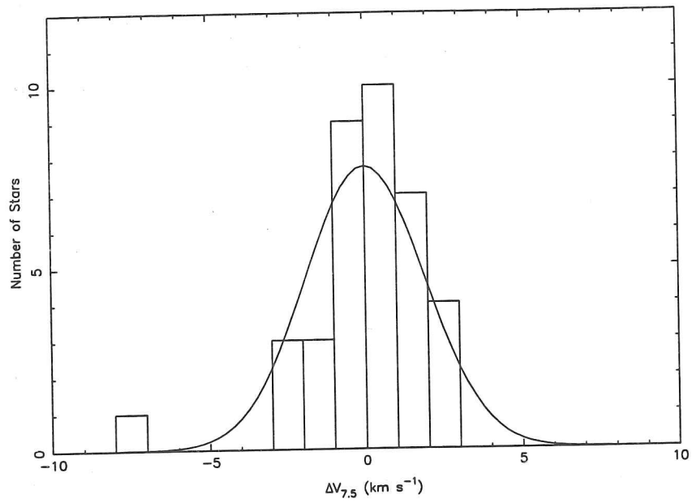

Figure 2.4: The Gaussian fit to the error distribution of the Sextans stars for R_{cut} of 7.5 with width 1.9 km s^{-1}. The K-S test of this fit produced a probability of 0.7.

calculated, leading to the values presented in Table 2.5. The standard deviations were then plotted against the R values for all the data, giving a representation of the accuracy variation with R. This plot is displayed in Figure 2.3, and illustrates the way the inaccuracy rises as expected with decreasing R. For R greater than about 8 the standard deviation is below about 3, but it is substantially higher for lower R values. A suitable cutoff value (R_{cut}) was taken to be somewhere between 7 and 8. All the results were calculated for R_{cut} values of 7, 7.5 and 8 although there was little difference between these three when compared with the case when no R threshold was imposed on the data.

Having found a cutoff value of R it was then necessary to calculate the measuring error on each observation in the remaining sample. Up to this point all the observations had been taken in isolation. It was possible, however to combine two spectra whose R values fell below R_{cut} to create a single spectrum with a sufficiently high R value for it to be used in the subsequent calculation. If the R values for the single observations were above the threshold R_{cut} then these observations were used separately, but if they fell below and that of the combined spectrum fell above, then the combination was used instead. The results for an R_{cut} value of 7.5 are shown in Table 2.4 where the 'c's in the 'Date' column mark

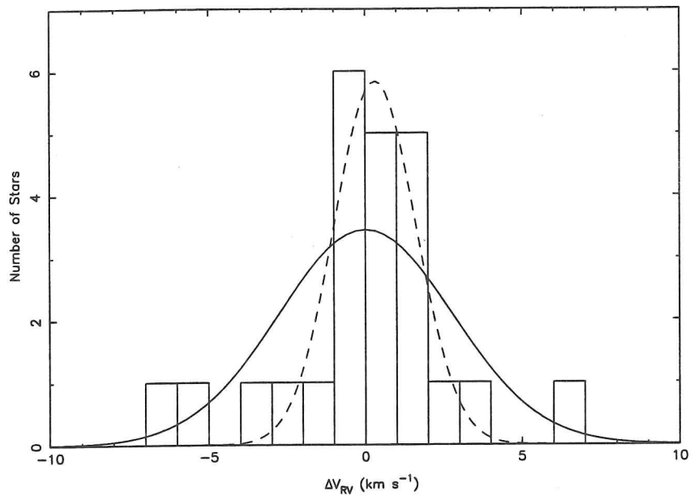

Figure 2.5: The Gaussian fit to the error distribution of the RV stars. The wider Gaussian is the fit to all the data and is of width 2.8 km s^{-1} with a probability of 0.5 for the fit. The narrower Gaussian is the fit for the distribution excluding the five most extreme velocities in the distribution. It is of width 1.3 km s^{-1} and the probability for the fit is 0.9. The relevance of the two different fits is explained in the text.

spectra that were combined to make the 'comb' spectra. Observations excluded at each value of R_{cut} are marked by dashes.

The standard deviations in Table 2.5 are basically the measuring errors for the observations at each value of R, so the standard deviation of the values of ΔV for the range of R greater than R_{cut} gives the measuring error of the sample used. This is equivalent to finding the width of a Gaussian fitted to the distribution of ΔV, so the assumption being made is that the errors were Gaussian, which is a point which will be returned to later. The calculation was made for each value of R_{cut} yielding a width σ^2_{err}, and the error on this width was ϵ_1, where $\epsilon_1 = \sigma^2_{err}\sqrt{2/N}$. The values of σ_{err} obtained for R_{cut} values of 0, 7, 7.5 and 8 were 7.2 ± 0.6, $3.2^{0.3}_{\pm 0.4}$, 1.9 ± 0.2 and 1.9 ± 0.2 km s^{-1} respectively. Kolmogorov-Smirnov (K-S) tests were performed on each fitted Gaussian to see if the errors were indeed consistent with Gaussian distributions. For R_{cut} values of 0, 7, 7.5 and 8 the probabilities of a Gaussian distribution were 0.006, 0.4, 0.7 and 0.7. So the errors are consistent with Gaussian errors except in the case where no threshold is imposed on R. In

this case it would not be expected for the errors to be simply Gaussian because of the very much lower accuracy at the lower values of R making the distribution a summation of different Gaussian which would itself not be Gaussian in shape. The errors for R_{cut} of 7 have a lower probability of being Gaussian than those for the other two higher cutoffs, probably for the same reason. Figure 2.4 shows the error distribution and fitted Gaussian for R_{cut} of 7.5.

Comparison with the RV Stars

The RV stars were used to check the reduction procedure and to find a lower limit on the random errors. The velocities obtained for these stars are listed in Table 2.6. The reduction procedure and error calculation were identical to that used for the Sextans data so the results from the two sets could be compared. All the R values obtained for the correlations of these spectra were well above the threshold region, with an average value being around 17. The average velocities of the stars were within 1 km s^{-1} of the known velocities, verifying that the reduction procedure had worked well. The distribution of the differences from the mean velocities, ΔV, had a width of 2.8 km s^{-1} with a probability of being a Gaussian of 0.5, which is somewhat lower than the probability for the Sextans results for R_{cut} of 7.5 or more. Looking at the distribution of ΔV, extended wings can be seen in addition to a rather Gaussian shape close to the centre.

This shape is probably due to the star not always being placed centrally in the slit. An experiment to test this was conducted during the April 1992 run whereby consecutive exposures of the same RV star were made with the star in the top half, middle and bottom half of the slit as it was viewed on the television screen. The 'top','middle', and 'bottom' readings in Table 2.6 show the velocities obtained. A difference of more than 6 km s^{-1} was obtained between the two sides of the slit, and this is sufficient to account for the wings to the distribution. This would be a systematic error, with no signal-to-noise dependence. However, for the Sextans stars the effect of positioning in the slit should be considerably less because of the motion of the star in the slit due to the guiding errors of the telescope during the exposures which are 180 times longer than those for the RV stars. So to get some idea of the minimum possible random error, which was signal-to-noise dependent, a Gaussian was fitted to the centre of the distribution. The width was 1.3 km s^{-1} with a higher probability from the K-S test of 0.9. This is considerably less than

Table 2.6: Velocities for the radial velocity standard stars.

Star	Date	V_t km s^{-1}	$\overline{V}$ km s^{-1}	ΔV km s^{-1}	V_A km s^{-1}
HD908061	M91	36.7		0.5	
		37.6		1.4	
		36.0		-0.3	
		38.7		2.4	
	D91	30.6	36.2	-5.6	36.3
		42.4		6.2	
	A92	36.6		0.4	
		29.3		-7.0	
		36.7		0.5	
		37.8		1.5	
HD92588	M91	43.9		2.0	
	D91	38.5		-3.5	
		41.6	41.9	-0.3	42.8
	A92	42.3		0.3	
		43.4		1.5	
HD13273	M91	-19.9		4.0	
		-22.0		1.9	
		-26.7		-2.8	
	A92	-24.9	-23.9	-1.0	-24.1
		-24.1		-0.2	
		-24.7		-0.8	
	top	-21.4			
	middle	-25.2		-1.2	
	bottom	-27.6			
HD107328	M91	35.6	35.5	0.1	35.7
	A92	35.4		-0.1	

Notes.

The notation here is the same as in table 2.4; $\overline{V}$ is the mean velocity for each star and ΔV the difference of the velocity of each star from this mean. The values of V_A are the actual velocities of the radial velocity standard stars.

the errors for the Sextans data, as would be expected for lower signal-to-noise spectra, so that no matter how good the spectra obtained by similar observations are, the errors will not be less than 1.3 km s^{-1} for each observation.

The effect of slit positioning in the Sextans data may not be negligible, but as this would be expected to show up in the error distribution deviating from Gaussian in shape and no deviation of this sort is obvious, no contribution of this to the errors is included in the results in this paper. However, it is important to bear in mind that the effect of this systematic error would be to create wings to the velocity distribution of the galaxy, probably increasing the value calculated for the velocity dispersion. The error distribution for the RV stars along with both Gaussian fits are shown in Figure 2.5, and all the results from the error calculations are displayed in Table 2.7.

2.3 Results

2.3.1 The Velocity Dispersion Calculation

The observations which had produced R values above the threshold were used to calculate a mean velocity for each star. The width of the distribution of these velocities defines the velocity dispersion (σ_{obs}) of Sextans. An unweighted Gaussian fit to the data and a weighted calculation were both made, producing slightly different results. All the velocity dispersion results, weighted and unweighted, for R_{cut} values of 0, 7, 7.5 and 8 are displayed in Table 2.7. The results mentioned in the text are those for an R_{cut} value of 7.5

The velocity dispersion obtained by fitting a Gaussian to the unweighted distribution was $7.4\pm^{1.1}_{1.3}$ km s^{-1} for an R_{cut} value of 7.5. The variance of σ^2_{obs} is $2\sigma^4_{obs}/N$, so this is the error quoted. This dispersion has not had the contribution due to measuring errors removed. The inclusion of these, as in equation 2.22, gives a corrected velocity dispersion of $7.3\pm^{1.0}_{1.2}$ km s^{-1}.

From a theoretical point of view, the most accurate calculation should use the average velocity of each star weighted in some way to take account of its measuring error. The method used over the last few years for such a calculation was that of Armandroff & Da Costa (1986). The detail of this method is given in Section 2.6, the first Appendix. The result from this weighted calculation for an R_{cut} value of

Table 2.7: Widths of the error distributions and the velocity dispersions calculated for different values of R_{cut}

Distribution	$\overline{v}$ km s^{-1}	σ km s^{-1}	Error km s^{-1}	Prob	N
Sextans error calculation					
all R	0.1	7.2	± 0.6	0.006	75
$R \geq 7$	-0.03	3.3	$\pm^{0.3}_{0.5}$	0.4	44
$R \geq 7.5$	-0.0003	1.9	$\pm^{0.2}_{0.3}$	0.7	37
$R \geq 8$	-0.0003	1.9	$\pm^{0.2}_{0.3}$	0.7	37
RV stars error calculation					
all results	0	2.8	± 0.4	0.5	24
core	0.3	1.3	± 0.2	0.9	19
Sextans velocity dispersion					
Unweighted calculation (measuring errors included)					
all R	-3.8	8.7	$\pm^{1.2}_{1.3}$	0.7	25
$R \geq 7$	-1.7	6.7	$\pm^{1.0}_{1.1}$	0.9	21
$R \geq 7.5$	-1.1	7.3	$\pm^{1.0}_{1.2}$	0.8	21
$R \geq 8$	-2.5	6.4	$\pm^{1.0}_{1.2}$	0.8	18
Armandroff & Da Costa weighted calculation					
all R	-4.2	7.8	$\pm^{1.0}_{1.2}$	0.8	25
$R \geq 7$	-1.2	5.5	$\pm^{0.8}_{0.9}$	0.7	21
$R \geq 7.5$	-1.1	6.0	$\pm^{0.9}_{1.0}$	0.8	21
$R \geq 8$	-1.7	5.6	$\pm^{0.9}_{1.0}$	0.5	18
Maximum likelihood calculation					
all R	-4.0	8.1	$\pm^{1.7}_{1.4}$	0.8	25
$R \geq 7$	-1.6	6.2	$\pm^{1.3}_{1.1}$	0.9	21
$R \geq 7.5$	-1.1	7.0	$\pm^{1.3}_{1.0}$	0.9	21
$R \geq 8$	-2.5	6.1	$\pm^{1.3}_{1.0}$	0.8	18

Notes The value of $\overline{v}$ is the average value calculated by the fit to the distribution.
The value of σ is the width of the distribution; so in the case of the error distribution it is the value of the error and in the case of the velocity dispersion calculation it is the velocity dispersion.
Error is the error in the value of σ calculated as described in the text. N is the number of stars in the distribution. The value 'Prob' is the probability obtained by a K-S test comparing a Gaussian distribution with the calculated width and average to the actual distribution of data.

The differences between the different calculations are described in Section 2.3.1.

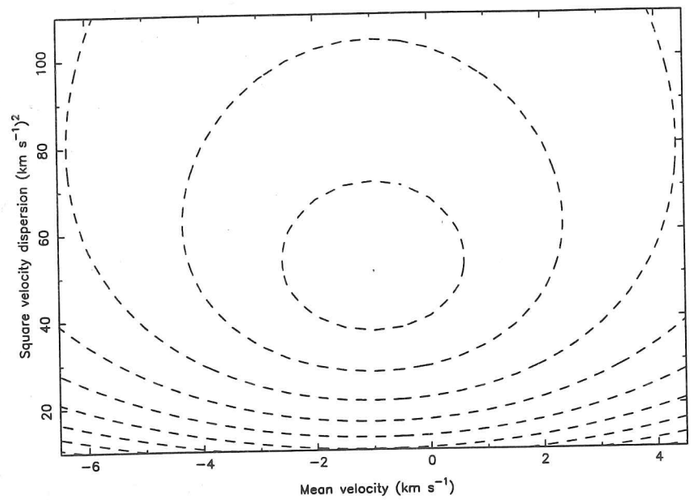

Figure 2.6: The log likelihood function described in Section 2.7, for the data with an R_{cut} value of 7.5. The central dot is at the maximum of the function, and the contours are analogous to the first to eighth sigma errors.

7.5 was $6.0\pm^{0.9}_{1.0}$ km s^{-1}. The K-S tests performed on all the results for the different R_{cut} values show consistency with Gaussian distributions.

We have used a different weighted calculation using a maximum likelihood estimator to simultaneously find the velocity dispersion (σ_{obs}) and mean velocity ($\overline{v}$) of the sample. Figure 2.6 shows the log likelihood function contoured in the $\overline{v}$, σ^2_{obs} space. The one sigma measuring errors are the first contour, where the log likelihood has fallen by 0.5 from its maximum. The theory is explained in the second Appendix, Section 2.7. Using this method the velocity dispersion for an R_{cut} value of 7.5 was $7.0\pm^{1.3}_{1.0}$ km s^{-1}. For a sample where the velocity dispersion is considerably larger than the measuring errors, it would be expected for this result to be similar to the unweighted calculation, as explained in the appendix. It can be seen, referring to Table 2.7, that this was indeed the case for our results.

We recommend use of the maximum likelihood estimator, with appropriate functional form for the intrinsic velocity dispersion, since not only does this give the 'best' estimate of σ_{obs} but it also enables reliable confidence limits to be readily determined. The Armandroff & Da Costa method gives too much weight to repeat measurements of the same stars, because the intrinsic dispersion of the sample is not allowed for. In cases where some stars are observed many more times than

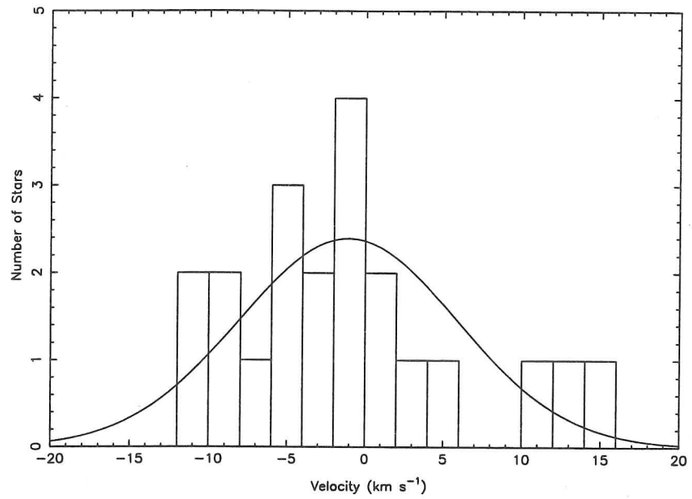

Figure 2.7: The velocity distribution of the Sextans dSph galaxy with R_{cut} of 7.5. There are twenty one stars in the sample and the Gaussian shown is that produced by the error weighted calculation. The velocity dispersion is 7.0 km s^{-1} and the average velocity -1.1 km s^{-1} with respect to the template.

others (as is common) this will cause the true velocity dispersion to be seriously underestimated. This effect can clearly be seen in Table 2.7.

The value of the velocity dispersion adopted for later calculations is 7.0 km s^{-1}, which was that for the maximum likelihood calculation at an R_{cut} value of 7.5. The cutoff value of 7.5 was used because the measuring errors are low, Gaussian with a high probability, without losing too many stars from the sample. Figure 2.7 shows the Gaussian with this width and the velocity distribution for an R_{cut} of 7.5.

Only a small change in the velocities occurs when the data are adjusted to Galactocentric coordinates, the average change being 0.1 km s^{-1}. The change in the velocity dispersion thereby produced (from $7.0\pm^{1.3}_{1.0}$ km s^{-1} to $7.1\pm^{1.3}_{1.0}$ km s^{-1}) is insignificant within the errors.

2.3.2 Comparison with Previous Results

The only other accurate measurements of the velocities of stars in the Sextans dSph galaxy are by Suntzeff et al. (1993). They measured velocities for forty

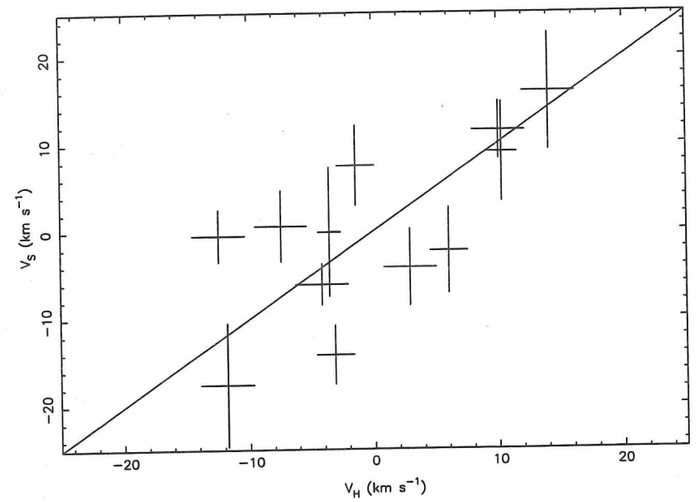

Figure 2.8: The velocities obtained from our data compared with those from Suntzeff et al. for the eleven stars for which we both have data. The V_S and V_H are the velocities from Suntzeff et al. and our velocities respectively, and the error bars show the upper and lower limits of each star's velocity according to the errors calculated by the two groups. The rectangles described by the error bars should intersect the straight line drawn on the diagram if the two sets of data were consistent; the error underestimate is a factor of 1.3.

three stars in Sextans during the period 25–27 March 1991 and obtained a velocity dispersion of 6.2 ± 0.9 km s^{-1}, analysing their results using the Armandroff & Da Costa method, and only using their most accurate thirty three stars. We have fifteen stars in common; for three of these our data were too poor to produce a reliable velocity and one is the variable star 6. Their observations were only one month before our first observations, and the velocity they obtained for star 6 is, within the errors, the same as the velocity we obtained during the May 1991 run, adding weight to our suggestion of its variability. Suntzeff et al. find their velocity measurement of star 5 (their star 17) statistically improbable for a Gaussian distribution and it is interesting to note that our result for this star is quite reasonable of itself but the two velocities measured by the different groups are not within each other's errors. They have several observations of each star so were

able to produce an individual error estimate for each star, and their measurements of the stars observed by both of us have errors between 2.4 and 7.4 $\mathrm{km\,s^{-1}}$.

Using the analysis described by Godwin & Lynden-Bell (1987) to compare our results with those of Suntzeff et al., and taking an average error estimate for the results of Suntzeff et al. of 5.2 $\mathrm{km\,s^{-1}}$, between us we have underestimated the measuring errors by a factor of 1.3. With only two sets of data it is not possible to say what the real errors are for each group, though since our errors are much smaller it is highly likely that the underestimate of the errors of Suntzeff et al. comprises most of the discrepancy; they would have to increase their errors by a much smaller factor to make up the difference. If the discrepancy was all due to us, our errors would have to be as large as theirs. Figure 2.8 shows our results plotted against those of Suntzeff et al. obtained for the twelve stars we both have velocities for, with our own predicted errors plotted as the error bars.

2.3.3 The Absolute Mean Velocity of Sextans

The other result obtained was that for the systematic velocity of the Sextans dSph galaxy. From the RV standard stars, the velocity of the template was found to be 223.3 $\mathrm{km\,s^{-1}}$. The maximum likelihood method output values for the velocity dispersion and the mean velocity of the sample simultaneously. For a value of R_{cut} of 7.5 the mean velocity of the sample with respect to the template was -1.1 ± 1.6 $\mathrm{km\,s^{-1}}$. The error here is derived from the log likelihood plot in the same way as the velocity dispersion (See the second Appendix). This gave the velocity of Sextans as 224.4 ± 1.6 $\mathrm{km\,s^{-1}}$, in line with the previous values of 230 ± 6 $\mathrm{km\,s^{-1}}$ (Da Costa et al. 1991), and 227.9 ± 1.8 $\mathrm{km\,s^{-1}}$ (Suntzeff et al. 1993).

2.4 Analysis

2.4.1 Mass-to-light Ratios

Theory

As discussed by Richstone & Tremaine (1986), the central mass-to-light ratio of a system may, dimensionally, always be written

$$\frac{\rho_0}{I_0} = \eta \frac{9\sigma_0^2}{2\pi G r_{hb} S_0}, \tag{2.1}$$

where $I_0 \approx S_0/2r_{hb}$, S_0 is the central surface brightness, r_{hb} is the half brightness radius and σ_0 is the measured central velocity dispersion. The factor η is given by

$$\eta = \frac{4\pi}{9} r_{hb} \frac{[\int_0^\infty \rho(r)\,dr]^2}{\int_0^\infty M(r)\rho(r)/r\,dr}, \tag{2.2}$$

so is dependent on the model fitted to the density profile. However it turns out that for all simple models producing realistic profiles, η is always close to 1. The equation for ρ_0/I_0 with η set to 1 is called King's method of core fitting; it was first derived by King in 1965 (see Richstone & Tremaine 1986) without use of a King model. This method is clearly independent of any model used to fit the density profile, all the variables being measurable quantities. However this is not quite true for dSph galaxies because of the difficulty of defining the central brightness, and hence the half brightness, without first fitting a model to the data. Therefore a King model has been fitted to the surface brightness profile (Irwin & Hatzidimitriou 1993) from which the half-brightness radius has been calculated.

King models are lowered isothermal spheres with velocity distributions given by,

$$f(v) = \begin{cases} k(e^{\beta(E-E_0)} - 1), & E < E_0, \\ 0, & E \geq E_0, \end{cases} \tag{2.3}$$

where $E = v^2/2 + \mathbf{\Phi(r)}$, $\mathbf{\Phi(r)}$ is the potential, and k, β ,and E_0 are constants. These models are parameterised by $W_0 = \beta[E_0 - \mathbf{\Phi(0)}]$ or by the concentration, $c = log(r_t/r_c)$ where r_t is the tidal cutoff radius and r_c is the core radius which King originally defined empirically (King 1962). As σ_0 is the measured central velocity

dispersion, we shall call $\sigma(r)$ the velocity dispersion as a function of distance from the centre of the galaxy. The value of β changes with the different models as is shown by the plot in Binney & Tremaine (1987) which relates $\sqrt{\beta\sigma^2(r)}$ to distance, r, from the centre of the galaxy. Rather confusingly their σ^2 is our $1/\beta$, whereas (assuming isotropy of the velocity dispersion) our $\sigma^2(r)$ is equal to one third of the mean square velocity which, in Binney & Tremaine's notation, is $\overline{v}^2/3$.

The central density of a King model (King 1966) is

$$\rho_0 = \frac{9}{4\pi G\beta r_c^2}. \tag{2.4}$$

For $W_0 \geq 5$, $1/\beta$ is close to σ_0^2 and r_c is close to r_{hb}, giving some feeling as to why this equation is equivalent to King's method of core fitting. In the same paper, King also developed an expression for the total mass of a system fitted by a King model. For different values of W_0 he calculated values for μ , where μ is the integral

$$\mu = \int_0^{R_t} \frac{\rho}{\rho_0} 4\pi R^2 \, dR. \tag{2.5}$$

Here $R = r/r_c$ and $R_t = r_t/r_c$. It therefore follows simply that

$$M_{tot} = \rho_0 \mu r_c^3 = \frac{9 r_c \mu}{4\pi G\beta}. \tag{2.6}$$

So the total mass-to-light ratio for a particular King model is given by

$$\frac{M_{tot}}{L_{tot}} = \frac{9 r_c \mu}{4\pi G\beta L_{tot}}. \tag{2.7}$$

This method (first used by Illingworth (1976) and hereafter called Illingworth's method) is more sensitive to the King model fitted to the density distribution than is the core fitting method (where the value of the η correction is 0.96 to 1.01 for W_0 from 2.5 to 11). It seems logical that this should be the case because obtaining a total mass must involve integration of the density over the whole galaxy, which must be a more model sensitive procedure than using only core parameters. For the two methods it would therefore be expected that the core fitting procedure is the more accurate. It should also be emphasised that Illingworth's method is only applicable to a King model whereas King's method of core fitting is applicable to all reasonable models.

When it comes to relating these equations to actual observations, there is another point which has to be considered. Both σ_0^2 and $1/\beta$ are values calculated through the centre of the galaxy, and as can be seen from the plot in Binney & Tremaine previously referred to, the measured line of sight velocity dispersion varies with distance from the centre of the galaxy. Now, in the case of real observations, all the stars looked at cannot be at the centre of the galaxy, particularly in such a diffuse system as Sextans, so the average distance of the stars observed was taken as the radius for the velocity dispersion measurement, σ_{obs}, the corrections at this radius can be read off the plot for the appropriate King model. Therefore $1/\beta$ can just be read off, and σ_0^2 is equal to one third of the mean square velocity at the centre for the particular value of W_0.

Putting equations 2.1 and 2.7 into units of $M_\odot/L_\odot$, with r_c in parsecs and the velocity dispersions in $km\,s^{-1}$, the factor $9(4\pi G)^{-1}$ becomes 166.5, so

$$\frac{\rho_0}{I_0} = \eta \frac{333\sigma_0^2}{r_{hb} S_0}, \tag{2.8}$$

and

$$\frac{M_{tot}}{L_{tot}} = \frac{166.5 r_c \mu}{\beta L_{tot}}. \tag{2.9}$$

Results

As already explained, it would be expected for the observed velocity dispersion to decrease with distance from the centre of the dSph galaxy. Table 2.8 shows how the velocity dispersion varies with radius for our results. Beyond 400 pc it does appear to drop off considerably, down from 8 $km\,s^{-1}$ to 3 $km\,s^{-1}$. The values

Table 2.8: How Velocity Dispersion Varies with Radius.

Radius (pc)	No. in bin	Velocity Dispersion. ($km\,s^{-1}$)
28-168	5	$6.7\pm^{1.9}_{2.7}$
194-243	5	$8.5\pm^{2.4}_{3.4}$
314-377	5	$8.2\pm^{2.3}_{3.2}$
404-612	6	$2.6\pm^{0.7}_{0.9}$

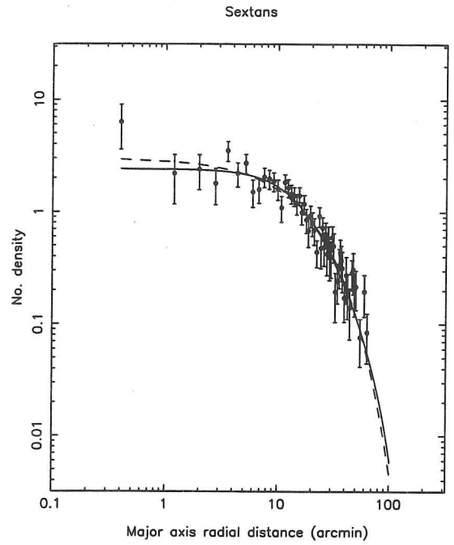

Figure 2.9: The best King model fitted to the Sextans dSph galaxy (by Irwin & Hatzidimitriou 1993 from the APM results) with a concentration of 0.98. The dashed line is the best exponential fit. One arcmin is equivalent to 24 parsecs at the distance of Sextans (83 kpc).

of 'No.' in the table give the number of stars within each range of radius. The dispersions and errors here were calculated as before, using a maximum likelihood estimator. Within the errors this drop off of velocity dispersion with radius is consistent with the range of possible King models.

Irwin & Hatzidimitriou (1993, 1995) have found the best King model fit to Sextans has a concentration, $c = 0.98$, which is equivalent to $W_0 = 4.8$. This model has the parameters $\eta = 0.98$ and $\mu = 11.4$. Figure 2.9 shows this model fitted to the photometric data. The brightness profile was obtained from the density in stars per unit area in the following way. It was assumed that surface brightness was proportional to surface density: in such a diffuse system there is unlikely to be mass segregation so this is a reasonable assumption. Therefore all that was required was the constant of proportionality. This was obtained by integrating the fitted profile of the number density distribution (in this case the King model) such that the integral was equal to the total magnitude of the dSph galaxy.

They also calculated the following parameters for the dSph galaxy:

$$r_c = 312 \pm 41 \text{ pc},$$
$$r_{hb} = 285 \pm 37 \text{ pc},$$
$$r_t = 3003 \pm 995 \text{ pc},$$
$$M_V = -9.0 \pm 0.5,$$
$$L_{tot,V} = (3.4 \pm^{2.0}_{1.3}) \times 10^5 \text{ L}_{\odot,V},$$
$$S_{0,V} = 0.5 \pm^{0.3}_{0.2} \text{ L}_{\odot,V}\text{pc}^{-2}.$$

All the distances quoted here are geometric mean distances. The average distance from the centre of the galaxy of our observations was 310.0 pc, which is very close to a core radius, leading to $\sigma_0 = \sigma_{obs}/0.93$ and $1/\beta = \sigma^2_{obs}/0.84^2$. Throughout the following calculations $\sigma_{obs} = 7.0 \pm^{1.3}_{1.0} \text{ km s}^{-1}$. Calculation of the core mass-to-light ratio using equation 2.8 gives $\rho_0/I_{0,V} = 124 \pm^{85}_{60}$. Similarly the total mass-to-light ratio calculation of equation 2.9 produces $M_{tot}/L_{tot,V} = 121 \pm^{84}_{58}$. The errors quoted here include those due to the half-brightness radius, the luminosity and the velocity dispersion, with the luminosity error contributing more than half the total error. Not only is there considerable uncertainty in the measurement of the total luminosity and central surface brightness of Sextans, but the values obtained by different people are not consistent. The problem is that on the survey plates there are only about twice the number of Sextans members as field stars so, depending on what the background luminosity is calculated to be, there is large variation in the luminosity obtained for Sextans. This is particularly true close to the centre of the galaxy where, because of the small area, there are correspondingly fewer stars, leading to larger errors. For example, Caldwell et al. (1992) have also calculated the luminosity parameters for Sextans. The results were $M_V = -10.0$, $L_{tot,V} = 8.2 \times 10^5 \text{ L}_\odot$, and $S_{0,V} = 1.5 \text{ L}_\odot\text{pc}^{-2}$. Using equations 2.8 and 2.9 as before, the mass-to-light ratios obtained are $\rho_0/I_{0,V} = 41$ and $M_{tot}/L_{tot,V} = 50$.

There is also an error not included so far caused by uncertainty in the King model fitted to the data. As an example, taking a probable lowest value for the concentration of $c = 0.8$, and Irwin & Hatzidimitriou's measurements for luminosity and core radius, all the model parameters are tweaked to produce $\rho_0/I_{0,V} = 134 \pm^{92}_{51}$, and $M_{tot}/L_{tot,V} = 103 \pm^{67}_{51}$. At this value of the concentration, the value of μ is quite variable depending on the exact concentration and the value

of β varies considerably with a small change in average radius, leading to lower reliability in Illingworth's method compared to core fitting.

So, taking all these things into consideration, treating Sextans as a simple lowered isothermal sphere produces a mass-to-light ratio of greater than 40 at the one sigma level. For the mass-to-light ratio to be 3 and taking Irwin & Hatzidimitriou's parameters for Sextans, σ_{obs} would need to be about 1 km s^{-1}. This is well outside the 99.9 % confidence level value of 4.4 km s^{-1} from the maximum likelihood calculation. Such a small dispersion would only just be detectable because the dispersion caused by our errors alone is 1.5 km s^{-1}.

The mass-to-light ratios obtained by Suntzeff et al. were $\rho_0/I_{0,V} = 30\pm^{20}_{13}$, and $M_{tot}/L_{tot,V} = 54 \pm^{44}_{24}$. Most of the discrepancy between these results and those derived from our data was due to the differences in the values of $S_{0,V}$ and M_V used. The values used by Suntzeff et al. were 1.3 $L_{\odot,V}pc^{-2}$ and -9.4 mag. respectively.

2.4.2 Other Possible Explanations of the Velocity Dispersion

Anisotropy of the Velocity Dispersion

The models used to calculate the mass-to-light ratio assumed isotropy in the velocity dispersion. That is,

$$\sigma^2_{total} = \sigma^2_{los} + \sigma^2_{\theta} + \sigma^2_{\phi} = 3\sigma^2_{los}, \tag{2.10}$$

where σ_{los} is the line of sight velocity dispersion and σ_θ, and σ_ϕ are the dispersions that would be seen along the other two perpendicular directions. So, the maximum effect that anisotropy could have on the mass-to-light ratio is a factor of three (the calculated mass-to-light ratio would be a factor of 3 bigger than the true answer) if all the dispersion were actually along the line of sight. It is impossible to measure this in any way since we can only measure the velocity dispersion in one direction, so some effect from anisotropy is always a possibility. However this alone cannot account for the huge discrepancy between the mass-to-light ratio we have calculated for Sextans and the values measured for larger and smaller stellar systems.

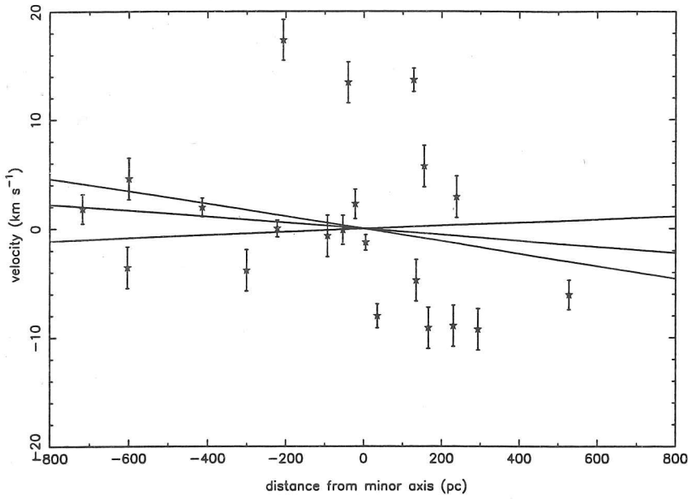

Figure 2.10: Rotation round the minor axis of Sextans. The best fit lines from the bootstrapping procedure, described in Section 3.3.2 are bounded by the errors. These are the 1 sigma errors for the slope of the fit, keeping the average velocity of the sample fixed.

Rotation of Sextans

Rotation of the dSph galaxy would artificially increase the observed velocity dispersion as long as that rotation was not in the plane of the sky. Therefore plots were made of the velocities of the stars with respect to their distance from the major and minor axes of Sextans as seen on the sky. In the centre of a galaxy such as Sextans it would be expected for the rotation curve to be linear and, as we have only observed close to the centre, linear least squares fits were made to the rotation plots. There is little sign of any rotation in either case. However, for consistency with the Ursa Minor results, the bootstrapping procedure described in Section 3.3.2 was carried out on the Sextans data. Using this method, the values derived for the rotation round the minor and major axes were $-0.3\pm^{0.4}_{0.3}$ km s^{-1} per 100 pc and $-0.8\pm^{0.7}_{0.8}$ km s^{-1} per 100 pc respectively, with other randomly chosen axes giving similar answers. The plot for the rotation around the minor axis of the galaxy is shown in Figure 2.10. The detection of rotation is hampered by all our stars being are close to the centre of the dSph galaxy making fitting of a realistic rotation curve impossible. All we can say with any degree of certainty is that the rotation is too small for us to detect, the values quoted being upper limits.

Binaries

The presence of binaries in the sample of observed stars would increase the observed velocity dispersion so that it was no longer a true indication of the mass of the galaxy. Suntzeff et al. (1993), made a calculation for Sextans using a Monte Carlo method. They obtained velocity dispersions of close to 6 $\mathrm{km\,s^{-1}}$ for a binary fraction of 0.25, assuming an intrinsic velocity dispersion of 2.1 $\mathrm{km\,s^{-1}}$, which is equivalent to a mass-to-light ratio of 2.5 according to the parameters they used. Use of Irwin & Hatzidimitriou's parameters make little difference to this result. The calculation involved several simplifications such as uniformity of mass ratios and inclinations and a flat period distribution which are not necessarily valid, but it is still useful for comparison with the observations.

We need to calculate how many binaries there were in our sample. The star that was not included in the calculations seemed to be obviously a binary but it is necessary to be more quantitative about this. There were five good quality observations of star 6. Observing such a large difference in velocity over the space of one year is an eight sigma result according to our calculated measuring errors and therefore extremely unlikely by chance. The other possible binary, star 8, was still included in the sample because of its fewer, lower quality observations. The observation of the velocities of this star is a 3 sigma result, if we have correctly estimated our velocity precision. If there were two binary stars out of the eight for which there were multi-epoch observations, there should be a fraction of 0.22 in the sample used to calculate the velocity dispersion. If only one out of those nine was a binary then the binary fraction is 0.11. However this is not the true picture because due to our observing criteria we could have detected only a fraction of the binary stars. Quantifying the possible binary fraction accurately requires continued velocity monitoring. Such efforts are important since a binary fraction of 0.1 still requires a true mass-to-light ratio of 50, whereas all extra mass above that found in globular clusters can be explained by a fraction of 0.25.

Tidal Interaction with the Galaxy

The other alternative is that the dSph galaxies are being tidally disrupted by the Milky Way Galaxy, so that the assumption of dynamical equilibrium underlying equations 2.8 and 2.9 is invalid. Structure observed in the Small Magellanic Cloud

along with the existence of the Magellanic stream are evidence that tidal disruption is currently occurring in this dwarf companion to the galaxy, and suggestive evidence for the existence of phase-space structure in the outer Galaxy, the reality of which would strongly support such a model of merging galaxies, continues to arise (Arnold & Gilmore 1992). Indeed the concept of the small galaxies close to the Milky Way undergoing tidal disruption and merger is fundamental to standard CDM cosmologies.

A completely disrupted dSph galaxy of freely expanding stars would be expected to disperse in the time it takes for the galaxy to orbit our Galaxy once or twice, so that it would be unlikely for a significant proportion of the nine known dSphs to be undergoing tidal disruption now. However it is possible that the dSph could still be visible as a collection of stars having been tidally disrupted some time ago, as shown by Kuhn (1993) who has performed N-body calculations demonstrating that, in the case of strong velocity anisotropy, the time for an unbound dSph galaxy to disperse may be an order of magnitude larger than a free expansion argument would suggest. If Sextans is a tidally disrupted dSph galaxy the velocity dispersion that we have been so diligently measuring would have nothing to do with the actual mass-to-light ratio of the galaxy.

The distance D_t that a dSph galaxy of mass M_{dSph} (in an orbit of ellipticity 0.5) would have to be from the Galaxy, mass M_G, for the force from the dSph on a star at distance r_t from the centre of the dSph to be balanced by the force from the Galaxy, assuming a Keplerian Galaxy potential is

$$D_t = r_t \left(\frac{3.5 M_G}{M_{dSph}} \right)^{1/3} . \tag{2.11}$$

This simple calculation can be made for all the dSph galaxies to gain an idea of whether they may be tidally disrupted. The distance D_t obtained is hereafter referred to as the tidal distance. Using Irwin & Hatzidimitriou's values for the luminosity and tidal radius for each dSph galaxy, a Galaxy mass of 10^{12} $\mathrm{M_\odot}$ and a supposed mass-to-light ratio of 3, all the dSph galaxies except Fornax, Leo I and Leo II could be suffering tidal interaction with the Galaxy at the moment. Sextans particularly with such a large tidal radius is well inside its tidal distance of 370 kpc at 84 kpc, and Sculptor, Draco and Ursa Minor are both more than 20 kpc inside their tidal distances.

Of course there is question here over the form of the Galactic potential. Tidal distances are slightly smaller for alternative Galaxy potentials like isothermal spheres and it is probably true that fewer of the dSphs are tidally disrupted than is suggested by this calculation. Nevertheless it is interesting to note that, with the exception of Sculptor, the dSph galaxies that are most likely to be undergoing disruption according to the preceding calculation, are those with the largest apparent mass-to-light ratios.

If the same calculation is performed taking the masses derived from the velocity dispersion as M_{dsph}, Sextans and Sculptor are inside their tidal distances with all the other galaxies being 30 kpc or more outside theirs.

Therefore there are two consistent alternatives. Either the dSph galaxies have small mass-to-light ratios implying that several of the galaxies are being tidally disrupted or that some other effect such as binaries are causing the velocity dispersion not to be a true representation of the masses, or the galaxies have higher masses and fewer of them are being tidally disrupted.

Dark Matter

Should all the ideas in the previous sections fail to account for the high mass-to-light ratios, the alternative is that dSph galaxies contain large amounts of dark matter, the brighter galaxies containing a lower proportion than the fainter ones. Each dSph galaxy would require a core dark matter density of around 0.07 $M_{\odot}pc^{-3}$. The implication is a range in total luminosity of a factor of 80 compared to a range in total mass of a factor of 7. In some senses it is simpler to view the problem as one of missing brightness rather than missing mass. This is demonstrated by Figure 2.11 which shows the absolute magnitude of globular clusters and dwarf spheroidals compared with their central velocity dispersion, central surface brightness and mass-to-light ratios respectively. The lines marked are the empirical relations for these values for elliptical galaxies and the bulges of spiral galaxies. Also marked on the magnitude verses central surface brightness diagram are some dwarf elliptical galaxies from the Virgo and Fornax clusters. The velocity dispersions of globular clusters and dSph galaxies are similar: the discrepancy comes with the low central surface brightness of the dSph galaxies and their correspondingly high mass-to-light ratios. So, the velocity dispersions of the dSph galaxies follow a similar trend to other objects in the universe. It

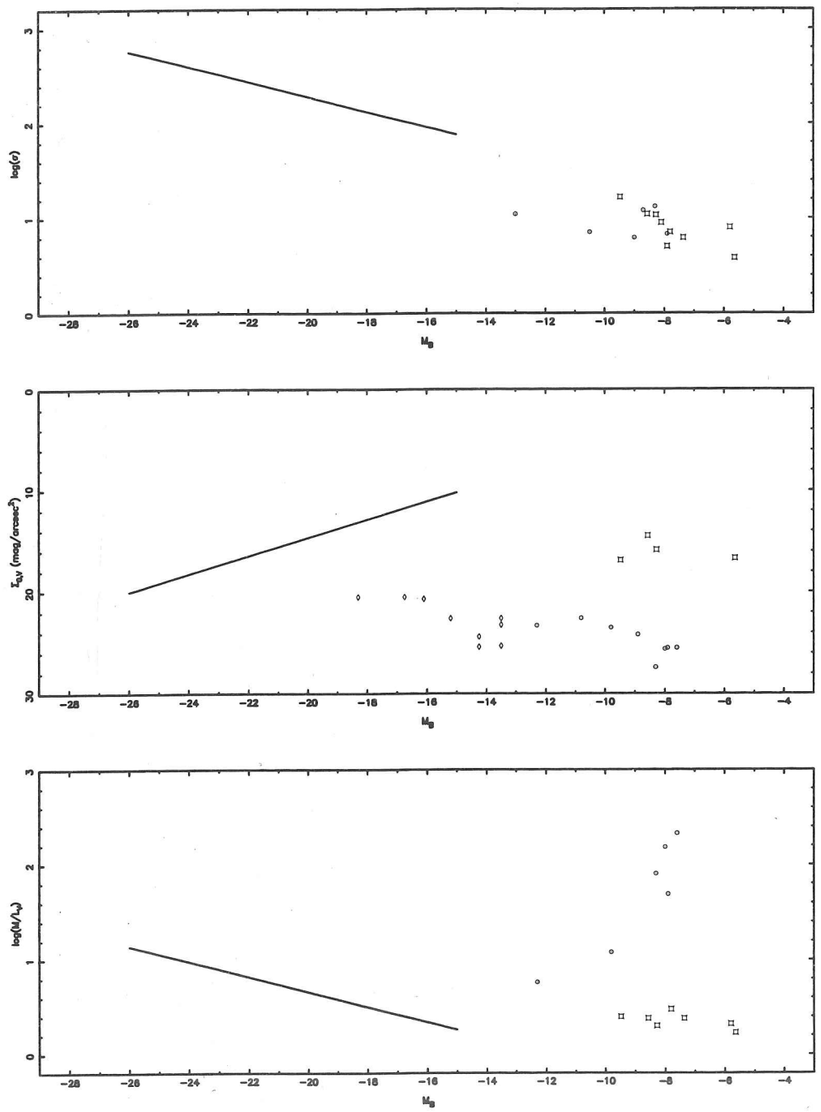

Figure 2.11: Absolute magnitude verses velocity dispersion, central surface brightness, and mass to light ratio for various systems. The straight lines show the relations for elliptical galaxies and the bulges of spirals. The squares are globular clusters, the circles, Galactic dSph galaxies, and the diamonds are dwarf galaxies in the Virgo and Fornax clusters. The velocity dispersions of dSph galaxies are similar to those of globular clusters; it is the low central surface brightness of the dSphs which results in their comparatively high mass to light ratios.

is the low surface brightness that is anomalous, resulting in equally anomalous mass-to-light ratios.

2.5 Conclusion

The internal central velocity dispersion of the Sextans dSph galaxy is $7.0 \pm^{1.3}_{1.0}$ km s^{-1} measured from twenty one giant stars. This leads to mass-to-light ratios of $124\pm^{85}_{60}$ and $121\pm^{84}_{58}$ in solar units, using core fitting and Illingworth's methods respectively. By comparison, apparently purely stellar systems such as globular clusters and the stellar Galactic disk, have mass-to-light ratios of about 3. Thus, the observed internal velocity dispersion of the Sextans dSph galaxy is several times larger than the value of about 1 km s^{-1} which is expected if the galaxy is a self gravitating stable system whose gravitational potential is dominated by the mass in visible stars.

Of the possible explanations, there are two explanations of this discrepancy which we think are more likely than the others. The first is as yet undetected binaries in the observed stellar tracers. We have found two possible binary stars in the sample of nine stars for which we have good multi epoch observations, one of these being a more positive identification than the other. Since a binary fraction of 0.25 is sufficient to explain the excess mass-to-light ratio over about 3, further observations are required to rule out this possibility. The second possibility is failure of the dynamical assumptions due to current tidal disruption. There is quite a high likelihood that Sextans is being tidally disrupted, since simple calculation shows it to be the most likely of the dSph galaxies to be in this state. It may be relevant that the three dSph galaxies which are a priori the most likely to be undergoing tidal disruption are also the three with the highest apparent mass-to-light ratios. Other possible explanations include a substantial dark matter density in this galaxy or a serious underestimate of the measuring errors. We think the latter possibility is unlikely. Other effects which may contribute include velocity anisotropy and rotation in the dSph, although they are unlikely to provide a major part of the answer.

Acknowledgements

The spectroscopy reported here was obtained with the William Herschel Telescope operated on the island of La Palma by the Royal Greenwich Observatory in the Spanish Observatorio del Roque de los Muchachos of the Instituto de Astrophysica de Canarias.

References

Arnold, R. & Gilmore, G., 1992, MNRAS, 257, 225.

Armandroff, T.E. & Da Costa, G.S., 1986, AJ, 92, 777.

Binney, J.J. & Tremaine, S., 1987, Galactic Dynamics, 236. Princeton University Press, Princeton.

Caldwell, N., Armandroff, T.E., Seitzer, P., Da Costa, G.S., 1992, AJ, 103, 840.

Da Costa, G.S., Hatzidimitriou, D., Irwin, M.J., McMahon, R.G., 1991, MNRAS, 249, 473.

Eadie, W.T., Drijard, D., Jame, F.E., Roos, M., Sadoulet, B., 1982, Statistical Methods in Experimental Physics. North-Holland Publishing Company, Amsterdam.

Godwin, P.J. & Lynden-Bell, D., 1987, MNRAS, 229, 7P.

Irwin M.J. & Hatzidimitriou D., 1993, Brodie, J., ed, in Proc. ASP Symp vol 48, 322.

Irwin M.J. & Hatzidimitriou D., 1995 (in preparation).

Illingworth, G.D., 1976, ApJ, 204, 90.

Irwin, M.J., Bunclark, P.S., Bridgeland, M.T., McMahon, R.G., 1990, MNRAS, 244, 16P.

King, I., AJ, 1962, 67, 471.

King, I., AJ, 1966, 71, 64.

Kuhn, J.R., 1993, ApJL, 409, L13.

Richstone, D.O. & Tremaine, S., 1986, AJ, 92, 72.

Suntzeff, N.B., Mateo, M., Terndrup, D.M., Olszewski, E.W., Geisler, D., Weller, W., 1993, ApJ, 418, 208.

Tonry J. & Davis, M., 1979, AJ, 84, 1511.

2.6 Appendix 1. The Armandroff and Da Costa Method

The mean velocities, equivalent to the values of $\overline{V}_{7.5}$ in Table 2.4, are written as v_i in the following equations. The error on a single observation is σ_{err}, so the variance of the average squared velocity of a star is σ_{err}^2/N_i, where N_i is the number of observations of star i used to calculate the velocity. The weight on star i is w_i, and is the inverse of this variance. The average velocity of the galaxy is then defined as

$$\overline{v} = \frac{\sum w_i v_i}{\sum w_i}, \tag{2.12}$$

and the velocity dispersion is defined by

$$\sigma_{obs}^2 = \left[\frac{\sum w_i (v_i - \overline{v})^2}{\sum w_i} - \frac{N}{\sum w_i}\right] \frac{N}{N-1}. \tag{2.13}$$

Here the first term in the brackets is simply the the square of the observed velocity dispersion while the second term is the contribution to this dispersion from the measuring errors, which must be subtracted to produce σ_{obs}, the intrinsic velocity dispersion.

The error on the square of the velocity dispersion is quoted as $\epsilon = \sqrt{\epsilon_1^2 + \epsilon_2^2}$ where $\epsilon_1 = \sigma^2\sqrt{2/N}$. and $\epsilon_2 = (2/N)\sqrt{\sum_{i=1}^{N} \varepsilon_i^2 \epsilon^2(\varepsilon_i)}$. Here ε_i is the error in velocity i and $\epsilon(\varepsilon_i)$ is the uncertainty in this error. The values of ϵ_2 were all very small, $\epsilon(\varepsilon_i)$ being of the order of 0.5 $\mathrm{km\,s^{-1}}$.

To illustrate the over weighting this method gives, take the following extreme example. Suppose the true velocity dispersion in a system is 10 $\mathrm{km\,s^{-1}}$ and the measuring errors 1 $\mathrm{km\,s^{-1}}$. Further suppose we have only observed two stars, the first ten times, the second once. If these two stars are a fair sample then their unweighted dispersion about the mean will be 10.0 $\mathrm{km\,s^{-1}}$. To one decimal place this will also be the maximum likelihood estimate of the dispersion. The Armandroff & Da Costa method, however would estimate a dispersion of 6.0 $\mathrm{km\,s^{-1}}$ mainly due to the mean velocity estimate being severely biassed toward the star with most measurements. The simple weighting of the velocity dispersion summation then compounds the problem.

2.7 Appendix 2. The Maximum Likelihood Method

Consider a series of velocity measurements v_i, $i = 1, 2 \cdots N$ with associated errors σ_i, $i = 1, 2 \cdots N$. We wish to estimate the systemic velocity, $\overline{v}$, and the velocity dispersion, σ_{obs}, of the system. Assume that both the measuring errors, σ_i, and the intrinsic system velocities are Gaussian distributed (it is straight forward to generalise to other intrinsic forms). Then the probability of observing velocity v_i is given by

$$P(v_i) = \frac{1}{\sqrt{2\pi(\sigma_i^2 + \sigma_{obs}^2)}} \exp\left(\frac{-(v_i - \overline{v})^2}{2(\sigma_i^2 + \sigma_{obs}^2)}\right), \tag{2.14}$$

and the likelihood of observing the series of observations $\{v_i, i = 1, N\}$ is given by

$$L(v_1, v_2, \cdots v_N) = \prod_i P(v_i). \tag{2.15}$$

Using the log likelihood function for convenience we see that

$$\ln\left(L(\overline{v}, \sigma_{obs}^2)\right) = \sum_i -\frac{(v_i - \overline{v})^2}{2(\sigma_i^2 + \sigma_{obs}^2)} - \frac{1}{2}\sum_i \ln(\sigma_i^2 + \sigma_{obs}^2) + constant. \tag{2.16}$$

$\ln(L)$ is a function of $\overline{v}$ and σ_{obs}^2 only, and is to be maximised with respect to these variables. Numerically this is easily accomplished by constructing a two dimensional grid of suitably fine mesh and simply 'contouring' the resulting array. By making use of the Central Limit Theorem we can argue that the error ellipses for $\overline{v}$ and σ_{obs}^2 are then simply given by steps down in $\ln(L)$ from the peak where (peak$-1/2$) corresponds to the one sigma error or 68 % confidence limit, (peak$-4 \times 1/2$) to the two sigma error or 95 % confidence limit, and so on).

To proceed analytically we differentiate equation 2.16 with respect to $\overline{v}$ and σ_{obs}^2 to yield

$$\frac{\partial \ln(L)}{\partial \overline{v}} = \sum_i \left(\frac{v_i - \overline{v}}{\sigma_i^2 + \sigma_{obs}^2}\right) = 0, \tag{2.17}$$

and

$$\frac{\partial \ln(L)}{\partial \sigma_{obs}^2} = \sum_i \left[\frac{(v_i - \overline{v})^2}{2(\sigma_i^2 + \sigma_{obs}^2)^2} - \frac{1}{2(\sigma_i^2 + \sigma_{obs}^2)}\right] = 0. \tag{2.18}$$

Re-arranging 2.17 and 2.18 yields an iterative scheme (cf. Gauss-Seidel) for finding the unknowns. This gives

$$\widehat{\overline{v}} = \frac{\sum_i w_i v_i}{\sum_i w_i}, \tag{2.19}$$

and

$$\widehat{\sigma}_{obs}^2 = \frac{\sum\left[(v_i - \overline{v})^2 - \sigma_i^2\right] w_i^2}{\sum_i w_i^2}, \tag{2.20}$$

where $w_i = 1/(\sigma_i^2 + \sigma_{obs}^2)$ is updated each cycle. If $\sigma_{obs}^2 \gg \sigma_i^2$ then

$$\widehat{\overline{v}} = \frac{1}{N}\sum_i v_i, \tag{2.21}$$

and

$$\widehat{\sigma}_{obs}^2 = \frac{1}{N}\sum_i \left[(v_i - \overline{v})^2 - \sigma_i^2\right]. \tag{2.22}$$

Since $\overline{v}$ is also estimated simultaneously, a factor $N/(N-1)$ is required for equation 2.20 (and equation 2.22) to make σ_{obs}^2 an unbiased estimator. Note that both the functionality of the 'weighting' factor and its form differ from that used by Armandroff & Da Costa (1986).

To estimate the analytic errors for $\overline{v}$ and σ_{obs}^2 we first construct the Information matrix (eg Eadie et al. 1982),

$$I = \begin{bmatrix} \frac{\partial^2 \ln(L)}{\partial \overline{v}^2} & \frac{\partial^2 \ln(L)}{\partial(\sigma_v^2)\overline{v}} \\ \\ \frac{\partial^2 \ln(L)}{\partial(\sigma_v^2)\overline{v}} & \frac{\partial^2 \ln(L)}{\partial(\sigma_v^2)^2} \end{bmatrix}. \tag{2.23}$$

The parameter covariance matrix is then given by I^{-1}. The off-diagonal term is given by

$$\frac{\partial^2 \ln(L)}{\partial(\sigma_v^2)\overline{v}} = \sum_i -\frac{(v_i - \overline{v})}{(\sigma_i^2 + \sigma_{obs}^2)^2} \approx 0, \tag{2.24}$$

which is small relative to the diagonal terms (cf equation 2.17) since

$$\frac{\partial^2 \ln(L)}{\partial \overline{v}^2} = \sum_i -\frac{1}{\sigma_i^2 + \sigma_{obs}^2}, \tag{2.25}$$

and

$$\frac{\partial^2 \ln(L)}{\partial (\sigma_v^2)^2} = \sum_i \left[-\frac{(v_i - \overline{v})^2}{(\sigma_i^2 + \sigma_{obs}^2)^3} + \frac{1}{2(\sigma_i^2 + \sigma_{obs}^2)^2} \right]. \tag{2.26}$$

Therefore to a good approximation

$$var\{\overline{v}\} = \left[\sum_i \frac{1}{\sigma_i^2 + \sigma_{obs}^2} \right]^{-1} \approx \frac{\sigma^2}{N}, \tag{2.27}$$

and

$$var\left\{\sigma_{obs}^2\right\} = \left\{ \sum_i \left[\frac{(v_i - \overline{v})^2}{(\sigma_i^2 + \sigma_{obs}^2)^3} - \frac{1}{2(\sigma_i^2 + \sigma_{obs}^2)^2} \right] \right\}^{-1} \approx \frac{2\sigma^4}{N}, \tag{2.28}$$

where $\sigma^2 = < \sigma_i^2 > + \sigma_{obs}^2$.

Chapter 3

The Ursa Minor Dwarf Spheroidal Galaxy

Abstract

We have observed forty six giant stars in the Ursa Minor dwarf spheroidal galaxy and obtained high quality spectra for thirty five of these. The velocity dispersion of the sample calculated by the maximum likelihood method was $7.5\pm^{1.0}_{0.9}$ km s^{-1} and the mean velocity was -249.2 ± 1.5 km s^{-1}. There was evidence for rotation around the major axis: a straight line fit, equivalent to solid body rotation, gives a gradient of $-4.7\pm^{2.0}_{2.2}$ km s^{-1} per 100 pc from the axis where the positive distances are to the north west of the major axis. This discovery adds evidence to the suggestion that Ursa Minor may be being tidally disrupted. If further work eliminates this possibility then, assuming dynamical equilibrium, isotropy in the velocity dispersion (which was $6.7\pm^{0.9}_{0.8}$ km s^{-1} once rotation had been subtracted) and a negligible contribution from binary stars, the core mass-to-light ratio is $59 \pm^{41}_{25}$ $M_\odot/L_{\odot,V}$ and the total mass-to-light ratio is $40 \pm^{29}_{17}$ $M_\odot/L_{\odot,V}$, implying the presence of large quantities of dark matter.

3.1 Introduction

This paper presents the results from the most accurate velocity measurements yet available for stars in the Ursa Minor dSph galaxy. These are used to calculate a velocity dispersion, look for rotation around the axes, and find the mean velocity for Ursa Minor.

Ursa Minor is the closest of the eight dSph galaxies known to be in orbit around the Milky Way. It is also distinguished by the detection of structure (Olszewski & Aaronson 1985): the luminosity contours show two clumps of stars along the major axis separated by 16 arc minutes (Irwin & Hatzidimitriou 1993. 1995). It is the most elongated of the dSph galaxies, with the major axis aligned along the polar ring, in the plane of the Magellanic Stream. In general these galaxies contain a mixture of old and intermediate population stars and show no evidence for gas or recent star formation. In Ursa Minor the population is dominated by old (15 Gyr) metal poor stars (Olszewski & Aaronson 1985): this is illustrated by a strong blue horizontal branch in the colour-magnitude diagram (CMD). The dSph galaxies have similar total luminosity to most globular clusters ($10^5 - 10^7$ $L_\odot$) but their core radii are around an order of magnitude larger for the same luminosity.

Study of the kinematics of stars in both globular clusters and dSph galaxies by application of various simple models has been used to produce measurements for the mass-to-light ratios of these systems. The answers for globular clusters are around 2 or 3 $M_\odot/L_\odot$, whereas those for the different dSph galaxies vary between 6 and 250 (Irwin & Hatzidimitriou 1995), and at face value imply that all the dSph galaxies are of similar mass but contain different proportions of luminous matter.

Finding the smallest scale on which large quantities of dark matter exist is important because it places constraints on what form that dark matter might take; for example, cold (or dissipative) dark matter can cluster on arbitrarily short scales while relativistic matter (eg. neutrinos) cannot. Therefore, since dSph galaxies are the next largest scale objects after globular clusters they are also the next largest scale on which to look for dark matter. However a mass-to-light ratio of 250 for a dSph galaxy does seem inconsistent with the general trend of mass-to-light ratio compared to size in the rest of the universe; for example, the value for the Milky Way Galaxy is only about 30, measured out to 80 kpc, and that for the Local Group is closer to 100 (Gilmore, 1990). This and the wide range of measurements for the mass-to-light ratios of the different dSph galaxies leads to a question over whether the stellar kinematics are quite such simple indicators of the mass of these galaxies as is assumed by the simple models employed to date.

One possible complicating factor would be the presence of rotation, and quantifying rotation about either axis is important for several reasons: the axis about which the dSph rotates can gives clues about possible triaxiallity and anisotropy in the velocity dispersion, and is a test for dissipation; rotation may also be related to possible tidal disruption by the Galaxy; and it is important to obtain both the rotation, the rotation curve and the velocity dispersion profile for a complete mass determination of the system. In assessing possible rotation it is important to allow for the effects of finite size which coupled with a high transverse motion can mimic rotation.

The results from observations taken during the same observing runs as those discussed here but for the Sextans dSph galaxy have been presented in an earlier paper (Chapter 2 of this thesis). Since the reduction and analysis of the data was conducted in an identical manner for both sets of data, the discussion of the fine points of the procedures employed is not repeated here.

The rest of this paper is divided into several sections. First, the observations and the reduction procedure are described. Next, the errors on the observations are discussed. Then the velocity dispersion calculation is described, the search for rotation explained and a value for the mass-to-light ratio obtained. Finally, other possible contributions to the velocity dispersion are discussed.

3.2 Observations, Data Reduction and Error Analysis

3.2.1 Observations

The observations were made on the nights of 4th–7th May 1991, 7th–9th and 26th–27th April 1992. All the observations were made using the William Herschel Telescope (WHT) on La Palma.

The spectral range observed was 8300–8750 Å, which is the region containing the prominent calcium II triplet absorption lines. We used the red arm of ISIS, the R1200R grating, a slit width of one arc second with the slit aligned with the parallactic angle and an EEV 1280x1180 CCD as detector. The CCD was windowed to 400 pixels, which is about 2 arcmin, in the spatial direction. The resulting dispersion was about 0.35 Å per pixel, and the resolution measured from sky and arc lines was twice this. Arc lamp frames were taken before and after each stellar exposure using a CuNe lamp for the May 1991 run and CuAr and CuNe lamps for the others.

The stars observed were giant branch stars ranging in brightness from 15 to 18 magnitudes in the R band. Sixty Ursa Minor candidates were observed of which forty five turned out to be members. Thirteen of the Ursa Minor targets were kindly provided by Ed Olszewski (private communication). The proper motion membership probabilities of Cudworth, Olszewski & Schommer (1986) together with proximity to the giant branch locus of our photographic CMD were used to select 'inner' candidates, whilst the photographic CMD on its own was sufficient to elect the 'outer' candidates. Good spectra were obtained for thirty five members, with repeat observations for twenty one of these, and nine had good spectra at two epochs. Out of these nine there was no firm evidence that any were binary

stars. This topic is discussed further in Section 3.4.3. Stars from the Sextans dSph galaxy were also observed during these runs as well as during one other in December 1991. The results of these observations have already been reported in the earlier paper (Chapter 2). The data for the stars observed in Ursa Minor and Sextans were considered together for definition of the internal and external errors, since the two data sets are of uniform precision.

Additionally four bright radial velocity standard stars (RV stars) were observed with integration times of only 5 seconds, one or two on each night of each run. These spectra provided an estimate of the random and systematic errors for high signal-to-noise, short exposure spectra. The random part of this error gave an estimate of the minimum random error for the dSph galaxy data, though it appears that the RV stars may have greater systematic error due to slit centering problems. The details of this are discussed in Section 2.2.3. The RV stars were also used as a check on the data reduction procedure because their actual velocities were already known, and as a base to obtain the absolute mean velocity of Ursa Minor.

The coordinates of all the Ursa Minor member stars observed are shown in Table 3.1, and Table 3.2 contains a list of the coordinates of the observed non members.

3.2.2 Data Reduction

The processing of the CCD frames, data reduction and analysis was carried out in a very similar way to the Sextans data already published. A brief summary will suffice.

Preliminary processing of the CCD frames to remove bias and cosmic ray events was done, mostly at the telescope, using FIGARO routines. IRAF was then used to wavelength calibrate, sky subtract, and cross correlate the data against the same template used for the Sextans data. The same line selection was used to throw out very poor lines from the spectra. The cross correlation programme FXCOR produces a Tonry and Davis R value (Tonry & Davis 1979) for each correlation, and it was this parameter that was used to produce a cutoff value below which the results were considered too inaccurate and therefore discarded. In the case of star UMJI12 it was possible to combine the two spectra with quality below the cutoff to produce one spectrum with quality above the cutoff.

Table 3.1: Coordinates of the Ursa Minor stars. The centre of the Ursa Minor dSph galaxy is at $15^h\ 8.4^m$, $67^\circ\ 25'$.

Star	RA 1950	DEC 1950	Star	RA 1950	DEC 1950
CUD1	15 08 52.6	67 28 25	EDO199	15 09 22.8	67 27 38
CUD9	15 08 53.3	67 24 18	EDO233	15 07 33.5	67 28 49
CUD34	15 10 02.4	67 24 55	EDO345	15 07 57.3	67 21 56
CUD37	15 10 07.8	67 24 08	EDON24	15 06 05.3	67 20 42
CUD87	15 09 41.9	67 27 11	EDON32	15 10 51.9	67 27 29
CUD96	15 08 38.8	67 29 05	EDON33	15 10 53.0	67 25 55
CUD107	15 09 03.8	67 28 58	EDON37	15 10 30.0	67 24 29
CUD122	15 09 56.3	67 30 23	EDON40	15 08 59.0	67 15 39
CUD132	15 08 52.7	67 31 32	EDON42	15 07 58.0	67 15 04
CUD189	15 08 05.6	67 24 35	EDOE	15 08 52.7	67 20 48
CUD267	15 08 30.3	67 28 28	EDOH	15 08 15.4	67 24 09
CUD234	15 07 33.9	67 28 31	UMJI1	15 10 03.1	67 38 55
CUD267	15 08 30.3	67 28 28	UMJI2	15 09 52.3	67 35 53
CUD297	15 07 49.9	67 21 30	UMJI5	15 10 45.0	67 33 49
CUD311	15 07 38.4	67 23 15	UMJI7	15 11 04.2	67 31 28
CUD366	15 08 13.3	67 21 32	UMJI8	15 11 13.7	67 30 50
CUD390	15 07 27.9	67 19 58	UMJI12	15 11 01.5	67 29 21
CUD397	15 08 04.2	67 20 07	UMJI13	15 10 10.7	67 27 57
CUD429	15 07 46.8	67 17 07	UMJI15	15 10 50.1	67 25 03
CUD459	15 09 15.3	67 23 36	UMJI18	15 09 18.0	67 23 22
CUD486	15 09 33.8	67 21 55	UMJI19	15 09 35.2	67 19 47
EDO26	15 09 32.9	67 24 09	UMJI20	15 07 17.5	67 18 43
EDO171	15 07 28.0	67 25 25	UMJI23	15 05 42.2	67 15 34

Notes. The stars labelled CUD are those listed by Cudworth, Olszewski & Schommer (1986) as high probability members from their derived proper motions, while the EDO stars are those found by Olszewski (1991) and the UMJI stars are new members found purely using their spatial location and proximity to the giant branch locus on a photographic CMD.

Table 3.2: Coordinates of the non-members found

Star	RA 1950	DEC 1950
CUD442	15 07 55.0	67 15 53
CUD508	15 09 39.6	67 17 11
UMJI3	15 07 15.6	67 34 10
UMJI4	15 09 46.8	67 43 39
UMJI6	15 10 24.1	67 32 17
UMJI9	15 09 10.1	67 30 36
UMJI11	15 06 26.1	67 29 14
UMJI14	15 09 00.5	67 26 54
UMJI16	15 06 42.9	67 24 27
UMJI17	15 06 48.3	67 24 21
UMJI21	15 06 23.0	67 18 24
UMJI22	15 08 56.8	67 16 57
UMJI25	15 09 04.8	67 13 56
UMJI26	15 09 20.0	67 13 43
UMJI27	15 06 22.3	67 13 18

Notes. The stars labelled UMJI are those stars we observed for the first time that turned out not to be members. The two CUD stars were those identified as high probability members from their proper motions by Cudworth, Olszewski & Schommer (1986). CUD442 has the colours and kinematics of a halo K-giant.

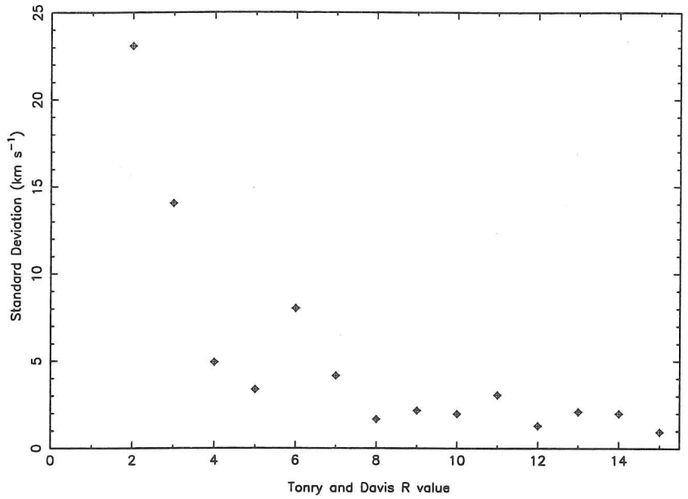

Figure 3.1: The standard deviations for the Sextans repeats, shown in Table 2.4, along with the equivalent data for the Ursa Minor repeats, compared with the Tonry and Davis R value; the steep increase in the standard deviation with decreasing R at low R is as expected for an accuracy verses R diagram. The deduced cutoff value for R is between 7 and 8.

3.2.3 Errors in the Velocities

The errors on the Ursa Minor data were calculated in the same way as for the Sextans data using the differences in the velocities obtained for repeat measurements. The cutoff value for R (R_{cut}) was found by comparing these differences in velocity with the R values of the measurements. There are considerably fewer repeat measurements per star for the Ursa Minor observations compared with those in Sextans, so the error information for the two data sets was combined, and the result is the appropriate measuring error for Ursa Minor. The repeat measurements for the possible binary, star 8, in the Sextans data (see Chapter 2) were removed from this data set.

The mean for each star was calculated, sigma clipping the most extreme velocities. This is $\overline{V}_{ex}$ in Table 3.3 and the velocities which were clipped out of the average are marked by an asterisk. The difference of each measurement from this mean value is ΔV_{ex} in the same table. Figure 3.1 is the σ_{ex} versus R diagram for the combined data set where σ_{ex} is the standard deviation of the values of ΔV_{ex} at each value of R. Figure 3.1 shows clearly how the value of σ_{ex} rises with decreasing

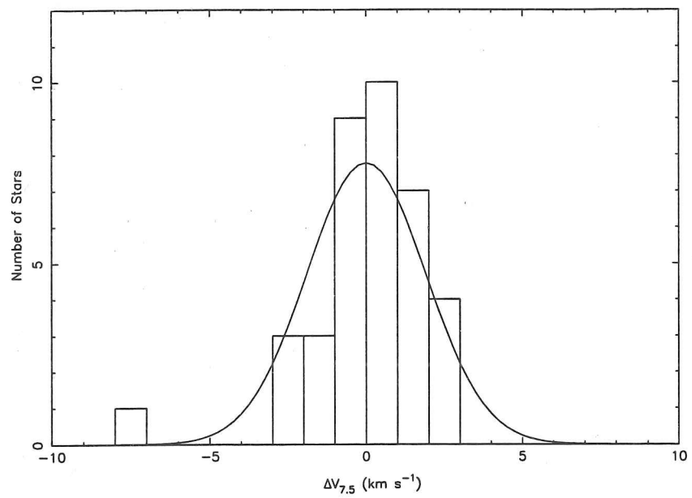

Figure 3.2: The Gaussian fit to the error distribution of the Sextans and Ursa Minor repeats for R_{cut} of 7.5 with width 2.0 km s^{-1}. The K-S test of this fit produced a probability of 0.6.

R value, a suitable cutoff value being somewhere between 7 and 8.

For a variety of values of R_{cut} an error distribution was created from the differences of the velocities obtained from individual observations for a star compared with the real mean velocity of that star. The Gaussian one sigma width of this distribution was the appropriate error on an individual observation.

The widths of the error distributions for R_{cut} of 0, 7, 7.5 and 8 were 5.5 ± 0.3, 2.3 ± 0.2, $2.0 \pm^{0.1}_{0.2}$ and 2.0 ± 0.2 km s^{-1} respectively. If the width of the distribution is denoted by σ_{err} then the error quoted here is such that the variance on σ^2_{err} is $2\sigma^4_{err}/N$. Komolgorov-Smirnov tests to compare the actual error distributions with Gaussians gave probabilities which implied consistency, except for the case for R_{cut} of 0 where the probability was 0.003. The failure of the K-S test was expected for this case because the wide range of R values for the velocities made a single value for the measuring error inappropriate. Table 3.4 contains all the error results for the different cutoff values.

The cutoff value used for the rest of the analysis was 7.5 since this was the value at which the error first dropped to a low value whilst still retaining a large number of the stars. Figure 3.2 shows the error distribution, for the Ursa Minor and Sextans data, and fitted Gaussian for R_{cut} of 7.5.

Table 3.3: The Velocities and Tonry and Davis R values for the Ursa Minor Observations. (The columns are explained in the table footnotes and the text.)

Star	Date	R	V_t km s^{-1}	$\overline{V}_{ex}$ km s^{-1}	ΔV_{ex} km s^{-1}	$\overline{V}_{7.5}$ km s^{-1}	$\Delta V_{7.5}$ km s^{-1}
CUD1	M91	9.78	0.6	4.1	-3.6	4.1	-3.6
	A92-1	11.50	7.4		3.3		3.3
	A92-1	12.14	4.4		0.3		0.3
CUD9	M91	4.35	2.6	2.6	—	—	—
CUD34	M91	9.33	3.8	3.8	—	3.8	—
CUD37	M91	4.61	4.5	0.9	3.5	—	—
	M91	9.24	-2.6		-3.5	-2.6	—
CUD87	M91	17.79	-5.0	-5.0	—	-5.0	—
CUD96	M91	11.46	-4.4	*	-4.6	-1.4	-3.1
	M91	9.26	-0.5	0.2	-0.7		0.8
	A92-1	8.13	0.9		0.7		2.2
CUD107	M91	11.48	-4.5	-4.5	—	-4.5	—
CUD122	A92-1	8.74	0.6	0.6	—	0.6	—
CUD132	M91	7.68	-2.8	-2.8	—	-2.8	—
CUD189	M91	10.83	-0.6	-0.6	—	-0.6	—
CUD234	M91	5.19	-9.8	-9.8	—	—	—
CUD267	M91	6.66	-0.9	-0.9	—	—	—
CUD297	M91	15.56	11.6	9.2	2.4	9.2	—
	A92-2	14.19	6.8		-2.4	—	—
CUD311	M91	5.00	-11.6	-11.6	—	—	—
CUD366	M91	6.62	-4.1	-8.3	4.2	—	—
	M91	8.23	-12.4		-4.2	-12.4	—
CUD390	M91	4.56	-35.4	-35.4	—	—	—
CUD397	M91	5.98	17.5	17.5	—	—	—
CUD429	A92-1	3.21	16.8	16.8	—	—	—

Table 3.3 continued...

Star	Date	R	V_t km s^{-1}	$\overline{V}_{ex}$ km s^{-1}	ΔV_{ex} km s^{-1}	$\overline{V}_{7.5}$ km s^{-1}	$\Delta V_{7.5}$ km s^{-1}
CUD442	M91	6.67	87.3	(81.7)	5.7	—	—
	A92-1	5.43	76.0		-5.7	—	—
CUD459	M91	7.44	-7.8	-7.8	—	—	—
CUD486	M91	6.11	2.8	2.8	—	—	—
	A92-1	3.95	—	—	—	—	—
EDO26	M91	18.04	10.9	*	-2.5	12.5	-1.6
	A92-1	11.78	13.7	13.3	0.4		1.2
	A92-2	12.67	12.9		-0.4		0.4
EDO171	M91	13.88	-13.1		0.7	-13.8	0.7
	A92-1	10.89	-14.6	-13.8	-0.7		-0.7
	A92-2	6.70	-7.8	*	6.0	—	—
EDO199	M91	16.47	-3.1		0.1	-2.7	-0.5
	A92-1	13.57	-3.4	-3.3	-0.1		-0.7
	A92-2	12.82	-1.5	*	1.8		1.2
EDO233	M91	12.52	-17.0	-17.0	-0.1	-17.9	0.8
	A92-1	13.17	-19.7	*	-2.7		-1.8
	A92-2	30.24	-16.9		0.1		1.0
EDO345	M91	15.44	-3.2	-3.4	0.2	-3.4	0.2
	M91	10.48	-3.6		-0.2		-0.2
EDON24	M91	19.83	-6.6	-6.6	—	-6.6	—
EDON32	M91	7.42	-4.4	-4.4	—	—	—
EDON33	M91	9.80	1.7	-1.5	3.2	-1.5	3.2
	A92-2	14.02	-4.7		-3.2		-3.2
EDON37	M91	13.30	2.2	3.0	-0.8	3.0	-0.8
	M91	9.79	3.8		0.8		0.8

Table 3.3 continued...

Star	Date	R	V_t km s^{-1}	$\overline{V}_{ex}$ km s^{-1}	ΔV_{ex} km s^{-1}	$\overline{V}_{7.5}$ km s^{-1}	$\Delta V_{7.5}$ km s^{-1}
EDON40	M91	9.13	25.0		5.7		6.9
	M91	4.08	24.0		-4.7	—	—
	M91	8.30	14.2	19.3	-5.2	18.2	-4.0
	A92-1	6.80	14.3		-5.0		-3.9
	A92-2	9.43	19.1		-0.2		1.0
EDON42	M91	6.91	7.9	6.6	1.3	—	—
	M91	11.11	5.4		-1.3	5.4	—
EDONE	M91	7.68	-12.9	-12.9	—	-12.9	—
EDONH	M91	14.39	3.3	3.4	—	3.3	—
UMJI1	A92-1	12.39	-1.0		0.2	-3.0	2.1
	A92-1	8.88	-7.3	*	-4.3		-4.3
	A92-2	14.62	-1.4	-1.2	-0.2		1.6
	A92-2	7.67	-2.5	*	-1.3		0.6
UMJI2	A92-1	12.39	-13.9	-12.8	-1.1	-12.8	-1.1
	A92-2	21.53	-11.7		1.1		1.1
UMJI5	A92-1	14.70	10.0	8.1	1.9	8.1	1.9
	A92-2	9.24	6.1		-1.9		-1.9
UMJI7	A92-1	7.60	-2.7	-2.8	0.1	-2.8	0.1
	A92-2	9.90	-2.9		-0.1		-0.1
UMJI8	A92-1	10.06	1.9	0.5	1.4	0.5	1.4
	A92-2	13.98	-1.0		-1.4		-1.4
UMJI12	A92-1	6.47	5.0	-0.2	5.2	—	—
	A92-2	6.10	-5.4		-5.2	—	—
	comb	8.40	0.8	—	—	0.8	—
UMJI13	A92-1	9.94	-7.9	-6.1	-1.8	-6.1	-1.8
	A92-2	10.74	-4.3		1.8		1.8

Table 3.3 continued...

Star	Date	R	V_t km s^{-1}	$\overline{V}_{ex}$ km s^{-1}	ΔV_{ex} km s^{-1}	$\overline{V}_{7.5}$ km s^{-1}	$\Delta V_{7.5}$ km s^{-1}
UMJI15	A92-1	10.90	-6.6	-6.3	-0.4	-6.3	-0.4
	A92-2	8.39	-5.9		0.4		0.4
UMJI18	A92-1	8.26	-4.4	-4.1	-0.3	-4.1	-0.3
	A92-2	10.44	-3.8		0.3		0.3
UMJI19	A92-1	10.27	0.2	0.4	-0.2	0.4	-0.2
	A92-2	9.34	0.6		0.2		0.2
UMJI20	A92-1	5.24	9.3	7.6	1.8	—	—
	A92-2	12.18	5.8		-1.8	5.8	—
UMJI23	A92-1	9.50	-10.8	-8.6	-2.3	-8.6	-2.9
	A92-2	10.79	-6.3		2.3		2.9

Notes. Date: M91, A92-1 and A92-2 are abbreviations for the May 1991 and April 1992 runs, A92-1 being the run at the start of April and A92-2 the one at the end.

V_t: This is the heliocentrically corrected velocity with respect to the template.

R is the Tonry & Davis R value.

$\overline{V}_{ex}$: This is the average for each star of all the values of V_t excluding those that caused a change in the mean of more than 2.5 standard deviations. The excluded stars are marked by an asterisk.

CUD442 is not a member of Ursa Minor: it is probably a halo star, but since we happen to have two observations of it, its errors were included in the analysis.

$\overline{V}_7$: This is the average velocity for a star where data which produced a correlation with $R < 7$ are not included, and $\Delta V_7 = (V_t - \overline{V}_7)$.

For UMJI12 the combination of the two spectra produced a spectrum with an R value above the threshold. The combined spectrum is marked by 'comb'.

The observations not included at the cutoff are marked by a dash.

Table 3.4: Widths of the error distributions and the velocity dispersions calculated for different value of R_{cut}.

Distribution	$\overline{v}$	σ	Error	Prob	N
	km s^{-1}	km s^{-1}	km s^{-1}		
Ursa Minor and Sextans error calculation					
all R	0.1	5.5	$\pm^{0.3}_{0.3}$	0.003	138
$R \geq 7$	−0.01	2.3	$\pm^{0.2}_{0.2}$	0.48	92
$R \geq 7.5$	3x10^{-4}	2.0	$\pm^{0.1}_{0.2}$	0.60	87
$R \geq 8$	2x10^{-4}	2.0	$\pm^{0.2}_{0.2}$	0.71	84
Ursa Minor velocity dispersion					
Unweighted calculation					
all R	-1.6	9.6	$\pm^{1.0}_{1.1}$	0.79	45
$R \geq 7$	-1.8	7.6	$\pm^{0.8}_{0.9}$	0.90	37
$R \geq 7.5$	-1.6	7.7	$\pm^{0.9}_{1.0}$	0.92	35
$R \geq 8$	-1.2	7.7	$\pm^{0.9}_{1.0}$	0.93	33
Unweighted calculation (measuring errors included)					
all R	-1.6	8.7	$\pm^{0.9}_{1.0}$	0.96	45
$R \geq 7$	-1.8	7.4	$\pm^{0.8}_{0.9}$	0.92	37
$R \geq 7.5$	-1.6	7.6	$\pm^{0.9}_{1.0}$	0.93	35
$R \geq 8$	-1.2	7.5	$\pm^{0.9}_{1.0}$	0.94	33
Maximum likelihood calculation					
all R	-1.5	8.3	$\pm^{1.2}_{1.0}$	0.97	45
$R \geq 7$	-1.8	7.3	$\pm^{1.0}_{0.8}$	0.91	37
$R \geq 7.5$	-1.5	7.5	$\pm^{1.1}_{0.9}$	0.94	35
$R \geq 8$	-1.2	7.5	$\pm^{1.0}_{0.9}$	0.94	33
Maximum likelihood calculation for velocities minus rotation					
R ≥ 7.5	-0.7	6.7	$\pm^{0.9}_{0.8}$	0.91	35

Notes. The value $\overline{v}$ is the average value calculated by the fit to the distribution.
The value of σ is the width of the distribution; so, in the case of the error distribution, it is the value of the error and in the case of the velocity dispersion calculation it is the velocity dispersion.
Error is the error in the value of σ calculated as described in the text.
N is the number of stars in the distribution.
The value 'Prob' is the probability obtained by a K-S test comparing a Gaussian distribution with the calculated width and average to the actual distribution of data.
The differences between the different calculations (weighted and unweighted) are described in Section 3.3.1.

3.3 Results

3.3.1 The Velocity Dispersion Calculation

The observations which had produced R values above the threshold were used to calculate a mean velocity for each star. The width of the distribution of these velocities defined the velocity dispersion (σ_{obs}) of Ursa Minor. An unweighted Gaussian fit to the data was made to compare with the error weighted fit. The results reported in the text are those for an R_{cut} of 7.5. Table 3.4 contains the details of all the results for differing values of R_{cut}.

The velocity dispersion obtained by fitting a Gaussian to the unweighted distribution was $7.7\pm^{0.9}_{1.0}$ km s^{-1}. The variance of σ^2_{obs} is $2\sigma^4_{obs}/N$, so this is the error quoted. This dispersion has not had the contribution due to measuring errors removed. The inclusion of this, as in equation 2.22, gave a corrected velocity dispersion of $7.6\pm^{0.9}_{1.0}$ km s^{-1}.

A better way to calculate the results is to weight each velocity by its error in some way. In the Appendices of Chapter 2 we compared the method commonly used (Armandroff & Da Costa 1986) with the use of a maximum likelihood estimator and concluded that the maximum likelihood estimator was the more appropriate for this situation. The resulting definitions for the mean velocity and velocity dispersion are

$$\widehat{\overline{v}} = \frac{\sum_i w_i v_i}{\sum_i w_i}, \tag{3.1}$$

and

$$\widehat{\sigma}^2_{obs} = \frac{\sum [(v_i - \overline{v})^2 - \sigma_i^2]\, w_i^2}{\sum_i w_i^2}, \tag{3.2}$$

where v_i is the velocity of each star and σ_i is the error on each star. The equations were solved by an iterative procedure whereby $w_i = 1/(\sigma_i^2 + \sigma^2_{obs})$ was updated on each iteration.

Using the maximum likelihood method, the velocity dispersion for an R_{cut} value of 7.5 was $7.5\pm^{1.0}_{0.9}$ km s^{-1}. For a sample where the velocity dispersion is considerably larger than the measuring errors, it would be expected for this result to be similar to the unweighted calculation, as explained in the Appendices of Chapter 2. It

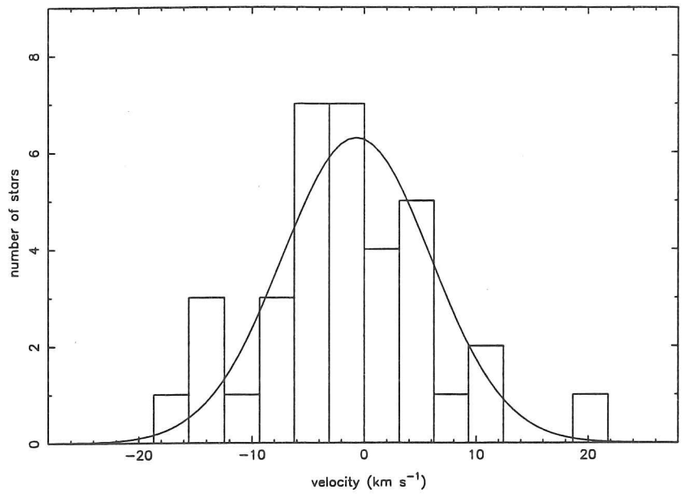

Figure 3.3: The velocity distribution of the Ursa Minor dSph galaxy with R_{cut} of 7.5. There are thirty five stars in the sample and the Gaussian shown is that produced by the maximum likelihood calculation. The velocity dispersion is 7.5 km s^{-1} and the average velocity -1.5 km s^{-1} with respect to the template plus 470 km s^{-1}.

can be seen, referring to Table 3.4, that this is indeed the case for our results. Figure 3.3 shows the velocity distribution for an R_{cut} of 7.5 with the fitted Gaussian derived by the maximum likelihood method.

Velocity measurements in Ursa Minor have been made over several years by Olszewski et al., the most recent published value for the velocity dispersion being 10.5 km s^{-1} (Pryor 1991). The error on this value is not published, but if it were similar in size to our error, then the values for the dispersion obtained by the two groups would be inconsistent.

3.3.2 Rotation

Ursa Minor is elliptical in shape, with an ellipticity of 0.56. This flattening could be caused by rotation of the dSph galaxy, anisotropy in its velocity dispersion, strong tidal interaction with the Milky Way, or some combination of the three. Rotation would artificially increase the observed velocity dispersion providing the rotation was not in the plane of the sky. Detection of rotation is important for

other reasons: the rotation curve and velocity dispersion are both required to correctly determine the mass of the system; and if the Galaxy is exerting a large tidal torque, disrupting the dSph, it would be expected to generate rotation. Finding the axis about which the dSph rotates is a test for triaxiality of the dSph galaxy, and dissipation.

Before looking for rotation, the velocities in Ursa Minor were corrected to a Galactocentric system to eliminate the differential heliocentric corrections over an object of large finite extent. The average change in the velocity of each star caused by this correction was 0.2 km s^{-1}. Then, to check for any sign of rotation, the distances of each star from the morphological major and minor axes were calculated, and straight lines were fitted to the velocity-distance plots: a straight line is the expected form of the rotation curve for solid body rotation. The gradient of the fit for rotation about the major axis was a factor of ten greater than for that about the minor axis (-4.4 km s^{-1} per 100 pc compared with -0.1 km s^{-1} per 100 pc) so more investigation was required.

Our data set is one of the many possible sets of data for Ursa Minor. The most complete way to calculate the significance of the apparent rotation would be to simulate data sets assuming values for the intrinsic velocity dispersion and rotation and see how likely it is that we would obtain apparent rotation as in our original data set. Bootstrap re-sampling is a simple and convenient way to make a similar calculation without having to do a full Monte-Carlo simulation.

It involves taking data points at random, with replacement, from the original data set, to build another sample data set. The analysis is repeated on this new data set as for the original and the parameters obtained are recorded. This is repeated many times, the median of the distribution of each parameter now being the best estimate of that parameter and the width of the distribution being the error. In our case we took one thousand samplings and found the values of the intercept and gradient for a straight line fitted to the data. The results were consistent with rotation about the major axis. The disadvantage of this method is that the 'new' samples are not independent from the original.

Fisher randomisation (Fisher 1958) is, in many ways, a superior procedure since it uses all the data points in such a way as to create independent samples. The velocities from our data set were randomly paired with the distances from the rotation axis to produce many new data sets. The number of times that the

straight line fit to the new data set produces a gradient larger than that obtained from our original set was calculated. The question answered here is how likely is it that the data with a velocity dispersion of $7.5\pm^{1.0}_{0.9}$ km s^{-1} and no rotation could produce apparent rotation of the magnitude we observed? For rotation around the major axis the answer was 0.58%, and around the minor axis, 45.97% which implies a three sigma effect around the major axis but no significant rotation around the minor axis.

The axis of greatest rotation was found by fitting solid body rotation curves to the distance-velocity information around every possible axis at one degree intervals. The position angle giving the greatest apparent rotation was 58°, in agreement with the morphological major axis calculated by Irwin & Hatzidimitriou (1993) which was 53° ± 5°. The effect of changing the position angle for the rotation by around 20° was to produce a significant decrease, of about 30%, in the magnitude of the apparent rotation. Whilst this is not the the error on the position angle of greatest rotation because one will always see a component of the rotation about any other axis which is not perpendicular to the true axis, it does give some idea of the rate of change of rotation with position angle. The following values for our estimate of the rotation effect are the median values of the intercept and gradient produced taking a position angle of 58° and applying the bootstrapping procedure one thousand times.

Around the major axis,

intercept = -2.5 ± 1.5 km s^{-1}, gradient = $-4.7\pm^{2.0}_{2.2}$ km s^{-1} per 100 pc.

The positive distances are on the north western side of the major axis.

Around the minor axis,

intercept = $-1.4\pm^{2.3}_{2.0}$ km s^{-1}, gradient = $0.1\pm^{0.8}_{1.1}$ km s^{-1} per 100 pc.

The positive distances are on the north eastern side of the minor axis.

For both these cases the intercept is with respect to an arbitrary value which is actually the velocity with respect to the template plus 470 km s^{-1}. The errors quoted are the 68% level of the distribution for each variable, holding the other one fixed. The goodness of fit of the lines is of course very poor since the velocity dispersion about the mean rotation is large ($\chi^2 \sim 840$ for 35 stars), but it does appear that there is a real indication of rotation about the major axis at the three sigma level of significance from the Fisher randomisation test. Figures 3.5 and 3.4

show the velocity-distance data for the minor and major axes, the fitted lines being those with the parameters quoted above. For the rotation we have observed to be an artifact produced by our line of sight and the transverse motion of the dSph galaxy, Ursa Minor would have to be travelling at more than 2500 km s^{-1} in an orbit in the direction of its minor axis. It is highly unlikely that the dSph galaxy would have a transverse velocity this large as the expected transverse velocity for a bound orbit is more likely to be around 300 km s^{-1}. Furthermore, the evidence points towards the orbit being in the direction of the major axis, a point which is discussed in Section 3.4.3 of this paper.

The presence of rotation lowers the value of the velocity dispersion as the rotation curve has to be subtracted from the velocities. In our case this leads to a velocity dispersion, calculated using a maximum likelihood method, of $6.7\pm^{0.9}_{0.8}$ km s^{-1}. Comparing this to the value without correction for rotation ($7.5\pm^{1.0}_{0.9}$ km s^{-1}) it is apparent that both the derived dispersion and one sigma error range have been reduced. The difference in the derived velocity dispersion using velocities corrected to Galactocentric coordinates and uncorrected was negligible. Figure 3.6 shows the fit of the new velocity dispersion to the velocity distribution corrected for rotation. At the last measured distance on the minor axis, of close to 180 pc, the solid body rotation curve produces a maximum rotational velocity of 8.5 km s^{-1}. The rotational velocity divided by the velocity dispersion is $8.5/6.7 = 1.3$, implying considerable support in the galaxy from rotation as well as from the velocity dispersion. This value is consistent with a tri-axial galaxy with no anisotropy rather than a prolate galaxy rotating end over end, although this is not a definitive model.

The discovery of rotation in Ursa Minor is of particular interest when placed in the context of the other dSph galaxies. For example in Chapter 2 we found no sign of rotation about either axis of the Sextans dSph galaxy, whereas Paltoglou & Freeman (1986) claim a rotation velocity of 3.5 ± 2.5 km s^{-1} about the minor axis of Fornax at about one core radius, but this is not confirmed by Mateo et al. (1991).

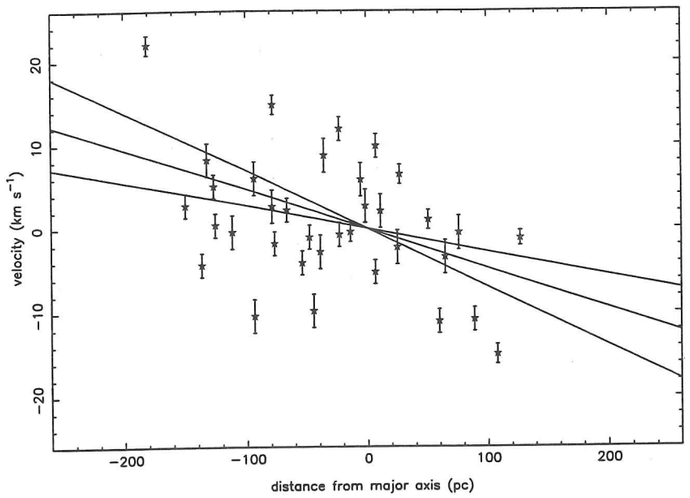

Figure 3.4: Rotation round the major axis of Ursa Minor. The best fit lines from the bootstrapping procedure, described in Section 3.3.2, are bounded by the errors. These are the one sigma errors for the slope of the fit, keeping the average velocity of the sample fixed.

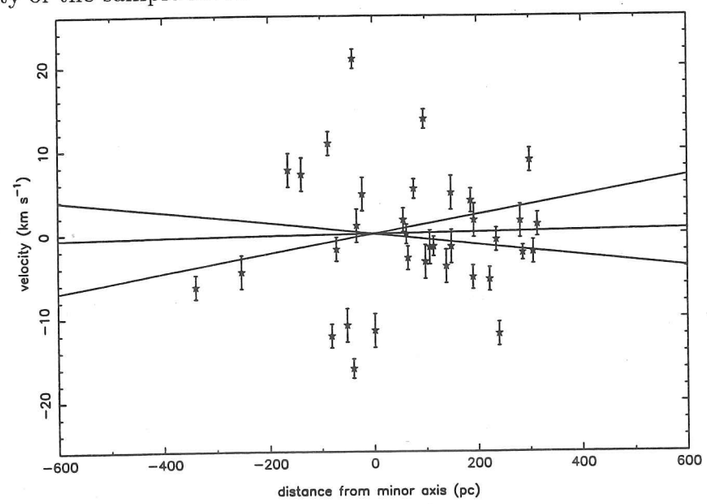

Figure 3.5: Rotation round the minor axis of Ursa Minor. The best fit lines from the bootstrapping procedure, described in Section 3.3.2 of, are bounded by the errors. These are the one sigma errors for the slope of the fit, keeping the average velocity of the sample fixed.

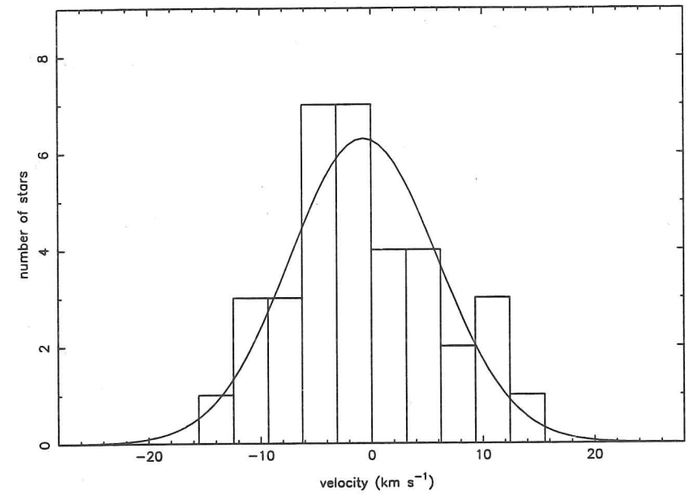

Figure 3.6: The velocity distribution of the Ursa Minor dSph galaxy with R_{cut} of 7.5 with the effect of rotation subtracted. The velocity dispersion calculated by the maximum likelihood method is 6.7 km s^{-1} and the average velocity is -0.5 km s^{-1}.

3.3.3 The Mean Velocity

The other result obtained was that for the systematic velocity of the Ursa Minor dSph galaxy. From the RV standard stars, the velocity of the template was found to be 223.3 km s^{-1}. The results quoted in Tables 3.3 and 3.4 are those relative to the template plus 470 km s^{-1}. These data gave a median intercept on the rotation curve of -2.5 ± 1.5 km s^{-1}. Therefore the velocity of Ursa Minor was $223.3 - 470 - 2.5 = -249.2 \pm 1.5$ km s^{-1}. This value is in agreement with the value of -249 ± 1 km s^{-1} given in Zaritsky et al. (1989).

3.4 Analysis

3.4.1 Variation of Velocity Dispersion with Radius

For a King model (King 1962, 1966) of a stellar system without an extended massive halo it would be expected for the velocity dispersion to decrease with distance from the centre of the galaxy (see Section 2.4.1). Table 3.5 shows how the velocity dispersion varies with distance for our results, the 'radius' being the

Table 3.5: How Velocity Dispersion Varies with Radius.

Radius range (pc)	Average radius (pc)	No. in bin	Velocity dispersion. Straight data ($km\,s^{-1}$)	Rotation subtracted ($km\,s^{-1}$)
16–67	49	7	$6.0\pm^{1.6}_{2.1}$	$6.7\pm^{1.7}_{2.3}$
70–104	89	7	$9.3\pm^{2.3}_{3.0}$	$8.0\pm^{2.0}_{2.6}$
104–152	130	7	$7.3\pm^{1.8}_{2.4}$	$5.8\pm^{1.5}_{2.0}$
158–227	190	7	$4.7\pm^{1.2}_{1.7}$	$4.1\pm^{1.1}_{1.6}$
235–290	261	7	$4.5\pm^{1.2}_{1.6}$	$5.3\pm^{1.3}_{1.8}$

geometric mean radius since Ursa Minor is elliptical in shape (Irwin & Hatzidimitriou, 1993). The two columns of values displayed contain the results for the data with R_{cut} of 7.5 and those for these same data with the effect of rotation subtracted. The dispersions and errors here were calculated as before, using the maximum likelihood method.

The velocity dispersion shows some sign of decrease at radii greater than the core radius of 196 pc. Figure 3.7 shows the results for the data corrected for the effect of rotation. Within the errors, the variation of the velocity dispersion for the data with and without rotation subtracted are consistent with the King model with $c = 0.51$ derived for Ursa Minor by Irwin & Hatzidimitriou (1993). We emphasize that the combination of an apparent rotation and a decrease in velocity dispersion with distance in Ursa Minor means that a detailed dynamical analysis of this Galactic dSph is in principle possible. Velocities for stars further from the centre of Ursa Minor are required to extend this result.

3.4.2 Mass-to-light Ratios

The background to the methods used to calculate the mass-to-light ratio are given in Section 2.4.1. The resulting equations for the core and total mass-to-light ratios, hereafter called the core fitting method and Illingworth's method respectively, are

$$\frac{\rho_0}{I_0} = \eta \frac{333\sigma_0^2}{r_{hb} S_0}, \tag{3.3}$$

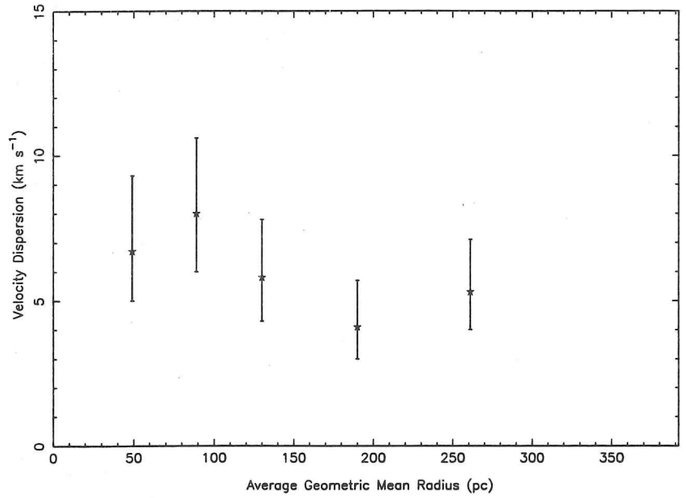

Figure 3.7: The variation of the velocity dispersion with distance from the centre of Ursa Minor. The data are from Table 3.5 and have been corrected for the effect of rotation.

and

$$\frac{M_{tot}}{L_{tot}} = \frac{166.5 r_c \mu}{\beta L_{tot}}, \tag{3.4}$$

where η and μ are parameters given by the particular King model, σ_0^2 and $1/\beta$ are the observed square velocity dispersion (σ_{obs}^2, adjusted according to the King model and average radius of the stars observed, I_0 and L_{tot} are the central surface brightness and total luminosity of the dSph, and r_c and r_{hb} are the core and half brightness radii respectively. Illingworth's method is far more model sensitive because η is always close to 1 but μ varies considerably with small changes in the concentration of the King model.

Irwin & Hatzidimitriou (1993) have found the best King model fit for Ursa Minor is that with $c = 0.51$, implying $W_0 = 2.4$, $\eta = 0.96$ and $\mu = 2.7$. Figure 8 shows the photometric data fitted by this King model (solid line) and the best fit exponential profile (dashed line).

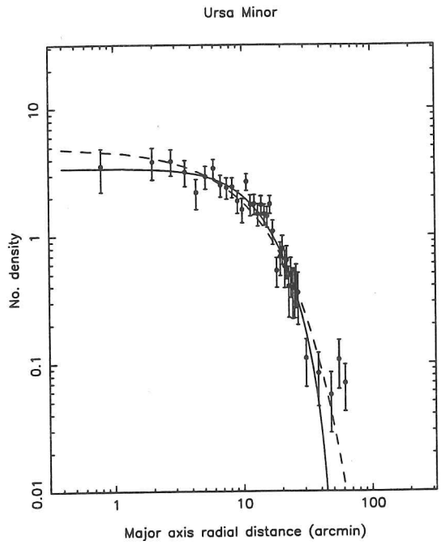

Figure 3.8: The best King model fitted to the Ursa Minor dSph galaxy (by Irwin & Hatzidimitriou (1993) from the APM results) with a concentration of 0.51. The dashed line is an exponential fit. One arc minute is equivalent to 18.6 parsecs at the distance of Ursa Minor (64 kpc).

Irwin & Hatzidimitriou (1993, 1995) also calculated the following parameters for the dSph galaxy:

$$r_c = 196 \pm 24 \text{ pc},$$

$$r_{hb} = 150 \pm 18 \text{ pc},$$

$$r_t = 628 \pm 74 \text{ pc},$$

$$M_V = -8.7 \pm 0.5,$$

$$L_{tot,V} = (2.5 \pm^{1.6}_{0.9}) \times 10^5 \text{ L}_{\odot,V},$$

$$S_{0,V} = 2.0 \pm^{1.2}_{0.8} \text{L}_{\odot,V}\text{pc}^{-2}.$$

All the distances quoted here are geometric mean distances. The average distance from the centre of the galaxy of our observations was 144 pc, which is $0.73r_c$, leading to $\sigma_0 = \sigma_{obs}/0.90$ and $1/\beta = \sigma^2_{obs}/0.54^2$ where σ_{obs} is the observed velocity dispersion. The velocity dispersion for the data with R_{cut} of 7, with the effect of our derived rotation subtracted, was $\sigma_{obs} = 6.7 \pm^{0.9}_{0.8}$ km s^{-1}. The mass-to-

light ratios were calculated by simulating a distribution assuming Gaussian errors and taking the median value. The result for the core mass-to-light ratio was $\rho_0/I_{0,V} = 59 \pm^{41}_{25}$. Similarly the total mass-to-light ratio was $M_{tot}/L_{tot,V} = 40 \pm^{29}_{17}$. The errors quoted here include those due to the half brightness and core radii, the luminosity and the velocity dispersion and they are taken at the 68% level of the derived distribution, the luminosity error contributing more than half the total error. For the velocity data without rotation subtracted the results were $\rho_0/I_{0,V} = 74 \pm^{51}_{31}$ and $M_{tot}/L_{tot,V} = 50 \pm^{36}_{22}$. Our values for the mass-to-light ratios are considerably less than the values previously published for Ursa Minor, which have been between 80 and 150 (Aaronson 1987, Pryor 1991). The differences are due mostly to our lower velocity dispersion.

For the mass-to-light ratio to be 3, σ_{obs} would need to be about 2 km s^{-1}. This is well outside the 99.9% confidence level value of 4.3 km s^{-1} from the maximum likelihood calculation. Such a small dispersion would only just be detectable because the dispersion caused by our errors alone is 1.5 km s^{-1}.

3.4.3 Other Possible Explanations of the Velocity Dispersion.

Anisotropy of the Velocity Dispersion

The models used to calculate the mass-to-light ratio assumed isotropy in the velocity dispersion. That is,

$$\sigma^2_{total} = \sigma^2_{los} + \sigma^2_\theta + \sigma^2_\phi = 3\sigma^2_{los}, \tag{3.5}$$

where σ_{los} is the line of sight velocity dispersion and σ_θ, and σ_ϕ are the dispersions that would be seen along the other two perpendicular directions. So, the maximum effect that anisotropy could have on the mass-to-light ratio is a factor of three (the calculated mass-to-light ratio would be a factor of 3 bigger than the true answer) if all the dispersion were actually along the line of sight. If we assume Ursa Minor to be oblate rather than triaxial and with the line of nodes in the plane of the sky, the dispersion we see is larger than one third of the total as we look in the major axis, implying some overestimate of the mass-to-light ratio. It is, however, likely that Ursa Minor is triaxial, a suggestion strengthened by the fact that it is possible to sustain rotation around the major axis of such a system.

The effect of anisotropy in this case would be more difficult to calculate as we do not know the size of the axis down which we are looking. Signs of triaxiallity may be seen as twisting of the surface brightness isophotes and rotation of the apparent rotation axis with increasing radius. Anisotropy alone cannot account for the large discrepancy between the mass-to-light ratio we have calculated for Ursa Minor and the values measured for larger and smaller stellar systems.

Binaries

The presence of binaries in the sample of observed stars would increase the observed velocity dispersion so that it was no longer a true indication of the mass of the galaxy. Suntzeff et al. (1993), made a calculation for Sextans using a Monte Carlo method. They obtained velocity dispersions of close to 6 $\mathrm{km\,s^{-1}}$ for a binary fraction of 0.25, assuming an intrinsic velocity dispersion of 2.1 $\mathrm{km\,s^{-1}}$, which is equivalent to a mass-to-light ratio of 2.5 according to the parameters they used. Applying this same result to Ursa Minor merely implies that the starting mass-to-light ratio was 3, otherwise the result is the same. The calculation involved several simplifications such as uniformity of mass ratios and inclinations and a flat period distribution which are not necessarily valid, but it is still useful for comparison with the observations.

Olszewski & Aaronson (1987) have found three velocity variables among eighteen stars in Ursa Minor. Two of these are likely to be variable because of motions in the atmospheres of the stars, but the other could well be a binary star. These results imply an observed binary fraction between 0.06 and 0.17.

We have spectra at two epochs, separated by a year, for nine stars. For all these stars the agreement between the velocities at the different epochs is almost within two sigma of the measuring errors, however for two of these stars we only have one observation at each epoch and for none do we have as many as two observations at both epochs, which compares poorly with the equivalent data for Sextans where we had two or three spectra at different epochs for several of the stars. Since for a binary fraction of 0.25 we would require only about two of these stars to be binaries, the result is inconclusive, although with the velocities of five of our nine stars being with one sigma of the measuring errors it is unlikely that the binary fraction as defined by Suntzeff et al. is much more that 25%.

However this is not the true picture because due to our observing criteria we could have detected only a fraction of the binary stars. Quantifying the possible binary fraction accurately requires continued velocity monitoring. Such efforts are important since a binary fraction of 0.1 still requires a true mass-to-light ratio of 50, whereas all extra mass above that found in globular clusters can be explained by a fraction of 0.25.

Tidal Interaction with the Galaxy

The other alternative is that the dSph galaxies are being tidally disrupted by the Milky Way Galaxy, so that the assumption of dynamical equilibrium underlying equations 3.3 and 3.4 is invalid. Tidal disruption caused by both the Galaxy and the Large Magellanic Cloud can account for much of the structure observed in the Small Magellanic Cloud as well as the existence of the Magellanic Stream (Gardiner, Sawa & Fujimoto, 1994), and suggestive evidence for the existence of phase-space structure in the outer Galaxy, the reality of which would strongly support such a model of merging galaxies, continues to arise (Arnold & Gilmore 1992). Indeed the concept of the small galaxies close to the Milky Way undergoing tidal disruption and merger is fundamental to standard CDM cosmologies.

A completely disrupted dSph galaxy of freely expanding stars would be expected to disperse in the time it takes for the galaxy to orbit our Galaxy, so that it would be unlikely for a significant proportion of the nine known dSphs to be undergoing tidal disruption now. However it is possible that the dSph could still be visible as a collection of stars having been tidally disrupted some time ago, as shown by Kuhn (1993) who has performed N-body calculations demonstrating that, in the case of strong velocity anisotropy, the time for an unbound dSph galaxy to disperse may be an order of magnitude larger than a free expansion argument would suggest. If this were so, the velocity dispersion that we have been so diligently measuring would have nothing to do with the actual mass-to-light ratio of the galaxy.

For a mass-to-light ratio of 3, the mass of Ursa Minor would be 7.8×10^5 $\mathrm{M_\odot}$. Assuming this mass and a Keplerian potential for the Galaxy implies that the tidal distance of Ursa Minor is 104 kpc. This tidal distance is the distance at which a galaxy of a certain size and mass would have to be to be disrupted by the galaxy according to a simple balance of forces argument (see Section 2.4.2). The

actual distance of Ursa Minor is 64 kpc, indicating that Ursa Minor ought to be undergoing tidal disruption at present.

Calculations by Hodge & Michie (1969), and several numerical simulations since then, have suggested that a tidally disrupted satellite of the Galaxy ought to become elongated along the direction of its orbit. In the case of Ursa Minor preliminary calculations of the proper motion indicate an orbit consistent with the direction of the Magellanic Stream (although the measuring errors here are large) and in the same orbital direction as the motion of the LMC (Scholz & Irwin 1994). The major axis is within 10 degrees of the direction of the likely orbital plane of the LMC suggesting that Ursa Minor could have been elongated as predicted by the tidal disruption calculations. This, along with the discovery of structure in the luminosity contour map and the fact that Ursa Minor does have a profile indicative of truncation (Irwin & Hatzidimitriou 1995) adds evidence to the suggestion of tidal disruption.

A tidally disrupted dSph galaxy would become elongated along its orbit, losing stars because of frictional forces. Any stars on prograde orbits in the dSph galaxy would be expected to be preferentially lost. Therefore rotation in this direction may be lost as the dSph galaxy is disrupted, whereas the component of rotation in a direction perpendicular to the orbit of the dSph galaxy round the Galaxy would remaining intact, eventually producing rotation only around the major axis, as we have found in Ursa Minor. Additionally, it is possible to maintain rotation around the major axis in a triaxial system, suggesting that Ursa Minor is likely to be triaxial.

Dark Matter

Should all the ideas in the previous sections fail to account for the high mass-to-light ratios, the alternative is that Ursa Minor contains large amounts of dark matter, with a core dark matter density of around 0.4 $M_{\odot}pc^{-3}$.

3.5 Conclusion

The internal central velocity dispersion of the Ursa Minor dSph galaxy is $7.5\pm^{1.0}_{0.9}$ $km\,s^{-1}$ measured from thiry five giant stars. There is rotation round the major axis with

a gradient of $-4.7\pm^{2.0}_{2.2}$ $km\,s^{-1}$ per 100 pc where positive distance is the north western side of the major axis. This leads to a corrected velocity dispersion of $6.7\pm^{0.9}_{0.8}$ $km\,s^{-1}$. The mass-to-light ratios calculated using this value $59\pm^{41}_{25}$ and $40\pm^{29}_{17}$ in solar units, using core fitting and Illingworth's methods respectively. By comparison, apparently purely stellar systems such as globular clusters and the stellar Galactic disk, have mass-to-light ratios of about 3. Thus, the observed internal velocity dispersion of the Ursa Minor dSph galaxy is several times larger than the value of about 2 $km\,s^{-1}$ which is expected if the galaxy is a self gravitating stable system whose gravitational potential is dominated by the mass in visible stars.

However there is considerable evidence to indicate that things are not as simple as the mass-to-light ratio calculations assume. The discovery of rotation about the major axis coupled with the evidence of structure in this dSph galaxy is a clear indication of this. What exactly causes these effects is by no means as clear but it is not unreasonable, given Ursa Minor's size and distance, that it should be undergoing tidal disruption, and we have suggested a possible explanation assuming this. This is that, as the dSph expands along the direction of its orbit, those stars which are causing the component of rotation round the axis perpendicular to the direction of motion are most likely to be lost, leaving only the other perpendicular component of rotation remaining. It is also possible that binary stars may be affecting the velocity dispersion since binary fractions of only 0.25 can account for a dispersion of 6 $km\,s^{-1}$. With measurements at two dates, separated by about a year, for nine stars the velocities for five of these were within one sigma of the measuring errors, the other four being within two sigma, so we have no firm identification of any binaries. However we have too few observations at each epoch to say with any certainty that none of these stars are binary stars. Further observations are required to ascertain the actual number of binaries in our sample of thirty five stars.

Other possible explanations for our results include a substantial dark matter density in this galaxy or a serious underestimate of the measuring errors. We think the latter unlikely. Another possible effect which may contribute is velocity anisotropy, although it is unlikely to provide a major part of the answer.

Acknowledgments

We would like to thank E.W. Olszewski for giving us the positions of members of Ursa Minor found through his observations.

The spectroscopy reported here was obtained with the William Herschel Telescope operated on the island of La Palma by the Royal Greenwich Observatory in the Spanish Observatorio del Roque de los Muchachos of the Instituto de Astrophysica de Canarias.

References

Aaronson, M. & Olszewski, E., 1987, Kormendy, J., & Knapp, G.R., eds, in Dark Matter in the Universe, Proc. IAU Symp. 117, 153. Reidel.

Arnold, R. & Gilmore, G., 1992, MNRAS, 257, 225.

Armandroff, T.E. & Da Costa, G.S., 1986, AJ, 92, 777.

Cudworth, K.M., Olszewski, E.W. &, Schommer, R.A., 1986, AJ, 92, 766.

Fisher, R.A., 1958, Statistical Methods for Research Workers. Oliver and Boyd, Edinburgh and London.

Gardiner, L.T., Sawa, T., & Fujimoto, M., 1994, MNRAS, 266, 567.

Gilmore, G., 1990, Lynden-Bell, D., & Gilmore, G. eds, in Baryonic Dark Matter. Kluwer, Dordrecht.

Hodge, P.W., & Michie, R.W., 1969, AJ, 74, 587.

Irwin M.J. & Hatzidimitriou D., 1993, Brodie, J., ed, in Proc. ASP Symp vol 48, 322.

Irwin M.J. & Hatzidimitriou D., 1995 (in preparation).

King, I., AJ, 1962, 67, 471.

King, I., AJ, 1966, 71, 64.

Kuhn, J.R., 1993, ApJL, 409, L13.

Mateo, M., Olszewski, E., Welch, D.L., Fischer, P. & Kinkel, W., 1991, AJ, 102, 914.

Olszewski, E.W. & Aaronson, M., 1985, AJ, 90, 2221.

Olszewski, E.W. & Aaronson, M., 1988, in Large Scale Structure in the Universe, Proc. IAU Symp. 130, 409. Reidel.

Olszewski, E.W., 1991, Private Communication.

Paltoglou, G. & Freeman, K.C., 1987, de Zeeuw, T., ed, in Structure and Dynamics of Elliptical Galaxies, Proc. IAU Symp. 127, 447. Reidel.

Pryor, C., 1991, Busarello, G., Capaccioli, M., & Longo, G., eds, in Morphological and Physical Classification of Galaxies. Kluwer, Dordrecht.

Scholz, R.D., & Irwin, M.J., 1994, in MacGillivray, H.T. et al., eds, Proc. IAU Symp. 161, Astronomy from Wide-Field Imaging, 535. Kluwer, Dordrecht.

Suntzeff, N.B., Mateo, M., Terndrup, D.M., Olszewski, E.W., Geisler, D., Weller, W., 1993, ApJ, 418, 208.

Tonry J. & Davis, M., 1979, AJ, 84, 1511.

Zaritsky, D., Olszewski, E.W., Schommer, R.A., Peterson, R.C. & Aaronson, M., 1989, ApJ, 345, 759.

Chapter 4

The Draco Dwarf Spheroidal Galaxy

Abstract

We have observed nineteen giant stars in the Draco dwarf spheroidal galaxy and obtained good quality spectra for seventeen of these. The velocity dispersion of the sample, calculated by the maximum likelihood method, is $10.5 \pm^{2.2}_{1.7}$ km s^{-1}. The mean velocity is $-293.8 \pm^{2.6}_{2.7}$ km s^{-1}. The data were taken at a single epoch, so there is no direct information about possible binary star contamination. Assuming dynamical equilibrium, isotropy in the velocity dispersion and a negligible contribution from binary stars, the core mass-to-light ratio is $166 \pm^{289}_{107}$ $M_\odot/L_{\odot,V}$ and the total mass-to-light ratio is $145 \pm^{116}_{71}$ $M_\odot/L_{\odot,V}$ consistent with the presence of large quantities of dark matter.

4.1 Introduction

This chapter presents the results for the Draco stars which were observed during the same runs as the Sextans and Ursa Minor stars discussed in the previous two chapters. A velocity dispersion and a mean velocity were calculated for Draco, and the possibility of rotation round either axis was explored as was the variation of the velocity dispersion with distance from the centre of the galaxy. The analysis of the data was identical to that employed for the other two galaxies, and so a full discussion of the procedures is not repeated here.

Draco is the second closest of the eight dSph galaxies known to be in orbit around the Milky Way. It has no signs of extended or recent star formation, with a red horizontal branch on the HR diagram and low metal abundance and range. Its orbit, like that of Ursa Minor, is consistent within the errors with a polar orbit along the direction of the Magellanic stream in the same direction as the motion of LMC (Scholz & Irwin 1994).

The rest of this chapter is divided into several sections. First, the observations and the reduction procedure are described. Next, the errors on the observations are discussed. Then the velocity dispersion calculation is described, the results of the rotation analysis presented and a value for the mass-to-light ratio obtained. Finally, other possible contributions to the velocity dispersion are discussed.

4.2 Observations, Data Reduction and Error Analysis

4.2.1 Observations

The observations were made on the nights of 7th–9th and 26th–27th April 1992. All the observations were made using the William Herschel Telescope (WHT) on La Palma.

The observations were carried out in the same way as those for the other two galaxies, using the red arm of ISIS and the R1200R grating to observe the calcium II triplet lines in the 8300–8750 Å wavelength range. The arc lamp was CuAr & CuNe. See Chapter 2 for further details.

The stars observed were giant branch stars ranging in brightness from 15 to 18 magnitude in the R band. The nineteen Draco targets were kindly provided by Ed Olszewski (private communication).

Good spectra were obtained for seventeen members, and as no stars were observed more than once, no multi-epoch results were obtained. With no repeat measurements, it was impossible to estimate directly the measuring errors on individual spectra. The spectra were, however, obtained during the same runs as spectra from similar stars in the Sextans and Ursa Minor galaxies. The internal and external errors on the Draco velocities were therefore estimated by considering the combined data sets from the other two galaxies.

Additionally four bright radial velocity standard stars (RV stars) were observed with integration times of only 5 seconds, one or two on each night of each run. These spectra provided an estimate of the random and systematic errors for high signal-to-noise, short exposure spectra. The random part of this error gave an estimate of the minimum random error for the Sextans, Ursa Minor and Draco data, although it appears that the RV stars may have greater systematic error due to slit centering problems. The details of this are discussed in Chapter 2. The RV stars were also used as a check on the data reduction procedure, because their actual velocities were already known, and as a base to obtain the absolute mean velocity of Draco.

The coordinates of all the Draco member stars which were observed are shown in Table 4.1.

Table 4.1: Coordinates of the Draco stars. The centre of the Draco dSph galaxy is at 17^h 19.5^m, 57^o $58'$.

Star	RA	DEC
	1950	1950
24	17 19 10.3	58 00 16
249	17 19 15.5	58 02 04
267	17 18 56.1	58 00 34
361	17 19 45.0	57 56 27
473	17 18 47.3	57 59 26
536	17 19 43.9	57 54 38
562	17 20 04.4	57 58 49
576	17 19 49.0	58 02 05
iv-20	17 21 25.0	57 55 53
vi-1	17 19 54.6	57 51 37
vii-4	17 18 58.5	57 51 33
ix-5	17 18 24.5	57 55 32
xi-2	17 18 29.2	58 04 06
3053	17 18 46.9	58 01 45
3150	17 18 47.3	57 54 22
3157	17 18 52.9	57 55 16
3316	17 20 15.1	57 59 59
3363	17 19 59.5	58 02 48
3369	17 19 53.5	58 03 18

4.2.2 Data Reduction

The processing of the CCD frames, data reduction and analysis was carried out in a very similar way to the Sextans and Ursa Minor data. The details are presented in Chapter 2 so a brief summary will suffice.

Preliminary processing of the CCD frames to remove bias and cosmic ray events was done, mostly at the telescope, using FIGARO routines. IRAF was then used to perform the wavelength calibration, sky subtraction, and the cross correlation of the data against the same template used for the Sextans data. The same line selection was used to throw out very poor lines from the spectra. The cross correlation programme FXCOR produces a Tonry and Davis R value (Tonry & Davis 1979) for each correlation, and it was this parameter that was used to produce a cutoff value below which the results were considered too inaccurate and therefore discarded.

4.2.3 Errors in the Velocities

There were no repeat measurements for the Draco stars so the errors on the Draco data were calculated by combining the data from the Sextans and Ursa Minor measurements, excluding the possible binary, star 8, in the Sextans data set. The procedure for calculating the errors was identical to that performed on the Sextans and Ursa Minor data in Chapters 3 and 4: repeat measurements of the same stars (from the Sextans and Ursa Minor galaxies) were used to derive the error and calculate a suitable cutoff (R_{cut}) for the Tonry & Davis R value. See Figure 3.2, for the results of the error calculation for the combined data set. We had four spectra (from stars 24, vii-4, ix-5 and 3150) which were very noisy over particular wavelength ranges, and this skewed the resulting cross-correlation profiles. In these cases, when the offending area was excluded from the analysis, the profile was improved and the remaining spectrum produced a consistent velocity. The poor areas were around the first or third calcium II triplet lines, the second line at 8542 Å being the strongest of the three. The velocities obtained from these stars were considered to be 'half' measurements, making them less strongly weighted in the later calculations, because only two of the three lines were contributing to the result. In other words, the error on these velocities was estimated to be a factor of $\sqrt{2}$ greater than that on the other velocities.

For a variety of values of R_{cut}, the error distribution for the Sextans and Ursa Minor repeat velocities was created from the differences of the velocities obtained from individual observations for a star compared with the real mean velocity of that star. The Gaussian one sigma width of this distribution was the appropriate error on an individual observation. The widths of the error distributions for R_{cut} of 0, 7, 7.5 and 8 were 5.5 ± 0.3, 2.3 ± 0.2, $2.0^{0.1}_{0.2}$ and 2.0 ± 0.2 respectively (see Table 3.4). If the width of the distribution is denoted by σ_{err} then the error quoted here is such that the variance on σ^2_{err} is $2\sigma^4_{err}/N$.

In the case of Draco, we adopted a value of R_{cut} of 7.0, because the value of 7.5 adopted for the other two galaxies excluded too high a proportion of the stars from the analysis. Having more stars is advantageous when it comes to looking at the rotation or the variation of velocity dispersion with radius. The error per star is, therefore, slightly greater for Draco than for the other two galaxies.

The resulting velocity for each star is displayed in Table 4.2, along with the Tonry and Davis R value for the correlation, and the weight assigned to each star according to the procedure described above.

4.3 Results

4.3.1 The Velocity Dispersion Calculation

Only the velocities derived from the observations which had produced R values above the threshold were used in the velocity dispersion calculation. The width of the distribution of these velocities defined the velocity dispersion (σ_{obs}) of Draco. An unweighted Gaussian fit to the data was made to compare with the error weighted fit. Thirteen out of the seventeen stars have identical measuring errors on the velocities. Therefore we would expect the velocity dispersion obtained by calculating the standard deviation of the velocities, and then subtracting the error, to be very similar to the maximum likelihood method, where the individual weight of each star is included separately. The results reported in the text are those for an R_{cut} of 7.0. Other values of R_{cut} made little difference to the velocity dispersion result.

The velocity dispersion obtained by fitting a Gaussian to the unweighted distribution was $11.2^{1.8}_{2.1}$ km s^{-1}. The variance of σ^2_{obs} is $2\sigma^4_{obs}/N$, so this is the error

Table 4.2: The Velocities and Tonry and Davis R values for the Draco Observations. (The columns are explained in the table footnotes)

Star	Date	R	V_t km s^{-1}	V_7 km s^{-1}	Error Weight
24	A92-1	11.70	18.9	18.9	0.5
249	A92-1	7.18	-8.6	-8.6	1.0
267	A92-1	7.33	4.3	4.3	1.0
361	A92-1	3.69	26.7	—	1.0
473	A92-2	9.45	-4.5	-4.5	1.0
536	A92-2	10.75	-7.9	-7.9	1.0
562	A92-2	9.60	-4.6	-4.6	1.0
576	A92-2	8.70	7.5	7.5	1.0
iv-20	A92-2	7.60	-9.6	-9.6	1.0
vi-1	A92-2	11.96	9.8	9.8	1.0
vii-4	A92-2	9.86	13.0	13.0	0.5
ix-5	A92-2	8.38	5.1	5.1	0.5
xi-2	A92-2	8.38	-24.7	-24.7	1.0
3053	A92-2	5.00	-1.2	—	1.0
3150	A92-2	7.89	-11.3	-11.3	0.5
3157	A92-2	8.75	-5.6	-5.6	1.0
3316	A92-2	7.16	-1.0	-1.0	1.0
3363	A92-2	9.56	-5.2	-5.2	1.0
3369	A92-2	8.36	15.3	15.3	1.0

Notes. Date: A92-1 and A92-2 are abbreviations for the April 1992 runs, A92-1 being the run at the start of April, and A92-2 the one at the end.
V_t: This is the heliocentrically corrected velocity with respect to the template.
R is the Tonry & Davis R value.
V_7: This is the velocity for a star where data which produced a correlation with $R < 7.0$ is replaced by a dash.
Error weight: Those stars which were given $\sqrt{2}$ times the error were those which had part of the spectrum selected out of the correlation. They were considered to be half measurements in the velocity dispersion calculation so they are marked by a 0.5 in this column.

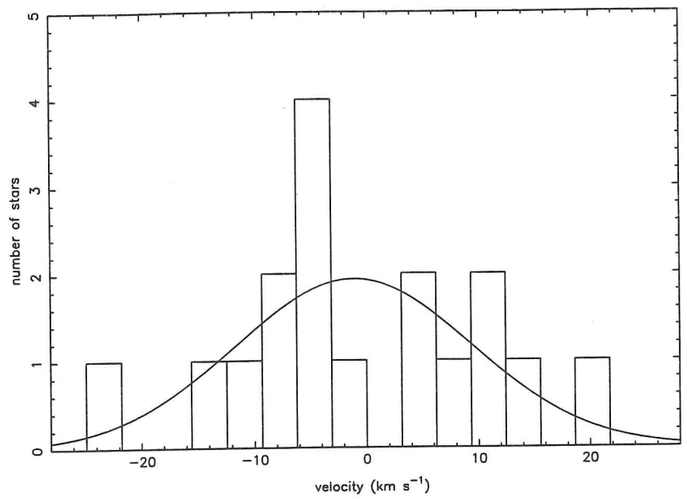

Figure 4.1: The velocity distribution of the Draco dSph galaxy with R_{cut} of 7.0. The velocity dispersion calculated by the maximum likelihood method is 10.5 km s^{-1} and the average velocity -1.1 km s^{-1} with respect to the template plus 516 km s^{-1}.

quoted. This dispersion has not had the contribution due to measuring errors removed. The inclusion of this, as in equation 2.22, gave a corrected velocity dispersion of $10.9\pm^{1.7}_{2.1}$ km s^{-1}.

Using the maximum likelihood method, the velocity dispersion for an R_{cut} value of 7.0 was $10.5\pm^{1.8}_{2.1}$ km s^{-1}. As expected, this is very similar to the unweighted calculation. Figure 4.1 shows the velocity distribution for an R_{cut} of 7.0 with the fitted Gaussian derived by the maximum likelihood method. Velocity measurements in Draco have been made over several years by Olszewski et al., the most recent published value for the velocity dispersion being 10.2 ± 1.8 km s^{-1} (Mateo 1994). More recently, Pryor, Olszewski & Armandroff (1995) have used a fibre system to measure the velocities of 84 Draco members with an accuracy between 1 and 10 km s^{-1} per observation and obtained a velocity dispersion of 9.2 ± 0.8 km s^{-1}. Both these results are consistent with the result we present here.

4.3.2 Rotation and the Mean Velocity

It is important to determine the degree of rotation about the axes of the dSph galaxy for several reasons: rotation would artificially increase the observed velocity dispersion providing that rotation was not in the plane of the sky; the rotation curve and velocity dispersion are both required to correctly determine the mass of the system; and if the Galaxy is exerting a large tidal torque which is affecting the dSph galaxy, this would be expected to generate rotation (Piatek & Pryor 1995). Finding the axis about which the dSph rotates is a test for dissipation, and triaxiality.

The details of the rotation calculation are explained in Section 3.3.2.

Before looking for rotation, the velocities for the stars in Draco were corrected to a Galactocentric system to eliminate the differential heliocentric corrections over an object of large finite extent. The average change in the velocity of each star caused by this correction was 0.02 km s^{-1}, and using these values rather than the heliocentric values made negligible difference to the value of the velocity dispersion.

The following values for the estimate of the rotation effect are the median values of the intercept and gradient produced taking a position angle of 82° and applying a bootstrapping procedure 1000 times.

Around the major axis,

intercept $= -1.9\pm^{2.4}_{2.0}$ km s^{-1}, gradient $= -5.0\pm^{3.3}_{3.1}$ km s^{-1} per 100 pc.

The positive distances are on the north western side of the major axis.

Around the minor axis,

intercept $= -2.3\pm^{2.7}_{2.6}$ km s^{-1}, gradient $= -0.7\pm^{2.3}_{2.1}$ km s^{-1} per 100 pc.

The positive distances are on the north eastern side of the minor axis.

For both these cases the intercept is with respect to an arbitrary value which is actually the velocity with respect to the template plus 516 km s^{-1}. The errors quoted are the 68% level of the distribution for each variable, holding the other one fixed. There is some evidence for rotation around the major axis, but this is only a two sigma result, and may well not be significant, given the relatively poor quality of the data set when compared with the Ursa Minor results presented in Chapter 3.

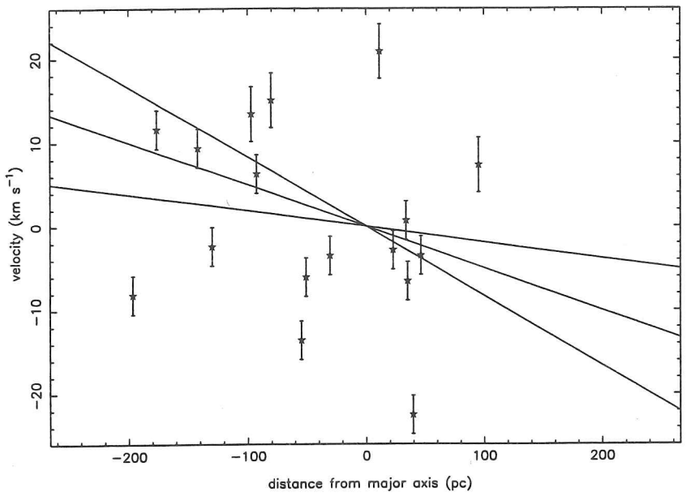

Figure 4.2: Rotation round the major axis of Draco. The best fit lines from the bootstrapping procedure, described in Section 3.3.2, are bounded by the errors. These are the 1 sigma errors for the slope of the fit, keeping the average velocity of the sample fixed.

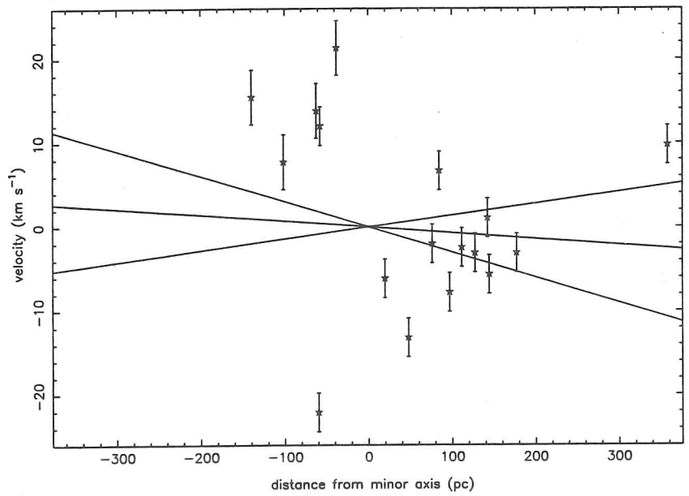

Figure 4.3: Rotation round the minor axis of Draco. The best fit lines from the bootstrapping procedure, described in Section 3.3.2, are bounded by the errors. These are the 1 sigma errors for the slope of the fit, keeping the average velocity of the sample fixed.

Figures 4.2 and 4.3 show the velocity-distance data for the major and minor axes, the central fitted lines being those with the parameters quoted above, the bounding lines are the 68% errors on the slope, holding the intercept fixed.

The other result obtained was that for the systematic velocity of the Draco dSph galaxy. From the RV stars, the velocity of the template was found to be 223.3 km s^{-1}. The results quoted in Tables 4.2 and 4.3 are those relative to the template plus 516 km s^{-1}. The average velocity obtained by the maximum likelihood method was $-1.1\pm^{2.6}_{2.7}$ km s^{-1}, making the velocity of Draco $223.3 - 516 - 1.1 = -293.8\pm^{2.6}_{2.7}$ km s^{-1}. Other estimates for this value are -289 ± 1 km s^{-1}, from a previous report of Olszewski's single star measurements, given in Zaritsky et al. (1989) and -291.9 ± 1.1 km s^{-1} from the fibre data of Pryor, Olszewski & Armandroff (1995). These results are consistent, assuming slight underestimates of the measuring errors.

4.4 Analysis

4.4.1 Variation of Velocity Dispersion with Radius

The velocity dispersion in a King model (King 1962, 1966) of a stellar system, without an extended massive halo, should decrease with distance from the centre of the galaxy (see Section 2.4.1). Table 4.3 shows how the velocity dispersion varies with distance for the Draco data, the 'radius' being the geometric mean radius since Draco is elliptical in shape ($e = 0.29$). The column in the table contains the results for the data with R_{cut} of 7.0. The dispersions and errors here were calculated as before, using the maximum likelihood method. The derived dispersions appear to show an increase rather than a decrease towards larger radii. They are also consistent with a flat profile. However, they are only consistent with the profile expected for a King Model with $c = 0.50$ (derived for Draco by Irwin & Hatzidimitriou, 1993) at the two sigma level. In this sample there are only three stars which lie outside the core radius of the dSph galaxy. Outside one core radius, the decrease of velocity dispersion is more pronounced in a King Model. Therefore, velocities for stars further from the centre of the galaxy are required to extend this result.

Table 4.3: How Velocity Dispersion Varies with Radius. $R_c = 158$ pc

Radius range (pc)	Average radius (pc)	No. in bin	Velocity dispersion ($\mathrm{km\,s^{-1}}$)
62–95	79	6	$9.3\pm^{3.8}_{2.4}$
99–119	110	6	$7.3\pm^{3.1}_{2.0}$
127–272	175	5	$13.8\pm^{6.0}_{3.7}$

4.4.2 Mass-to-light Ratios

The background to the methods used to calculate the mass-to-light ratio are given in Section 2.4.1. The resulting equations for the core and total mass-to-light ratios, hereafter called the core fitting method and Illingworth's method respectively, are

$$\frac{\rho_0}{I_0} = \eta \frac{333\sigma_0^2}{r_{hb} S_0}, \tag{4.1}$$

and

$$\frac{M_{tot}}{L_{tot}} = \frac{166.5 r_c \mu}{\beta L_{tot}}, \tag{4.2}$$

where η and μ are parameters given by the particular King model, σ_0^2 and $1/\beta$ are the observed square velocity dispersion (σ_{obs}^2), adjusted according to the King model and average radius of the stars observed, I_0 and L_{tot} are the central surface brightness and total luminosity of the dSph, and r_c and r_{hb} are the core and half brightness radii respectively. Illingworth's method is far more model sensitive because η is always close to one but μ varies considerably with small changes in the concentration of the King model.

Irwin & Hatzidimitriou (1993) have found the best King model fit for Draco is that with $c = 0.50$ implying $W_0 = 2$, $\eta = 0.96$ and $\mu = 2.7$. Figure 4.4 shows the photometric data fitted by this King model (solid line) and the best fit exponential profile (dashed line).

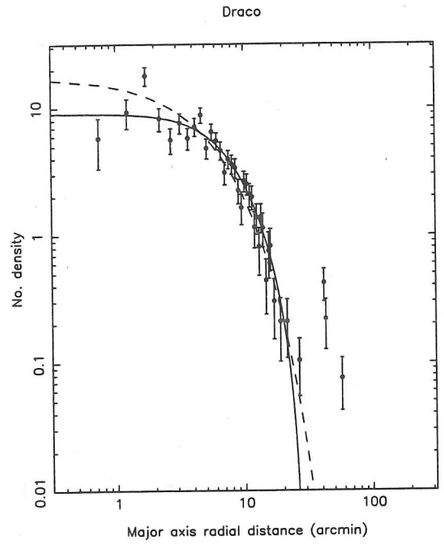

Figure 4.4: The best King model fitted to the Draco dSph galaxy (by Irwin & Hatzidimitriou 1993 from the APM results) with a concentration of 0.50. The dashed line is an exponential fit. One arc minute is equivalent to 20.9 parsecs at the distance of Draco (72 kpc).

Irwin & Hatzidimitriou (1993, 1995) also calculated the following parameters for the dSph galaxy:

$$r_c = 158 \pm 14 \text{ pc},$$
$$r_{hb} = 120 \pm 11 \text{ pc},$$
$$r_t = 498 \pm 47 \text{ pc},$$
$$M_V = -8.3 \pm 0.5,$$
$$L_{tot,V} = (1.8\pm^{1.0}_{0.7}) \times 10^5 \text{ L}_{\odot,V},$$
$$S_{0,V} = 2.2 \pm^{1.3}_{0.8} \text{L}_{\odot,V}\,\text{pc}^{-2}.$$

All the distances quoted here are geometric mean distances. The average distance from the centre of the galaxy of the observations was 118 pc, which is $0.75\mathrm{r_c}$, leading to $\sigma_0 = \sigma_{obs}/0.87$ and $1/\beta = \sigma_{obs}^2/0.54^2$ where σ_{obs} is the observed velocity dispersion. The velocity dispersion for the data with R_{cut} of 7.0 was $\sigma_{obs} = 10.5\pm^{2.2}_{1.7}$ $\mathrm{km\,s^{-1}}$. The mass-to-light ratios were calculated by simulating a

distribution assuming Gaussian errors and taking the median value. The result for the core mass-to-light ratio was $\rho_0/I_{0,V} = 165 \pm^{289}_{107}$. Similarly the total mass-to-light ratio was $M_{tot}/L_{tot,V} = 145 \pm^{116}_{71}$. The errors quoted here include those due to the half brightness and core radii, the luminosity and the velocity dispersion and they are taken at the 68% level of the derived distribution, the luminosity error contributing more than half the total error.

Our values for the mass-to-light ratios are consistent with previously published values, the most recent being Pryor, Olszewski & Armandroff (1995) who obtained 110 ± 20 $M_\odot/L_\odot$, the error quoted here being only that due to the error in the velocity dispersion.

For a mass-to-light ratio of 3, σ_{obs} would be about 1.5 $km\,s^{-1}$. This is well outside the 99.9% confidence level value of 5.6 $km\,s^{-1}$ from the maximum likelihood calculation. At this level, the error on the measurements would outweigh the actual velocity dispersion, since the dispersion caused by the errors alone is 2.5 $km\,s^{-1}$.

4.4.3 Other Possible Explanations of the Velocity Dispersion

Like both Sextans and Ursa Minor, the velocity dispersion observed here may not truly reflect the mass of the system. Anisotropy in the velocity dispersion could inflate the mass-to-light ratio by a factor of three at most, although the actual factor is likely to be considerably less. This is, however, an unmeasurable effect.

The data presented in this chapter tell us nothing about how many binaries may be contaminating the sample because there are no multi-epoch observations: the presence of binaries would increase the measured velocity dispersion.

Chapter 6 of this thesis contains a closer examination of the possible influence of binary stars on the velocity dispersion, and analyses how effective repeat observations may be in weeding out those binary stars which are affecting the results obtained from the sample.

The other alternative is that the dSph galaxies are being tidally disrupted by the Milky Way Galaxy, so that the assumption of dynamical equilibrium underlying equations 4.1 and 4.2 is invalid. For a mass-to-light ratio of 3, the mass of Draco would be 5.1×10^5 $M_\odot$. Assuming this mass and a Keplerian potential for the

Galaxy implies that the tidal distance of Draco is 187 kpc. This tidal distance is the distance at which a galaxy of a certain size and mass would have to be to be disrupted by the galaxy according to a simple balance of forces argument (see Section 2.4.2). The actual distance of Draco is 72 kpc, indicating that Draco ought to be undergoing tidal disruption at present. See Sections 2.4.2 and 3.4.3 for a more complete discussion.

Hodge & Michie (1969) have suggested that a tidally disrupted satellite of the Galaxy ought to become elongated along the direction of its orbit, and calculations of the proper motion of Draco, indicate that, like Ursa Minor, its orbit is consistent with the direction of the Magellanic Stream (although the measuring errors here are large) and in the same orbital direction as the motion of the LMC (Scholz & Irwin 1993). It is possible that Ursa Minor, Draco and the LMC used to be part of the same object: if this is the case, and Ursa Minor is undergoing tidal disruption at present, then it is likely, given the similarities in luminosity and size between the two dSph galaxies, that the same thing is happening to Draco.

Should all these ideas fail to account for the high mass-to-light ratios, the alternative is that Draco contains large amounts of dark matter, with a core dark matter density of around 1.5 $M_\odot pc^{-3}$.

4.5 Conclusion

The internal central velocity dispersion of the Draco dSph galaxy is $10.5 \pm^{2.2}_{1.7}$ $km\,s^{-1}$ measured from seventeen giant stars. It is possible that Draco may be rotating around the major axis but the value of $-5.0 \pm^{3.3}_{3.1}$ $km\,s^{-1}$ per 100 pc derived here is only a two sigma result. The limit on rotation round the minor axis is $-0.7 \pm^{2.3}_{2.1}$ $km\,s^{-1}$ per 100 pc. The mass-to-light ratios from core fitting and Illingworth's methods are, respectively, $165 \pm^{289}_{107}$ and $145 \pm^{116}_{71}$ in solar units.

Apparently purely stellar systems such as globular clusters and the stellar Galactic disk, have mass-to-light ratios of about 3. Thus the observed internal velocity dispersion of the Draco dSph galaxy is several times larger than the value of about 1.5 $km\,s^{-1}$ which is expected if the galaxy is a self gravitating stable system whose gravitational potential is dominated by the mass in visible stars.

Effects such as anisotropy in the velocity dispersion and contamination of the data with binary stars cannot be discounted as contributing factors to this very

large mass-to-light ratio. It is by no means unreasonable, given Draco's size and distance, that it may be undergoing tidal disruption by the Galaxy. Another possible explanation for the results is a substantial dark matter density in this galaxy. These questions are discussed further in the following chapter, which compares the Sextans, Ursa Minor and Draco dSph galaxies in the light of the results presented here and in the previous two chapters.

Acknowledgments

We would like to thank E.W. Olszewski for giving us the positions of members of Draco found through his observations.

The spectroscopy reported here was obtained with the William Herschel Telescope operated on the island of La Palma by the Royal Greenwich Observatory in the Spanish Observatorio del Roque de los Muchachos of the Instituto de Astrophysica de Canarias.

References

Armandroff, T.E. & Da Costa, G.S., 1986, AJ, 92, 777.

Irwin M.J. & Hatzidimitriou D., 1993, Brodie, J., ed, in Proc. ASP Symp vol 48, 322.

Irwin M.J. & Hatzidimitriou D., 1995 (in preparation).

King, I., AJ, 1962, 67, 471.

King, I., AJ, 1966, 71, 64.

Mateo, M., 1994, Meylan, G., & Prugniel, P., eds, in Dwarf Galaxies, ESO/OHP Workshop No. 49, 309.

Piatek,S. & Pryor, C., 1995, Preprint.

Pryor, C., Olszewski, E.W. & Armandroff, T.E., 1995, to appear in van der Kruit, P.C., Gilmore, G., eds, in Stellar Populations, Proc. IAU Symp. 164.

Scholz, R.D., & Irwin, M.J., 1994, in MacGillivray, H.T. et al., eds, Proc. IAU Symp. 161, Astronomy from Wide-Field Imaging, 535. Kluwer, Dordrecht.

Tonry J. & Davis, M., 1979, AJ, 84, 1511.

Zaritsky, D., Olszewski, E.W., Schommer, R.A., Peterson, R.C. & Aaronson, M., 1989, ApJ, 345, 759.

Chapter 5

Summary of the Observational Results

5.1 Introduction

This chapter contains a summary of the previous three chapters and discusses the conclusions and further questions which the results suggest. Table 5.1 shows the results for the most recent observations of K giant velocities in the dSph galaxies. There are now several fairly consistent sets of results for most of the galaxies (cf Chapter 1).

Table 5.1: Recent velocity dispersion measurements for dSph galaxies.

dSph	N	σ_0	δ	
		km s^{-1}	km s^{-1}	
Draco	19	$10.5\pm^{2.2}_{1.7}$	2.0	Chapter 4
	24	10.2 ± 1.8	1.0	Olszewski & Aaronson (Mateo 1994)
	84	9.2 ± 0.8	3.6	Pryor, Olszewski & Armandroff (1995)
Carina	17	6.8 ± 1.6	2.9	Mateo et al. (1993)
Ursa Minor	35	$7.5\pm^{1.0}_{0.9}$	2.0	Chapter 3
	19	12.0 ± 2.4	1.1	Olszewski & Aaronson (Mateo 1994)
	85	8.9 ± 0.8	3.6	Pryor, Olszewski & Armandroff (1995)
Sextans	21	6.0 ± 1.0	2.1	Chapter 2
	33	6.2 ± 0.8	5.5	Suntzeff et al. (1993)
Sculptor	32	7.0 ± 1.2	4.7	Da Costa (1992)
	24	6.5 ± 1.0	2.3	Dubath & Queloz (1994)
Fornax	80	$9.4\pm^{1.5}_{1.4}$	10	Paltoglou & Freeman (Pryor 1991)
	49	11.0 ± 2.0	2.5	Mateo et al. (1991)
Leo II	31	6.7 ± 1.1	2.4	Vogt, Mateo, Olszewski & Keane (1994)

Notes. N is the number of stars observed.
σ_0 is the velocity dispersion obtained.
δ is the approximate error per observation.

In view of the improving measurements of the velocities in these galaxies it is becoming possible to start making a more detailed study of the kinematics of these galaxies rather than just the simplistic calculations so far employed. There are several factors which could be affecting the measurement of the velocity dispersion of these galaxies, such as, the existence of binary stars, tidal disruption

by the Galaxy, and the presence of rotation or anisotropy in the velocity dispersion. In the rest of this chapter the assumptions on which the mass-to-light ratio calculation are based are discussed in the light of the results from Chapters 2, 3 and 4.

5.2 The Mass-to-Light Ratio Calculation

The mass-to-light ratio calculations made in the previous three chapters are dependent on two factors.

1. The King Model fitted to the density profile is defined by the ratio of the core and tidal radii. The half-brightness and core radii are used in King's method of core fitting and Illingworth's method respectively. Although King's method should be generally insensitive to the King model used, the fact that a King Model must be fitted in order to ascertain the size of the core radius (because of the uncertainty in the central brightness of dSph galaxies) means that both methods have some model dependency.

2. The velocity dispersion is obtained by fitting a Gaussian to the velocity distribution, and it is this dispersion which is then used in the following mass-to-light ratio calculations.

5.2.1 Suitability of the King Models

The answers to the mass-to-light ratio calculations imply that the dSph galaxies range over a factor of 7 in mass but a factor of 100 in visible mass. However, this is complicated by the uncertainty in the surface brightness of the galaxies. The surface brightness is measured by subtracting the field star density from the survey plates. Since the field star density is of the same order as, or even larger than, the dSph galaxy surface density, there is considerable uncertainty in the value obtained. It is the error in this parameter which now contributes more than half the error to the mass-to-light ratios (see Section 2.4.1).

As explained in Section 2.4.1, in a King Model, the velocity dispersion decreases with distance from the centre of the galaxy. King's method of core fitting is fairly independent of the model chosen to fit the luminosity profile (Richstone &

Tremaine, 1986), but this does assume that mass follows light. If the velocity dispersion does not fall with radius then this might be an indication of significant amounts of dark matter at large radii, although some models where mass follows light and there is a flat dispersion profile out to quite large radii can be made with an anisotropic dispersion tensor (Pryor 1994). If it were to be the case that mass does not follow light, the methods used in the previous chapters for calculating the mass-to-light ratio would be inappropriate.

5.2.2 Shape of the Velocity Distribution

If the shape of the velocity distribution is not Gaussian, then the derivation of the velocity dispersion is incorrect and so the mass-to-light ratios may have been under or over estimated. Broad wings to the distribution could imply the presence of binary stars and would lead to an overestimate of the derived velocity dispersion. On the other hand, a truncated distribution may be a sign of tidal interaction, whereby the fastest moving stars have escaped from the galaxy.

A dSph which was undergoing tidal disruption by the Galaxy would be pulled apart in the direction of the line from the centre of the Galactic potential to the dSph galaxy and so we might expect the observed velocity dispersion to increase as the disruption occurs. Piatek & Pryor (1995), in numerical simulations have found that, for orbits where the dSph should be destroyed on a single approach, the central velocity dispersion does not rise significantly before the galaxy is destroyed. Additionally the surface brightness decreases and the velocity dispersion profile is flat. Rather than causing an increase in the velocity dispersion above the 1–2 $\mathrm{km\,s^{-1}}$ required for a low mass-to-light ratio, the stars which are unbound from the dSph galaxy cause rotation round the minor axis of the galaxy. Oh, Lin and Aarseth (1994) made simulations for less violent tidal interactions where the dSph can make more than one orbit round the Galaxy without being totally disrupted. They obtained similar results, but found that the central density remained constant rather than decreasing as in the Piatek & Pryor case.

Alternatively, if the galaxies were unbound systems representing former galaxies that had been disrupted, the velocity dispersion may have no bearing at all on the mass of the system. Kuhn (1993) suggested rather specific conditions under which a dSph could survive for an extended period of time as a visible system while actually being unbound.

With the fairly small number of stars that have been observed, deviation of the velocity distribution from a Gaussian may not be apparent. As shown later in Chapter 6, the K-S test cannot be expected to bring up a negative result for non-Gaussian distributions caused by binary stars alone with fewer than about 40 stars.

Rotation or the existence of binary stars could lead to an artificial expansion of the velocity dispersion, as explained in Sections 3.3.2 and 2.4.2, which would have to be subtracted before the dispersion caused by the mass of the system could be found.

5.3 Comparison of the Sextans, Ursa Minor and Draco dSph Galaxies

The results for the three dSph galaxies studied are presented in Chapters 2, 3 and 4. Of the three, the Ursa Minor data are of the highest quality with more stars and repeat measurements. There are slightly fewer stars for Sextans, and the Draco data have no repeats and only seventeen stars.

Table 5.2:

Galaxy	Number of stars	Number of repeats	Number of multi-epoch
Sextans	21	9	9
Ursa Minor	35	21	9
Draco	17	0	0

5.3.1 Rotation

All three galaxies were investigated for signs of rotation about the major and minor axes. Table 5.3 and Figure 5.1 compare the results.

Ursa Minor shows rotation significant at the three sigma level about the major axis, but nothing significant round the minor axis. Pryor, Olszewski & Armandroff (1995) agree with this discovery, obtaining 2.0 ± 1.0 $\mathrm{km\,s^{-1}}$ per 100 pc from the major axis. The rotation in Sextans is well constrained to be small about both

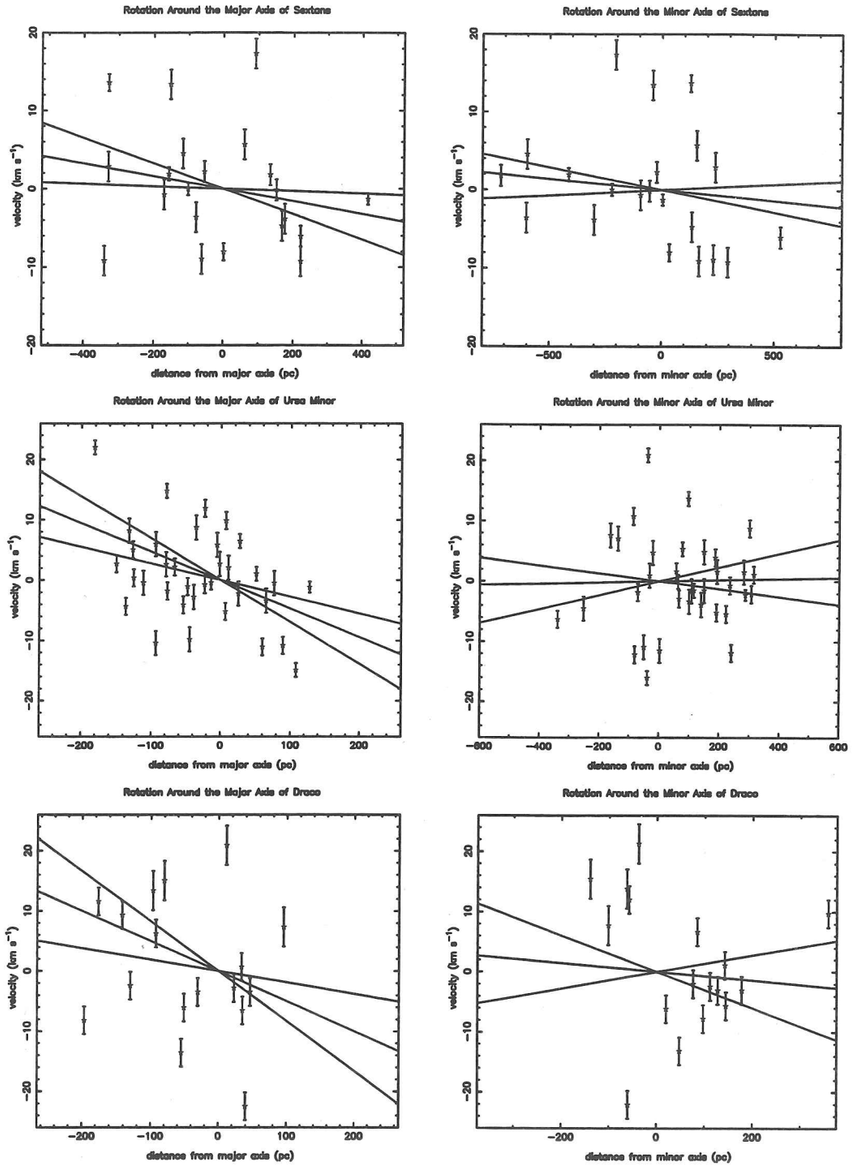

Figure 5.1: Rotation in the Sextans, Ursa Minor and Draco dSph galaxies. The best fit lines from the bootstrapping procedure, described in Section 3.3.2, are bounded by the errors. These are the 1 sigma errors for the slope of the fit, keeping the average velocity of the sample fixed.

Table 5.3: Rotation

Galaxy	Around minor axis ($\mathrm{km\,s^{-1}}$)	Around major axis ($\mathrm{km\,s^{-1}}$)
Sextans	$-0.3\pm^{0.4}_{0.3}$	$-0.8\pm^{0.7}_{0.8}$
Ursa Minor	$0.1\pm^{0.8}_{1.1}$	$-4.7\pm^{2.0}_{2.2}$
Draco	$-0.7\pm^{2.3}_{2.1}$	$-5.0\pm^{3.3}_{3.1}$

axes. In contrast, the rotation in Draco is poorly constrained; the rotation about the major axis being only significant at the two sigma level, whereas the rotation round the minor axis is only constrained to be less than about 2 $\mathrm{km\,s^{-1}}$ per 100 pc at the one sigma level.

Piatek & Pryor (1995) predicted the existence of rotation, of 0.4–0.5 $\mathrm{km\,s^{-1}}$ per 100 pc out to more than a core radius, around the minor axis of tidally disrupted dSph galaxies about the size of Ursa Minor, and, calculated that the slope of the rotation curve should be greater further out from the centre of the galaxy. As nearly all our stars are within a core radius of the centre of the dSph galaxies, it should be noted, with reference to Table 5.3, that the size of the rotation that they predict is too small to be detected by our data. They also suggested that rotation around the major axis as seen in Ursa Minor may not be inconsistent with the tidal disruption picture since, if the galaxy axes were suitably positioned with respect to the orbit round the Galaxy, tidal disruption could cause such rotation before turning the major into the minor axis.

When the effect of rotation from Ursa Minor is subtracted, the velocity dispersion decreases from $7.5\pm^{1.0}_{0.9}$ $\mathrm{km\,s^{-1}}$ to $6.7\pm^{0.9}_{0.8}$ $\mathrm{km\,s^{-1}}$. This means that the effect from rotation on the velocity dispersion is insufficient to account for the large mass-to-light ratio.

Figure 5.2 shows the variation of the velocity dispersion with radius for the 3 dSph galaxies. The errors are very large as each bin only contains a few stars. The drop off expected for a King Model is consistent with the Sextans and Ursa Minor data, but is only consistent with the Draco data at the two sigma level. The Draco and Ursa Minor data sets are both consistent with flat profiles.

More data, especially further from the centre of the dSph galaxies, are required to extend both the rotation and velocity dispersion profile results further.

From the observations described in Chapters 2, 3 and 4 there were one or two

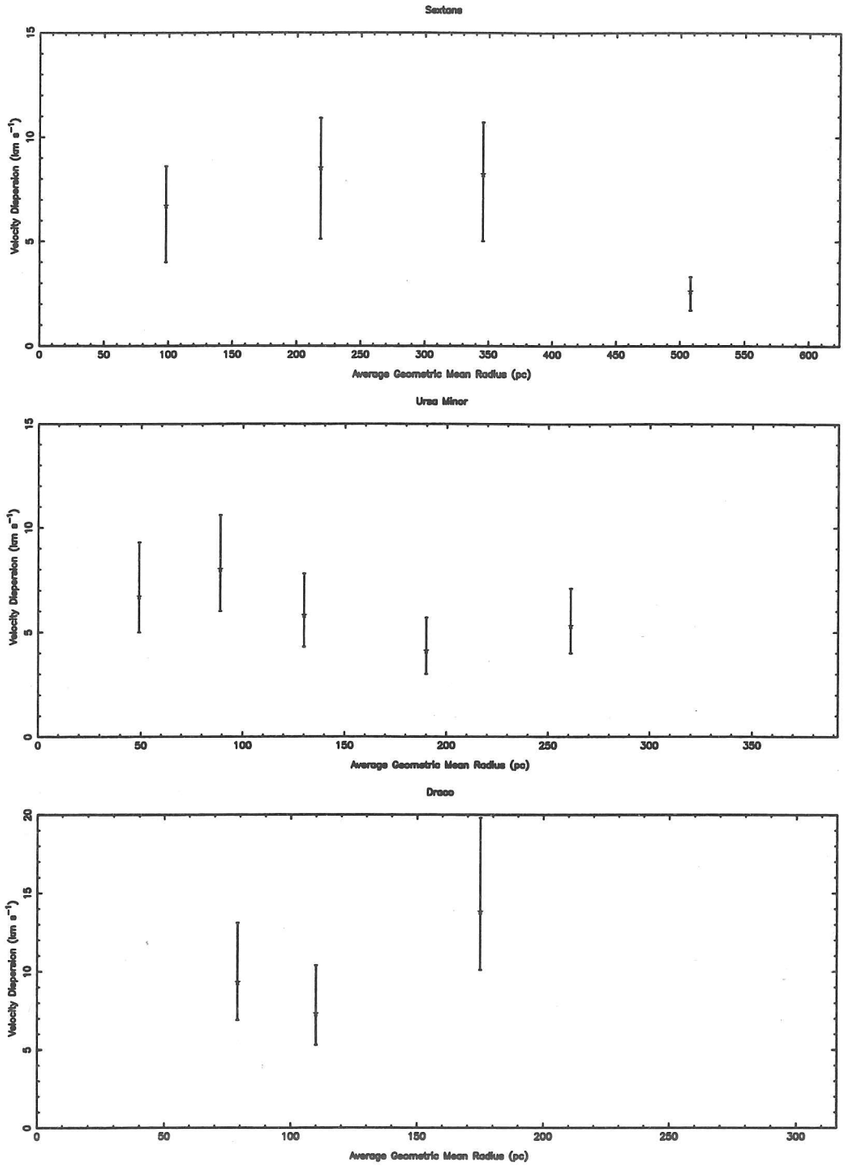

Figure 5.2: The velocity dispersion profiles for Sextans, Ursa Minor and Draco. The x-axes are scaled such that the length of each axis is twice the core radius of the dSph galaxy

binary stars out of eighteen stars with multi-epoch measurements, and other observations of binary stars have revealed a binary fraction of 0.1–0.2 with between two and ten years of observation of each star (Mateo 1994). Suntzeff (1993) suggested that a velocity dispersion of the size of that observed in Sextans could be accounted for by a binary fraction of 0.25. It is not clear from these results how many of the expected binary stars one would hope to observe in a certain number of multi-epoch measurements. If fewer than half of the binaries have been observed in two years this could imply that binary stars contribute all the dispersion over that expected for a small mass-to-light ratio. Chapter 6 describes the computer simulations made to explore these questions.

References

Da Costa, G., 1992, Barbury, B. & Renzini, A. eds, Proc. IAU Symp. 149, 191, Kluwer, Dordrecht.

Dubath, P. & Queloz, D., 1994, Meylan, G., & Prugniel, P., eds, in Dwarf Galaxies, ESO/OHP Workshop No. 49, 257.

Kuhn, J.R., 1993, ApJL, 409, L13.

Mateo, M., 1994, Meylan, G., & Prugniel, P., eds, in Dwarf Galaxies, ESO/OHP Workshop No. 49, 309.

Mateo, M., Olszewski, E., Welch, D.L., Fischer, P. & Kinkel, W., 1991, AJ, 102, 914

Mateo, M., Olszewski, E., Pryor, C., Welch, D.L. & Fisher, 1993, AJ, 105, 510

Oh, Lin & Aarseth, 1994, Preprint.

Piatek, S. & Pryor, C., 1995, Preprint.

Pryor, C., 1994, Meylan, G., & Prugniel, P., eds, in Dwarf Galaxies, ESO/OHP Workshop No. 49, 323.

Pryor, C., Olszewski, E.W. & Armandroff, T.E., 1995, to appear in van der Kruit, P.C., Gilmore, G., eds, in Stellar Populations, Proc. IAU Symp. 164.

Richstone, D.O. & Tremaine, S., 1986, AJ, 92, 72.

Suntzeff, N.B., Mateo, M., Terndrup, D.M., Olszewski, E.W., Geisler, D., Weller, W., 1993, ApJ, 418, 208.

Vogt, S.S., Mateo, M., Olszewski, E.W. & Keane, M.J., 1994, Preprint, submitted to AJ.

Chapter 6

The Influence of Binary Stars on Dwarf Spheroidal Galaxy Kinematics

Abstract

We have completed a Monte-Carlo simulation to estimate the effect of binary star orbits on the measured velocity dispersion in dwarf spheroidal galaxies. This chapter analyses previous attempts at this calculation, and explains the simulations which were performed with mass, period and ellipticity distributions similar to that measured for the solar neighbourhood. The conclusion is that with functions such as these, the contribution of binary stars to the velocity dispersion is small. The distributions are consistent with the percentage of binaries detected by observations, although this is quite dependent on the measuring errors and on the number of years over which measurements have been taken. For binaries to be making a significant contribution to the dispersion measured in dSph galaxies, the distributions of the orbital parameters would need to be very different from those of stars in the solar neighbourhood. In particular more smaller period orbits with higher mass secondaries would be required. The shape of the velocity distribution may help to resolve this issue when more data becomes available. In general, the scenarios producing a larger apparent dispersion have a velocity distribution which deviates more clearly from Gaussian.

6.1 Introduction

A binary star orbits its companion in an elliptical orbit, its velocity changing as it goes. This velocity depends on the masses of the stars, the period of the orbit and the eccentricity of the orbit. The orbit of the stars that we would observe has the centre of mass of the two stars as one of the foci. The velocity that we observe at a particular time depends on the position of the star in its orbit and the orientation of the orbit with respect to an observer. If every star observed was on an identical orbit, but at a different point in that orbit, a range of different velocities would be observed, the average velocity being zero. The standard deviation of these velocities is the dispersion produced by this orbit. A particular range of different orbits therefore contributes a specific amount to the velocity dispersion that would be observed. The size of the contribution of these binary stars to the dispersion can be calculated if the number of stars with each set of orbital parameters is known. It is this value that was estimated by the simulation described in this chapter.

6.1.1 Previously Published Results

Aaronson & Olszewski (1987) made the first simulations for binary stars in dSph galaxies, taking the mass and period distributions from Galactic studies by Mathieu (1983), and choosing a primary mass of 0.8 $M_\odot$. They chose the phase, inclination angle and eccentricity at random, possibly from uniform distributions, although this is not explicitly stated. They set the binary fraction to 0.5, assumed a certain intrinsic dispersion, and calculated, for each star, the velocities that would be measured from two observations taken one year apart. They did 500 trials for 10 stars in each case and measured the velocity dispersion after removing variations of greater than 4 $\mathrm{km\,s^{-1}}$ from the sample. They produced no significant deviation from the intrinsic dispersion in their results.

Mateo et al. (1993), Suntzeff et al. (1993), and Vogt et al. (1994) used similar simulations to estimate the effect of binaries in Carina, Sextans and Leo II dSph galaxies respectively. They took the period from a distribution that is uniform in log space, which they state is consistent with various studies, including Duquennoy & Mayor (1991). The mass was taken from a uniform distribution, the primary mass being 0.8 $M_\odot$. The inclination was taken from a cosine distribution, and the eccentricity and phase were chosen at 'random', again, presumably from uniform distributions. The sample sizes for the simulations were similar in size to the observed sample reported in the papers (between 17 and 33 stars), and they repeated the simulation for differing intrinsic velocity dispersions and binary fractions, making 1000 independent trials each time. They calculated the standard deviation and the biweight (Beers et al. 1990) of the resulting velocities. For small intrinsic dispersions of the order of 2 $\mathrm{km\,s^{-1}}$ which is that expected for dSph galaxies containing no dark matter, a binary fraction of 0.2 was required to produce an apparent velocity dispersion of the size observed in dSph galaxies (>6 $\mathrm{km\,s^{-1}}$). They also noticed a difference between the standard deviation and biweight measurements, and suggested that because this was not observed in their observations, it was an indication that binaries did not contribute significantly to the observed dispersion. This would require the binary star fraction in dSph galaxies to be considerably less than that observed in the solar neighbourhood.

6.1.2 Observations of Binary Stars

From the observations presented in this thesis, there may be two binary stars out of the eighteen that have measurements at more than one epoch (Sections 2.4.2 and 3.4.3), giving an observed binary fraction of 0.11. It is important to know what actual binary fraction this represents, since if less than half of the binaries were observed in two years this would imply a binary fraction of greater than 0.2. Other observations of stars in dSph galaxies (see Table 5.1) have obtained between four and twelve years of repeat measurements of sixty three stars in Sculptor, Fornax, Ursa Minor and Draco. These observations have found a binary fraction of between 0.1 and 0.16 (Mateo, 1994). For Draco where there are twenty four stars for which there are up to five observations of each, four appear to be binaries (Mateo, 1994). Our simulation was designed to place an estimate on the fraction of binary stars that would be observed over a certain period of observations, as well as to calculate the contribution binary orbits make to the measured velocity dispersion.

6.2 Details of the Model.

The model was constructed to examine the velocity distribution caused by the orbits of binary stars. The model made a Monte-Carlo simulation, choosing binary orbits with parameters chosen at random from empirical and theoretical and distributions for a large number of stars, and then evolved each star round its orbit. From this it was possible to ascertain what fraction of binary stars would be identified over the course of a certain number of equally spaced observations, given a certain velocity above which a velocity difference would become apparent to an observer. The velocity distribution obtained from evolving the stars round their orbits could be used to calculate the velocity dispersion caused by the binary stars.

The model chose the parameters of the binary orbits randomly from different distributions, The velocity that would be measured by an observer was calculated for equal time intervals all the way round each orbit. In this way, a distribution of velocities was obtained for each orbit. One hundred velocities were chosen at random from the set of velocities for each star and written to file 1, ensuring that

the distribution for each orbit represented in the file had equal weight. Thus, file 1 contained the velocity distribution for the set of binary orbits.

It was assumed that a specific difference in velocity, called the threshold velocity, could be detected between two velocity measurements made by the observer: the value depended on the assumed measuring errors. If the difference in velocity between time intervals, measured along the line of sight, was equal to or greater than this value, then the velocities concerned were marked. All the velocities that appeared in file 1 and were not marked in this way were written to file 2. Therefore file 2 contained the velocity distribution for the binary orbits which would not be identified by the assumed measuring errors. The fraction of the binary stars that would be identified was given by the ratio of the number of velocities in files 2 and 1. The velocity dispersion of the binary distribution (σ_b in equation 6.12) was equal to the standard deviation of the velocities in file 1, whereas the velocity dispersion that would be obtained if the stars were thrown out of the sample when identified as belonging to binary systems was the standard deviation of the stars in file 2. The standard deviations of the data in files 1 and 2 were consistent under repetition for given parameter distributions, provided that a sufficient number of stars were used in the sample.

The orbital parameters which need to be considered are: the masses of the two stars; the period of the orbit; the minimum approach distance of the stars; the ellipticity of the orbit; the inclination; the phase; and the position of the periastron with respect to the observer.

6.2.1 The Distributions of the Orbital Parameters

The best estimate for the distributions of the orbits of binary stars comes from the solar neighbourhood sample observed by Duquennoy & Mayor (1991), so it is these distributions that have been used to define the orbital parameters. The primary stars in the orbits of that study were solar mass G dwarfs. Although the masses of the stars observed in the dSph galaxies are fairly close to the masses of these dwarfs, it may well be the case that the orbital distributions discovered are not applicable in the very different conditions of a dSph galaxy. The simulations which used these orbit distributions, assuming the radius of the primary to be 10 and 30 $R_\odot$, are termed DM10 and DM30 respectively in the rest of the chapter.

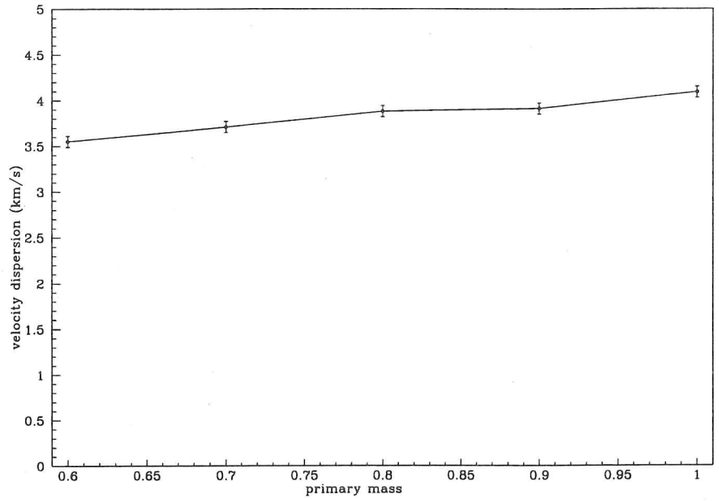

Figure 6.1: The velocity dispersion obtained for different primary masses for model DM10.

To compare this with previous simulations, the same distributions used by Mateo et al. in their simulations were also used (hereafter Ma). The secondary mass distribution calculated by Kroupa, Tout & Gilmore (1993), which rises rather than falls towards low masses, was also used. In these simulations, the DM distributions were used for the other parameters apart from mass: the simulations are called KTG10 and KTG30.

Mass

The K giants for which the velocities are presented in the previous chapters are the brightest stars in the dSph galaxies, occupying the tip of the giant branch. Given the stellar populations in dSph galaxies are predominantly of intermediate to old age, these stars will have mass of about 0.8 $M_\odot$, so this is the value of the primary in our simulations. Figure 6.1 shows that there is very little difference in the results of the simulation taking a primary mass of between 0.6 and 1.0 $M_\odot$.

The secondary mass distribution found by Duquennoy & Mayor is given by

$$\mathbf{P}(M2) \propto \exp\left(\frac{-(M2-0.23)}{0.42}\right)^2, \tag{6.1}$$

where $M2$ is allowed to vary between 0.05 $M_\odot$ and the mass of the primary.

Mateo et al. also took the primary mass to be 0.8 $M_\odot$, but their secondary masses were taken from a uniform distribution with masses varying between 0.05 and 0.8 $M_\odot$.

Kroupa, Tout & Gilmore's mass distribution has the following form:

$$\mathbf{P}(m) = \begin{cases} 0.035m^{-1.3} & 0.08 \leq m \leq 0.5 \\ 0.019m^{-2.2} & 1.0 \leq m \leq 1.0 \\ 0.019m^{-2.7} & 1.0 \leq m < \infty. \end{cases} \tag{6.2}$$

Period

The Duquennoy & Mayor period distribution is consistent with the estimate of Kroupa, Tout & Gilmore (1990). It is Gaussian in log space, and has the form

$$\mathbf{P}(\log(P_{days})) \propto \exp\left(\frac{-(x-4.8)}{2.3}\right)^2 \tag{6.3}$$

($x = \log(P_{days})$)

where P_{days} is the period in days. No maximum or minimum bounds were imposed on this distribution.

The distribution used by Mateo et al. was uniform in the logarithm of the period. They stated that this distribution is also consistent with the results of Duquennoy & Mayor.

Ellipticity

Here, the ellipticity, e, is defined to be $e = (1 - b/a)$, where b and a are the minor and major axes of the orbit respectively.

Duquennoy & Mayor found the ellipticity obeyed the following distributions.

$$\begin{array}{ll} \text{period} < 11 \text{ days} & e = 0.0 \\ 11 \text{ days} < \text{period} < 1000\text{days} & \mathbf{P}(e) \propto \exp\left(\frac{-(e-0.3)}{0.16}\right)^2 \\ \text{period} > 1000\text{days} & P(e) \propto e \end{array} \tag{6.4}$$

Mateo et al. took the ellipticity from a uniform distribution in the range 0.5 to 1.0.

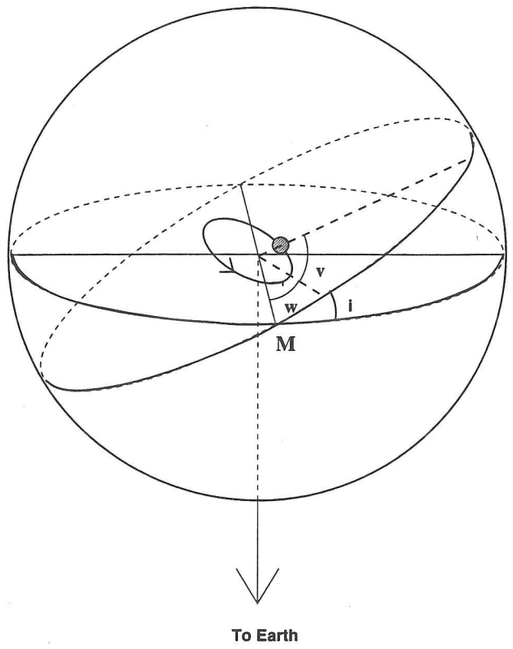

Figure 6.2: Orbit of a binary star round the centre of mass.

Angles

Figure 6.2 shows the orbit of a binary star round its centre of mass. Viewed from the earth, the star moves in an ellipse in the plane perpendicular to our line of sight. The inclination, i, is the angle between the orbital plane and the viewing plane. For spherical symmetry, the normal to the viewing plane must be evenly distributed over the sphere, implying that the distribution of the orbital inclinations is proportional to the sine of the inclination.

$$\mathbf{P}(i) \propto \sin i. \tag{6.5}$$

The angle w is the angle between the ascending node, M, and the apastron of the orbit. As in the diagram, the phase, v, is the angle between w and the current position of the star, taken in the direction shown. Both w and v were allowed to vary between 0 and 360 degrees, so, because of symmetry, i was allowed to vary

between 0 and 180 degrees. The angle w was chosen from a uniform distribution, and was a constant parameter of the orbit. The phase, v, however is the angle that varies with time, so that although its initial value was chosen from a uniform distribution, its value thereafter varied in accordance with Kepler's 2nd law.

6.2.2 Radius Cutoff

Orbits of very low period or high ellipticity may not be physically possible, since they can result in too close an encounter between the two stars in the binary. To estimate this minimum distance a simple gravitational Roche-Lobe radius estimate was used.

$$M2 = M1 \times \frac{a_p^2(a_p - R)}{R^3(2a_p - R)}. \tag{6.6}$$

Here a_p is the distance between the stars at periastron, and R is the radius of the primary star of mass $M1$, $M2$ being the maximum mass of the secondary before Roche-Lobe overflow occurs. The radius of the giant stars in dSph galaxies is not well known, as the evolution of stars in low metallicity environments such as that found in dSph galaxies is not understood in detail, so a range of between 10 and 30 $R_\odot$ was used in the simulations, which should cover the possibilities. This is a difference between the binaries in dSph galaxies and the binaries with solar mass primaries observed by Duquennoy & Mayor in the solar neighbourhood: some of the orbits which existed round the primaries when they were main sequence stars should no longer exist, so it may be expected for the fraction of binary stars to be somewhat lower than that observed in the solar neighbourhood.

6.2.3 Velocity

From the period, the semi-major axis of the real orbit, rather than that with respect to the centre of mass, is given by

$$a^3 = (M1 + M2)T^2 \tag{6.7}$$

where a is the semi-major axis in astronomical units, T is the period in years and $M1$ and $M2$ are the masses in solar masses.

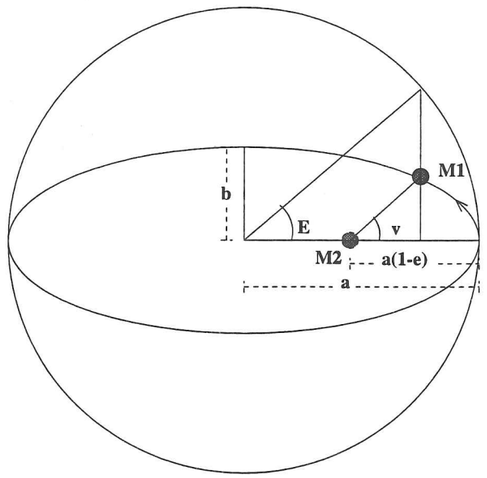

Figure 6.3: Geometry of the orbit of two binary stars

The line of sight velocity observed for a particular binary star with mass M1 at some phase, v is given by

$$V = 2\pi \frac{1.49598 \times 10^{11}}{365.25 \times 3600} \frac{M2 \sin i}{\sqrt{a(M1 + M2)}} \left[\frac{\cos(v + w) + e \cos w}{\sqrt{(1 - e^2)}} \right]. \tag{6.8}$$

Here the velocity is in ms^{-1}, and the semi-major axis, a, is in astronomical units. The ellipticity, e is $\sqrt{1 - (b/a)^2}$.

6.2.4 Time

To calculate the velocity that would be observed at equal time intervals round the orbit using equation 6.8, it was necessary to calculate the change in the phase resulting from a change in time.

Figure 6.3 shows the geometry of the orbit. The secondary, M2 sits at the focus of the ellipse orbited by M1. The phase, v, is also called the true anomaly and E, is the eccentric anomaly. Geometry and Kepler's 2nd law can be used to derive the following relationships between these two angles and time.

$$\tan \frac{E}{2} = \sqrt{\frac{(1 - e)}{(1 + e)}} \tan \frac{v}{2}. \tag{6.9}$$

$$E - \sin E = \frac{2(\tau)}{T}. \tag{6.10}$$

Here τ is the time since the stars were last at periastron.

So we obtain E from v using equation 6.9, iterate to find the new E from equation 6.10 and then use equation 6.9 once more to calculate the new v. In this way and using equation 6.8 the velocity can be calculated at every stage of the orbit.

6.2.5 Fraction of Binary Stars Identified

There were some binary stars that would never be identified because the range of their orbital velocities was small compared to the measuring error. These were the stars for which the difference between the maximum and minimum value of the velocity from equation 6.8 was less than the threshold velocity at which the difference would appear significant to the observer (this is explained for specific examples in Section 6.3). The maximum and minimum values were obtained by evaluating the equation at $v = -w$ and $v = \pi - w$. For these stars, the orbit was divided into 100 equal timesteps and each velocity produced was written to files 1 and 2.

The time difference between measurements in the simulations was taken to be one year. Therefore each star not already catered for by the criterion of the previous paragraph was evolved round its orbit, recording the velocity at one yearly time intervals. For periods of less than 100 years 1001 yearly velocities were taken. For periods greater than this the number of orbital revolutions was reduced to save computing time. For periods between 100 and 1000 years velocities were calculated five times round the orbit, and for those between 1000 and 10000 years two orbit's worth of velocities were calculated. Then all the differences between consecutive velocities were calculated, thus obtaining 1000 velocity differences for periods of less than 100 years.

The velocities were marked for which, if observations were started from the position on the orbit associated with that velocity, over the course of the observations,

the star would be identified as having a binary orbit. Therefore another parameter was used, which was the number of years over which observations were conducted. A velocity was marked if any of the subsequently obtained velocity differences, or their sum, was greater than the threshold velocity. Then 100 velocities were chosen at random with equal probability from the sample for each star, writing all 100 to file 1 and only those not marked to file 2.

For periods greater than 10000 years a slightly different approach was adopted. For such large periods the only portion of the orbit at which the star might possibly be identified as a binary was close to apastron, so 1001 velocities were calculated symmetrically about apastron, and calculated the phase angles about which the velocity differences were sufficiently large to be detected over the years of observation. Then the velocity was calculated at 100 equal timesteps right round the orbit (ie each timestep went 100th of the way round the orbit) and marked those which fell between the calculated phase points. These velocities were written to the files in the same way as the velocities for the other orbits.

For the periods of less than 10000 years, the probability of recognising a particular binary star orbit over the observing period was equal to the number of marked velocities, divided by the number of observations in total. For the larger periods, the probability was equal to the number of velocities within the calculated phase range where the binary could be identified, divided by the number of timesteps contained in an orbit. For a timestep of one year, this denominator is just the orbital period in years.

The average of the probabilities for all the stars is equal to the fraction of stars that would be recognised as having binary orbits.

6.3 Results

Figures 6.4, 6.5, 6.6, 6.7 and 6.8 show the results for the simulations. Each figure contains two plots. The upper plot shows the percentage of the binaries that would be identified for a certain threshold velocity. The different lines are for yearly observations spanning 2, 10 and 50 years. The solid line on the lower plot shows the standard deviation of the distribution arising from binary stars with the orbital parameters chosen: the dotted lines show the standard deviation of the distributions once the identified binary stars have been removed.

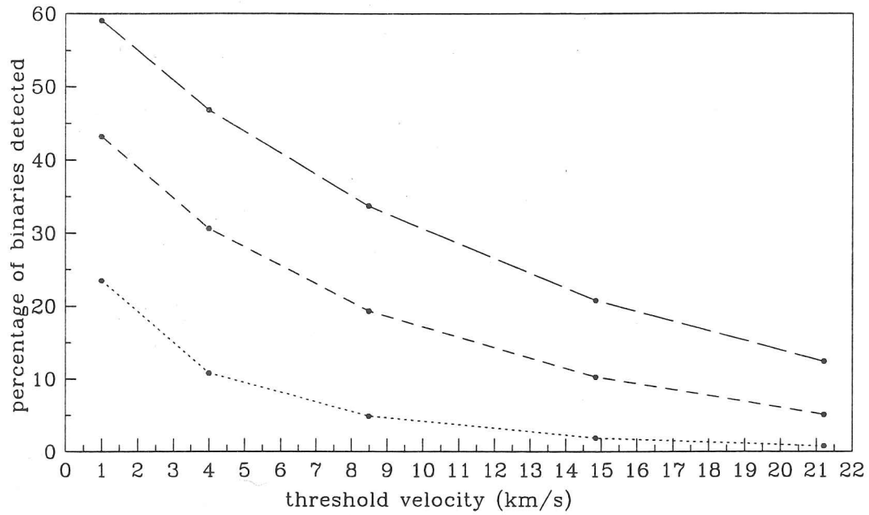

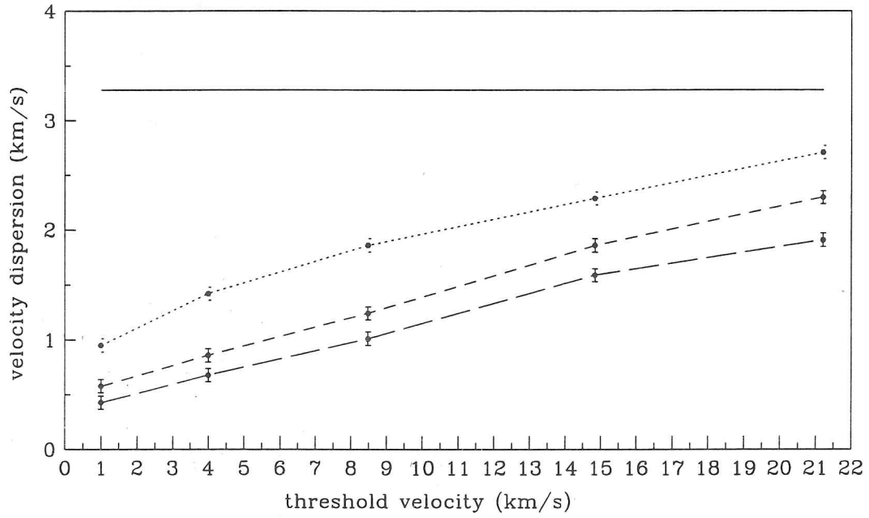

Figure 6.4: Model Ma. The solid line in the bottom plot shows the velocity dispersion of the whole sample. The dashed and dotted lines show the percentage of binaries that would be detected (top plot) and the velocity dispersion of the residual sample (bottom plot) after 2 years of observations. The short dashes and long dashes show the same statistics for 10 and 20 years of observations respectively

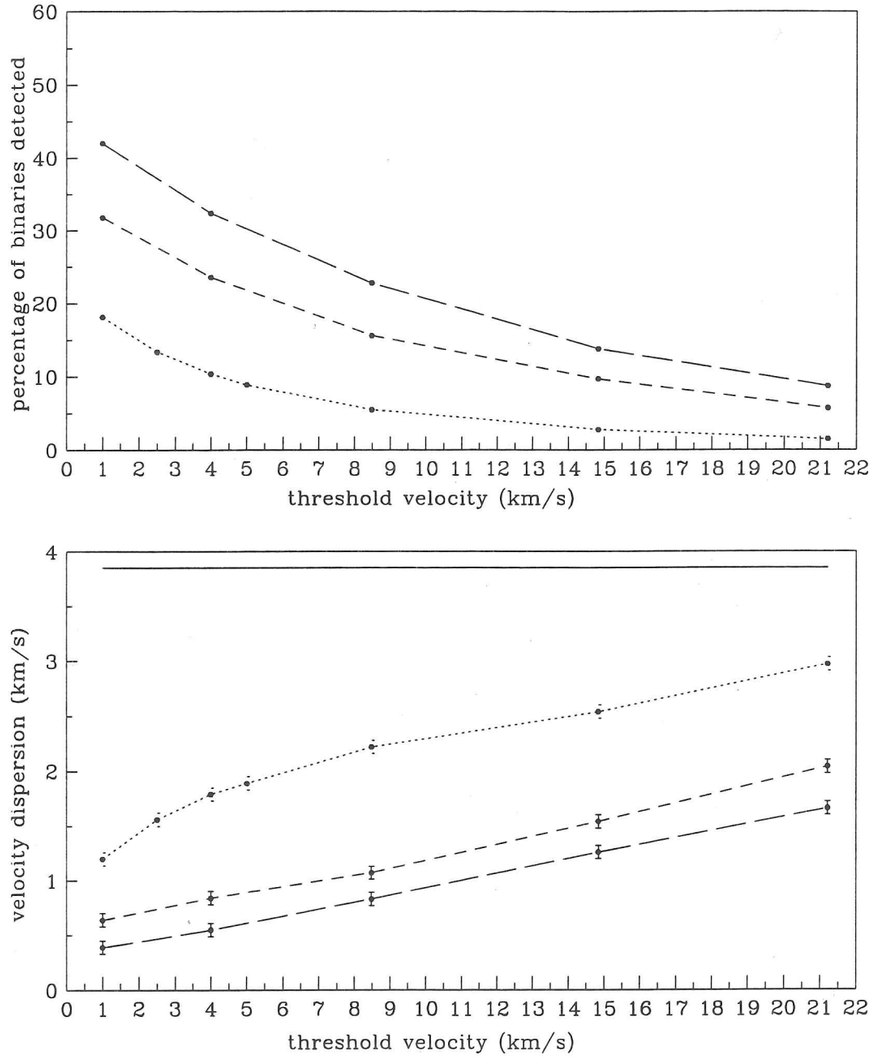

Figure 6.5: Model DM10. The solid line in the bottom plot shows the velocity dispersion of the whole sample. The dashed and dotted lines show the percentage of binaries that would be detected (top plot) and the velocity dispersion of the residual sample (bottom plot) after 2 years of observations. The short dashes and long dashes show the same statistics for 10 and 20 years of observations respectively

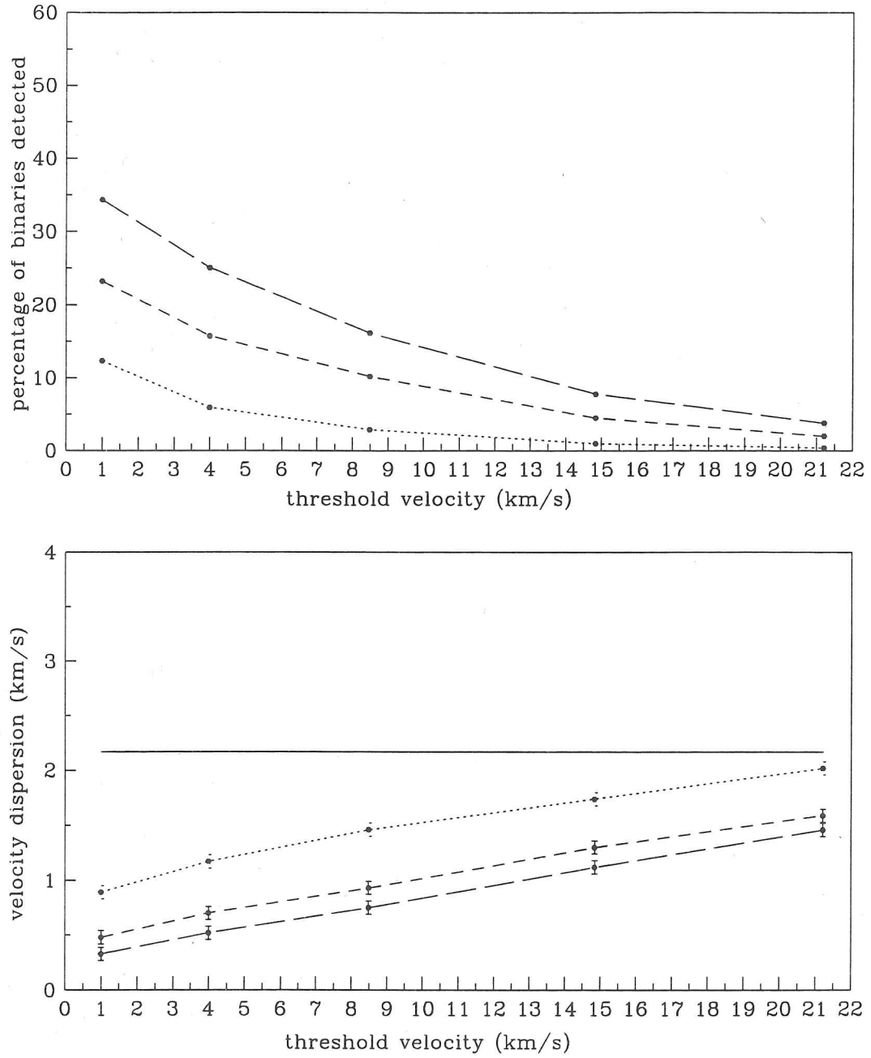

Figure 6.6: Model DM30. The solid line in the bottom plot shows the velocity dispersion of the whole sample. The dashed and dotted lines show the percentage of binaries that would be detected (top plot) and the velocity dispersion of the residual sample (bottom plot) after 2 years of observations. The short dashes and long dashes show the same statistics for 10 and 20 years of observations respectively

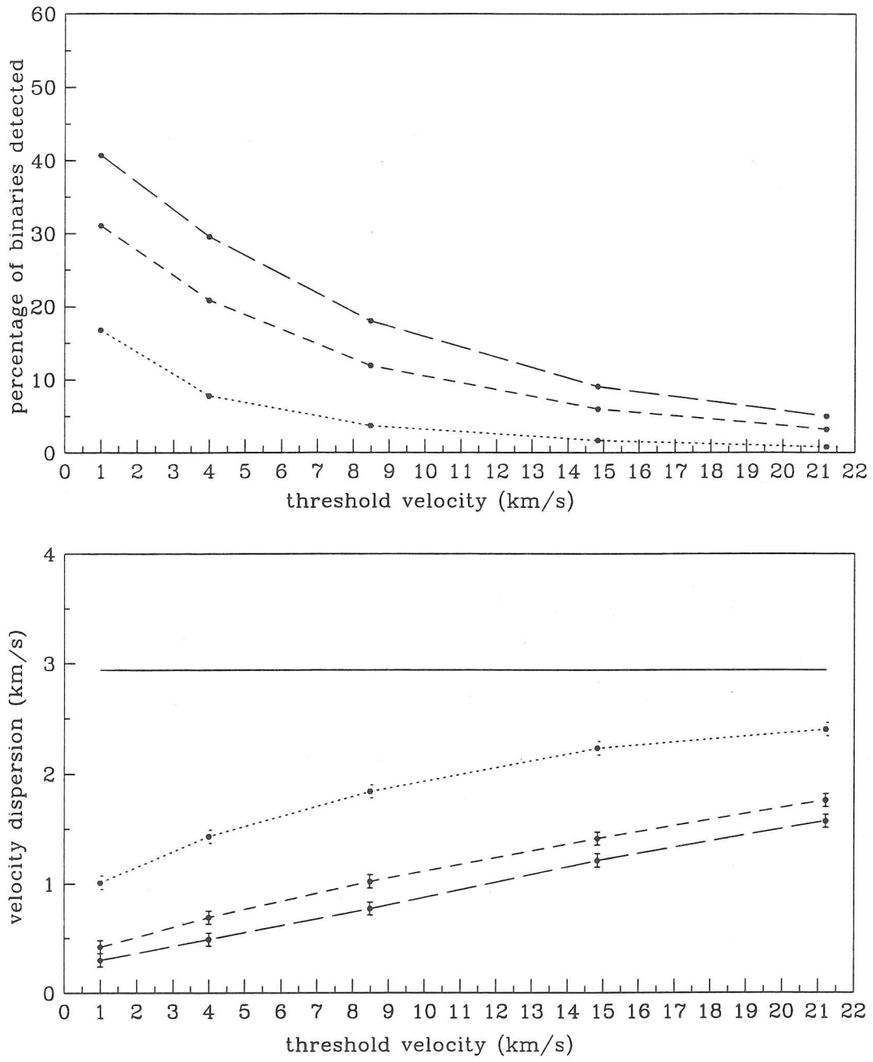

Figure 6.7: Model KTG10. The solid line in the bottom plot shows the velocity dispersion of the whole sample. The dashed and dotted lines show the percentage of binaries that would be detected (top plot) and the velocity dispersion of the residual sample (bottom plot) after 2 years of observations. The short dashes and long dashes show the same statistics for 10 and 20 years of observations respectively

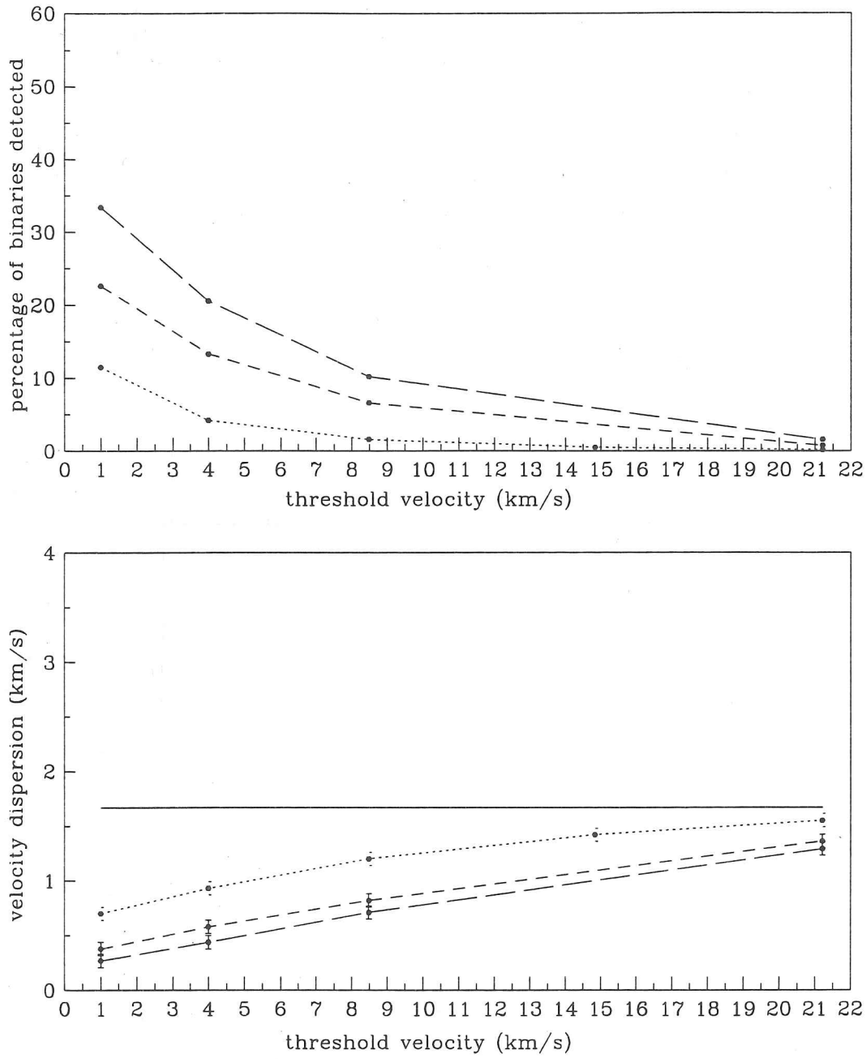

Figure 6.8: Model KTG30. The solid line in the bottom plot shows the velocity dispersion of the whole sample. The dashed and dotted lines show the percentage of binaries that would be detected (top plot) and the velocity dispersion of the residual sample (bottom plot) after 2 years of observations. The short dashes and long dashes show the same statistics for 10 and 20 years of observations respectively

For observations with a error for each velocity measurement of σ_{err}, the threshold velocity for a binary star to be detected was $3\sqrt{2}\sigma_{\rm err}$. For the observations presented in Chapters 2, 3 and 4, the error per velocity was close to 2 $\mathrm{km\,s^{-1}}$. Aaronson & Olszewski (1987), took 4 $\mathrm{km\,s^{-1}}$ as the threshold velocity in their simulation, whereas the average error on the velocities of Pryor, Olszewski & Armandroff (1995) was 3.6 $\mathrm{km\,s^{-1}}$, giving a threshold velocity of 15.3 $\mathrm{km\,s^{-1}}$. Threshold velocities of 1, 4, 8.5, 15.3, and 21.2 $\mathrm{km\,s^{-1}}$ were used, as shown in the plots, to cover the range of possible observations.

The simulation was made using 10000 stars since it was at this level that repeat simulations became easily recognisable. The one standard deviation of the percentage of identified binaries taken from repeat simulations was about 0.5%, whereas that for the velocity dispersion was about 0.06 $\mathrm{km\,s^{-1}}$.

Table 6.1 shows the standard deviation of the binary star distribution required for binary stars to be making a significant contribution to the measured dispersion in dSph galaxies; dispersions due to binary orbits alone are required to be greater than about 6 $\mathrm{km\,s^{-1}}$ to explain the observed dispersion assuming a low mass-to-light ratio. The results from the simulations from the chosen paramter range show that the highest dispersion caused by the binary orbits alone is about 3 $\mathrm{km\,s^{-1}}$, We conclude that either the velocity dispersions that have been observed are largely unaffected by binary stars, or that the orbital parameters, which were after all taken from Galactic observations, are inappropriate for dSph galaxies.

Comparing the results from the Ma, DM10 and DM30 models, it can be seen that the percentage of binaries detected in model Ma was considerably larger than that in the other two cases. This is largely due to the fact that the orbits in the Ma model have a maximum period of 10000 years. The periods in the DM model have no such upper bound and have about 30% of periods above 10000 years. These long periods alone produce only a small dispersion, and as they can only be detected during the few years close to apastron, they only slightly increase the total number of binary stars identified. When an extra 30% of stars are added analytically to the Ma model using equations 6.11 and 6.12, the percentages and dispersions (approximating the dispersion of the long periods alone to be negligible), lie somewhere between the results from the two DM models. The KTG mass distribution which rises towards the low mass end, does, as expected, produce lower percentages of binaries identified and lower velocity dispersions.

Table 6.1: Velocity dispersion required from the binary stars for binary orbits to account for the excess dispersion over that generated for a typical stellar mass-to-light ratio. All velocities are in $\mathrm{km\,s^{-1}}$.

Measured dispersion = 7 $\mathrm{km\,s^{-1}}$

binary fraction	intrinsic dispersion 2	4
0.25	13.4	11.5
0.5	9.5	8.1
0.75	7.8	6.6
1.0	6.7	5.7

Measured dispersion = 10 $\mathrm{km\,s^{-1}}$

binary fraction	intrinsic dispersion 2	4
0.25	19.6	18.3
0.5	13.9	13.0
0.75	11.3	10.6
1.0	9.8	9.2

Models Which Produce Large Velocity Dispersions

Figure 6.9 shows the standard deviation of the velocity distribution of the DM10 model at different periods. The periods were chosen from a uniform distribution within a small range around the average value shown on the plot. It was not sensible to take single periods because the dispersion would be greater at integer multiples of the time between measurements (because if the large apastron velocities were measured once then they were measured every orbit): this does not represent the real life situation where observations are not taken at exact intervals. Only 1000 rather than 10000 stars were used for each of these simulations since, with such a limited period distribution, the velocity distribution was quicker to converge.

Periods of less than 5 years can produce large standard deviations of greater than 6 $\mathrm{km\,s^{-1}}$. When the calculation of Mateo et al. was repeated, without their error in the phase distribution (see Section 6.4), simulations were made for period

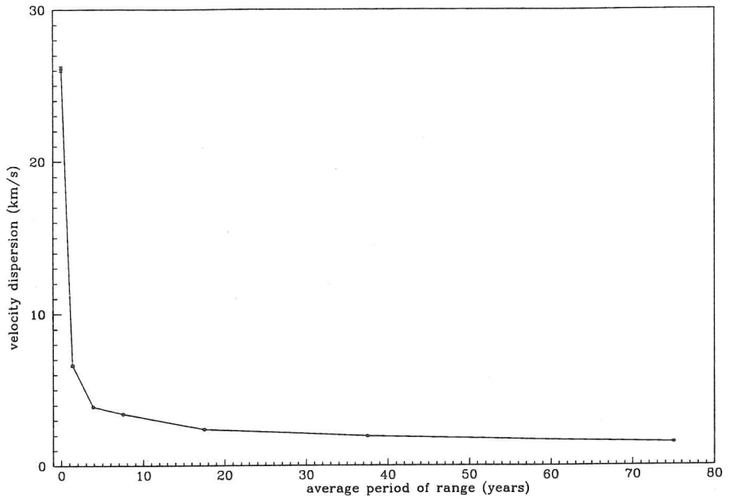

Figure 6.9: Variation of the velocity dispersion for different periods. Each point is positioned at the average period of the range for that simulation.

ranges of 0.5 to 10 years, and 0.5 to 100 years. These produced dispersions of 5.5 and 4.3 $\mathrm{km\,s^{-1}}$ respectively. This all implies that keeping the other parameters as before, only the situations where the binary fraction is close to 1.0 and the periods are almost all below 10 years, can the velocity dispersion produced by the binary stars be sufficient to account for that observed. For a threshold velocity of 4 $\mathrm{km\,s^{-1}}$ (equivalent to a one sigma error of 0.9 $\mathrm{km\,s^{-1}}$ on each velocity), one would expect to see more than 70% of the binaries in 10 years for periods below 10 years, requiring a far higher binary fraction observed than the 10–20% actually observed. This is true even allowing for the fact that not all these stars have been observed for 10 years.

Fixing the mass of the secondary to be equal to the mass of the primary also increases the standard deviation of the velocity distribution, the DM10 model producing a dispersion of over 6 $\mathrm{km\,s^{-1}}$ (see Figure 6.10). Here, only 30% of the binaries would be identified in 10 years, for a threshold velocity of 4 $\mathrm{km\,s^{-1}}$, which is much more in line with the observations.

As we have seen earlier, taking very high ellipticity orbits can produce high dispersions: however, these orbits are not physically possible and therefore not allowed using the cutoff radius method.

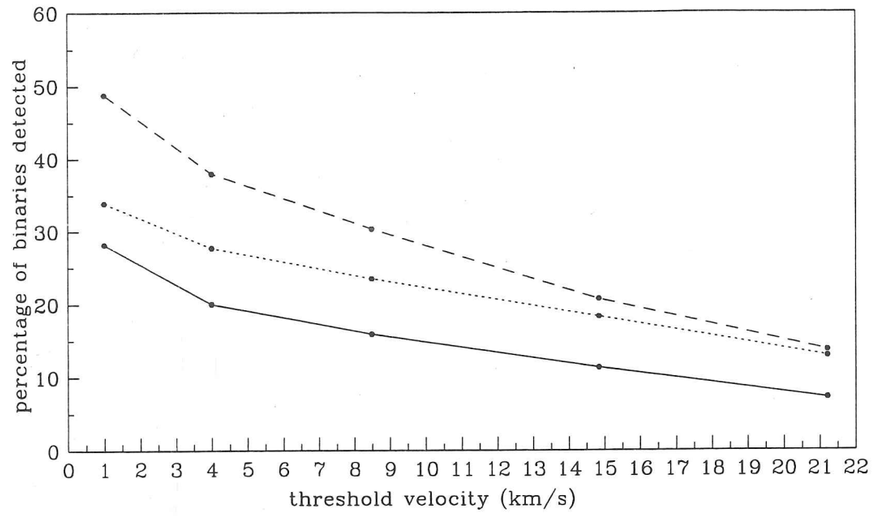

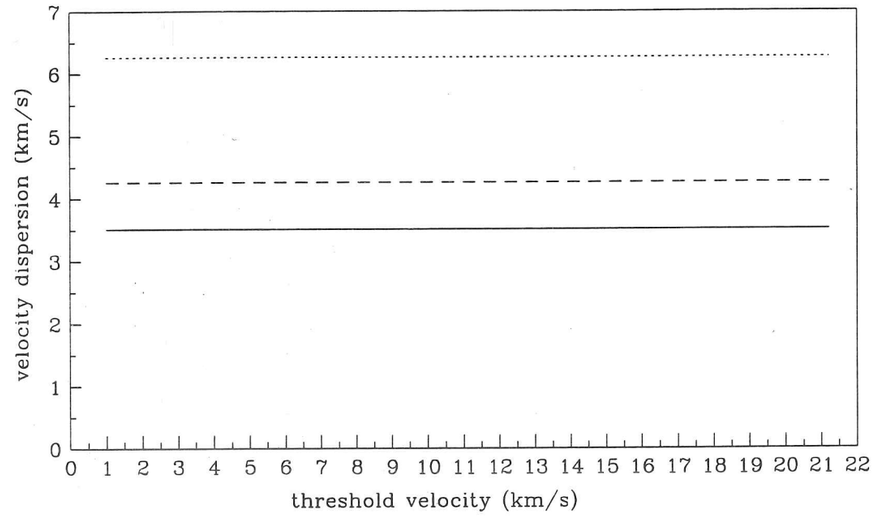

Figure 6.10: Ma, DM10 and DM30 models for M1=M2=0.8 $R_\odot$. These results are for 10 years of observations.

6.4 Main Differences Between the Simulations and Previous Work

Phase

Choosing the phase of an orbit randomly from a uniform distribution implies that the orbit has a constant angular velocity. This is only true for a circular orbit, as Kepler's 2nd law states that the line joining the two stars in an elliptical orbit sweeps out equal areas in equal times. The assumption of a constant angular velocity means that too many stars will be chosen in the part of the orbit close to peri centre where the true angular velocity is highest, relative to sampling equal time intervals throughout the orbit. It is around this part of the orbit that the stars have the largest orbital speed and this leads to an overestimate of the velocity dispersion caused by the binary stars.

For the results produced by the other groups mentioned in Section 6.1.1, the overestimate is of the order of a factor of three. Figure 6.11 shows the binary velocity dispersion (ie assuming 100 percent binary stars in the sample) obtained by Mateo et al. (1993) and the equivalent results choosing the orbital phase correctly using our model.

Binary Fraction

It is straightforward to calculate the size of the observed dispersion from the binary velocity dispersion, the binary fraction, and the intrinsic velocity dispersion.

Assuming the two dispersions both have a mean of zero,

$$\sigma_o^2 = (1-f)\sigma_i^2 + f\sigma_B^2, \tag{6.11}$$

where

$$\sigma_B^2 = \sigma_b^2 + \sigma_i^2. \tag{6.12}$$

Here σ_o is the observed dispersion, σ_i is the intrinsic velocity dispersion, σ_b the calculated dispersion due to a binary fraction of 1.0, and f is the binary fraction.

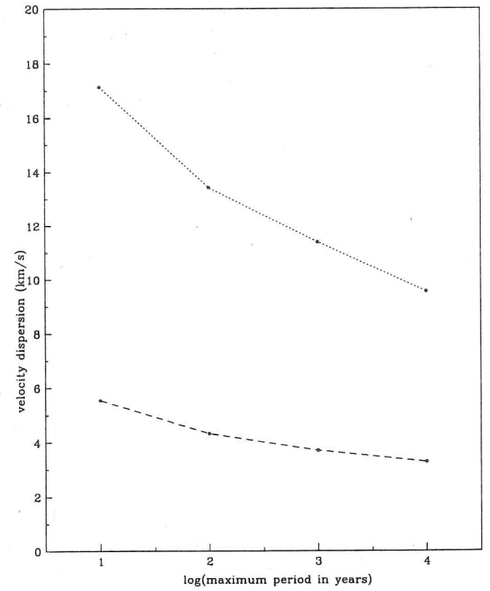

Figure 6.11: The velocity dispersion of the binary stars for the simulations published by Mateo et al., 1993 (dotted line) compared with the use here of their orbit distributions choosing the phase correctly (dashed line). The x-axis values are the upper cutoff period for the simulations, the lower cutoff in each case being 0.5 years

The difference between the standard deviation and biweight measurements noticed by Mateo et al. (1993) is an indication that the shape of the velocity distribution deviates from a Gaussian shape when binary stars are present. The fact that Mateo et al. chose the phase incorrectly suggests that this difference may not be as great for a more carefully chosen distribution. However, since the simulation reported in this chapter only simulates the binary stars, calculating the effect of different binary fractions using the equations 6.11 and 6.12, this comparison has not been made. Instead, samples of small numbers of stars were drawn from the velocity distribution and K-S tests were performed to see at what level the distribution deviated significantly from a Gaussian shape.

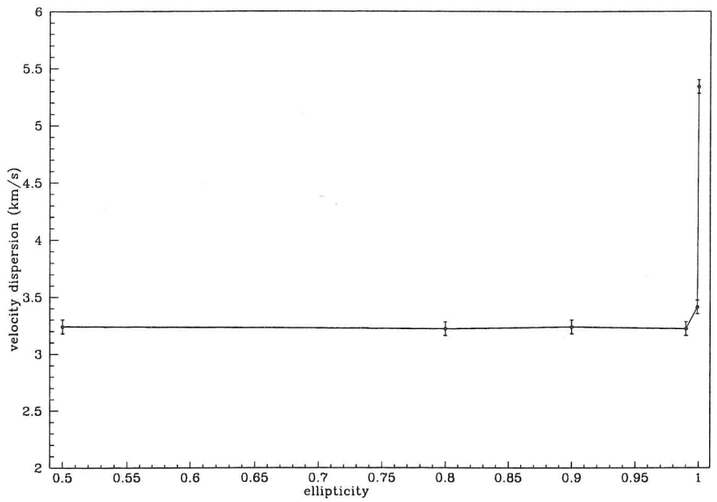

Figure 6.12: The velocity dispersion for the Ma model with periods between 0.5 and 10000 years, for different values of the ellipticity ($e = \sqrt{1-(b/a)^2}$)

Period and Radius Cutoffs

Previous simulations (for example Mateo et al. 1993) have taken an ellipticity range from a uniform distribution ranging from 0.5 to 1.0 and a period range with a lower bound of half or one year. Some cutoff value for the ellipticity must have been taken in previous simulations to avoid production of infinite velocities in the simulations, however this is not published and it is possible that unrealistic orbits with very high ellipticities were allowed. Figure 6.12 shows how the measured velocity dispersion varies for a fixed ellipticity. Here the period, taken from a distribution which is uniform in the logarithm of the period, ranges from 0.5 years to 10 years. As an alternative to this a minimum approach distance for the two stars in the binary has been taken, negating the need for artificial period and ellipticity cutoffs. When the same orbital distributions as those used by Mateo et al. were used a maximum ellipticity of 0.999 was taken (where ellipticity is $\sqrt{1-(b/a)^2}$), so as to avoid some of the unrealistic orbits shown by Figure 6.12. As can be seen from this figure and Figure 6.11, the effect is not sufficient to explain the difference between the simulations reported in this chapter and the previously published results.

Number of Stars

Previous calculations have been aimed at simulating the exact experimental conditions of the observations. They therefore simulated velocities for only a small number of stars at a single epoch. The simulations were repeated of the order of 1000 times to obtain an average result for the velocity dispersion. A more robust and exact way to conduct the simulation is to use a much larger number of stars and calculate velocities all the way round the orbits.

6.5 Analysis of the Results

6.5.1 Comparison with the Observations

If the parameters defining binary star distributions in the Galaxy and dSph galaxies are the same, except for some loss of close orbits due to the expansion of the primary in the older population, then the effect of binaries on the measured velocity dispersion is small. If so, then there must be some other explanation for the large velocity dispersions which have been measured in dSph galaxies. When all the multi-epoch observations from dSph galaxies are added together, a binary fraction of between 0.1 and 0.16 is observed, with four to twelve years of measurements (Mateo 1994). Olszewski & Aaronson have between five and ten roughly yearly measurements for their stars, and have detected a binary fraction of between 0.1 and 0.2. These results have not been fully published so there remain uncertainties about the exact answers, but they do claim a measuring error of about 1 $\mathrm{km\,s^{-1}}$, so a threshold velocity of about 4 $\mathrm{km\,s^{-1}}$ should be suitable for analysing their results. Duquennoy & Mayor found a binary fraction of 0.6 for the solar neighbourhood solar mass stars.

Considering the range of the results from the DM10 and DM30 models, between 12% and 24% of the binaries should be identified in 5 to 10 years, given a threshold velocity of 4 $\mathrm{km\,s^{-1}}$ (see Figure 6.13). If 60% of the stars are binary stars, this means that we should actually identify 7% to 14% of the stars as binary stars. If the threshold velocity is 8.5 $\mathrm{km\,s^{-1}}$ (equivalent to a 2 $\mathrm{km\,s^{-1}}$ measuring error), we would expect between 4% and 10% of the binaries to be identified as such. The percentage of binaries that has been detected is a little on the high side (see the

previous paragraph), but the discrepancy may well be caused by an underestimate of the measuring errors; for example, this could occur if there were broad wings on the error distribution. We correct for the fact that 28% of the binaries in DM30 and 15% in DM10 were rejected when compared with the DM1 model, where the radius of the primary was 1 $R_{\odot}$, because the minimum separation of the stars fell below the cutoff, and assume that these ex-binaries are still 'normal' stars in the sample. Then we conclude that the binary fraction should be 0.4 or 0.5, rather than 0.6. This results in a predicted percentage of binaries detected in 5–10 years, with a threshold velocity of 4 km s^{-1}, of 5% to 12%, which is more divergent from the observations. From the DM models, with a threshold velocity of 4 km s^{-1}, we should expect never to identify between 40% and 50% of the binary stars, however many years we observe for (Table 6.2). However, the dispersion caused by this fraction is very small, of the order of 1 km s^{-1} (see Figures 6.5 and 6.6). From the shape of the velocity distribution formed by the binary orbit velocities alone, it appears that one would not reject the Gaussian distribution hypothesis with only 20 stars, but would in most cases with 40 stars. Therefore, with a binary fraction of 0.6, we would expect no divergence from a Gaussian shape to be detected at the level of our current observations.

Olszewski & Aaronson's observations of Draco have detected a binary fraction of 0.17 with up to five observations at roughly yearly intervals and measuring errors of about 1 km s^{-1}. This again is slightly on the high side.

For the results discussed in Chapters 2, 3 and 4, one or two binaries out of eighteen stars with multi-epoch observations in Sextans and Ursa Minor (6% to 11%) may have been found with two years of observation and a measuring error of 2 km s^{-1}. The DM models, and a binary fraction of 0.6, predict that 1.8% to 3.3% of the binaries should have been identified. We would, therefore, have expected to see zero or one binary star. However, several of the multi-epoch measurements have more than one observation at each of the two epochs, as is the case for the strongest binary candidate. This leads to a considerably higher probability of identifying a binary star due to the effective decrease in measuring error resulting from the combination of several observations.

The results from the Ma model, restricting the period to various ranges (Figure 6.11) suggest that nearly all the binary stars which are identified within 10 years have periods of less than 100 years. This result was obtained by consid-

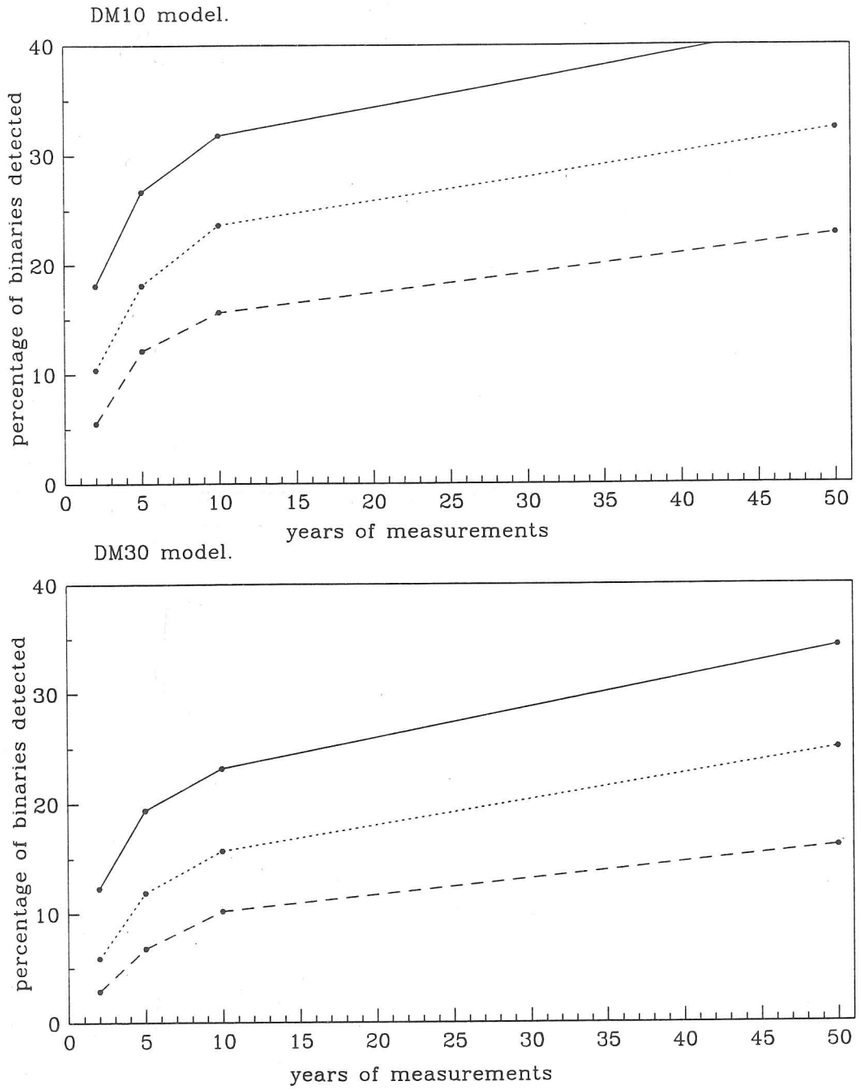

Figure 6.13: Variation of the percentage of binaries detected with number of years of observation. The top plot shows the results from the DM10 model with threshold velocities of 1, 4, and 8.5 km s^{-1}(solid, dotted and dashed lines respectively), and the lower plot presents results of the DM30 model adopting the same threshold velocities.

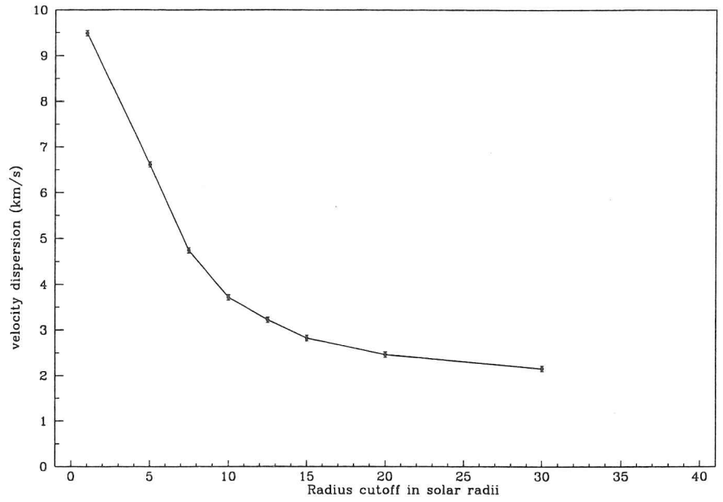

Figure 6.14: The velocity dispersion obtained from the DM models with different primary stellar radius cutoffs.

ering the sample with periods between 0.5 and 10000 year. Since we know that the distribution is uniform in the logarithm of the period, we can calculate the percentages of the total number of binary stars identified in the more restricted period ranges. The result is a negligible difference in the percentage between periods of 100 and 10000 years.

For the distribution to be such that the binary stars have a significant effect on the measurement of the velocity dispersion, we would require the sample to be biased towards lower periods and higher masses. In this case we would expect to detect between 30% and 70% of the binaries in 10 years of observation, assuming a threshold velocity of 4 $\mathrm{km\,s^{-1}}$ (Table 5.2). Thus, the observations imply a binary fraction between 0.14 and 0.50. This requires a dispersion of about 10 $\mathrm{km\,s^{-1}}$ or more for the binary stars to have a significant effect on the observed dispersion (Table 6.1). In these cases, the distributions of the orbital parameters of the binary stars are very different from the distributions of Galactic binary stars that have been detected through observations.

Simulations using a very small primary star radius can also produce large dispersions: if the radius of the primary star were as small as 5 $R_\odot$, then dispersions greater than 5.5 $\mathrm{km\,s^{-1}}$ could be produced, while stars of 1 $R_\odot$ can produce a dispersion of close to 10 $\mathrm{km\,s^{-1}}$ (Figure 6.14).

The percentages of binary stars detected with the KTG models are only slightly less than those for the DM models. Thus, it is impossible, from these results, to rule out the KTG secondary mass function, which rises towards lower masses. If anything it is slightly more in tune with the observations.

6.5.2 The Shape of the Velocity Distribution

The shape of the velocity distribution varies depending on the model chosen. Table 6.2 shows the sample size at which the distributions would probably be rejected at the three sigma level by a K-S test as being Gaussian. The distributions have broader wings than a Gaussian distribution. These sample sizes do not, however, reflect the number of stars that we would need to observe before recognising a component due to binary stars in an observed distribution. This is because the simulation has not taken into account the contribution to the distribution of the intrinsic velocity dispersion due to the mass of the galaxy.

A simple procedure was completed to illustrate the situation. Randomly chosen Gaussian deviates were added to the sample of velocities obtained from the binary star simulation. The intrinsic dispersion was chosen such that the total dispersion of the resulting sample was 6 $\mathrm{km\,s^{-1}}$. K-S tests were then conducted for different sample sizes drawn from the new distribution.

For the DM10 distribution forty stars were sufficient to reject the Gaussian hypothesis. This distribution had a dispersion of 3.8 $\mathrm{km\,s^{-1}}$ which was caused by binary star velocities alone. When we added a Gaussian deviate from an intrinsic dispersion of 4.6 $\mathrm{km\,s^{-1}}$ to each star (making 6 $\mathrm{km\,s^{-1}}$ in total, using equations 6.11 and 6.12), the K-S test did not reject the Gaussian hypothesis until samples contained as many as 1000 stars. The addition to each sample of 67% more stars, which had a velocity from the intrinsic dispersion, but no binary component, required the intrinsic dispersion to be 5.2 $\mathrm{km\,s^{-1}}$. This sample, with a binary fraction of 0.6, required about 5000 stars before it was rejected at the three sigma level by the K-S test.

This result was compared with a simulation for which the dispersion caused by the binary stars alone is larger. In this case the DM10 simulation was performed, restricting the periods of the orbits to less than 3 years, the periods being drawn from a uniform distribution. The dispersion caused by only the binary stars was

Table 6.2: The results for the simulations of the different models.

Model	Comments	σ_b km s^{-1}	N	V_T km s^{-1}	P_{10}	P_N
Ma	0.5–10 years	5.5	100	4	75	1
	1.0–10 years	4.7	100	4	73	2
	0.5–100 years	4.3	100	4	56	3
	0.5–1000 years	3.7	80	4	39	8
	0.5–10000 years	3.3	60	4	31	17
DM1		9.5	20	4	30	36
DM5		5.6	20	4	27	38
DM10		3.9	40	4	22	42
DM20		2.5	40	4	18	47
DM30		2.2	40	4	16	50
DM40		1.9	60	4	13	53
KTG10		2.9	40	4	48	49
KTG30		1.7	40	8.5	19	79
DM10	1–11 days	26.5	>200	4	98	0.4
	11–1000 days	6.6	180	4	84	5
	2.7–5 years	3.9	140	4	71	2
	5–10 years	3.2	100	4	69	5
	10–25 years	2.4	100–160	8.5	22	23
	25–50 years	1.9	100–160	8.5	9	31
	50–100 years	1.5	100–160	8.5	4	41
	100–1000 years	0.8	100–160	8.5	0.4	66
	1000–10000 years	0.4	100–160	8.5	0.01	87

Table 6.2 continued...

Model	Comments	σ_b km s^{-1}	N	V_T km s^{-1}	P_{10}	P_N
Ma	e=0.9999	5.3	40–60	4	28	0
	e=0.999	3.4	40–60	4	28	1
	e=0.99	3.2	40–60	4	28	7
	e=0.9	3.2	40–60	4	32	31
	e=0.5	3.2	100	4	33	51
	e=0.0	3.2	100	4	33	54
Ma	M2=M1	5.0	60	4	38	5
DM10	M2=M1	6.3	60	4	28	28
DM30	M2=M1	3.5	60	4	20	32

Notes. σ_b is the standard deviation of the velocity distribution caused by the binary orbits obtained from the model defined in the first two columns.
N is the number of stars in the sample before a K-S test rejected the Gaussian hypothesis at the three sigma level. The samples were taken from the whole distribution in steps of twenty stars.
V_T is the threshold velocity of the simulation for which the percentage P_{10} of the binaries were detected in 10 years of yearly observations. P_N is the percentage of the stars that would never be identified as binary stars because the velocity variations round the orbit are too small ever to be detected by the threshold velocity.

6.2 km s^{-1} and samples of about 220 stars were required before this distribution was rejected in the K-S test. We made the same calculation as described in the previous paragraph for this sample, but only conducted the experiment for a binary fraction of 0.6, because a binary fraction of 1.0 would require no contribution from an intrinsic dispersion. The intrinsic dispersion required by a binary fraction of 0.6 to make a total dispersion of 6 km s^{-1} was 3.2 km s^{-1}. In this case about 500 stars were required for the Gaussian hypothesis to be rejected. Figure 6.15 shows these results for the two simulations.

In the light of these examples it seems unlikely that there should be any clear evidence for binary stars in the shape of the velocity distributions which have been obtained from dSph galaxies, because the largest sample sizes are about 80 stars (see Table 5.1). As an illustration we have combined the data from the observations reported in Chapters 2, 3 and 4 for three dSph galaxies. Each velocity distribution was normalised to a dispersion of 1 km s^{-1} and then a K-S test was

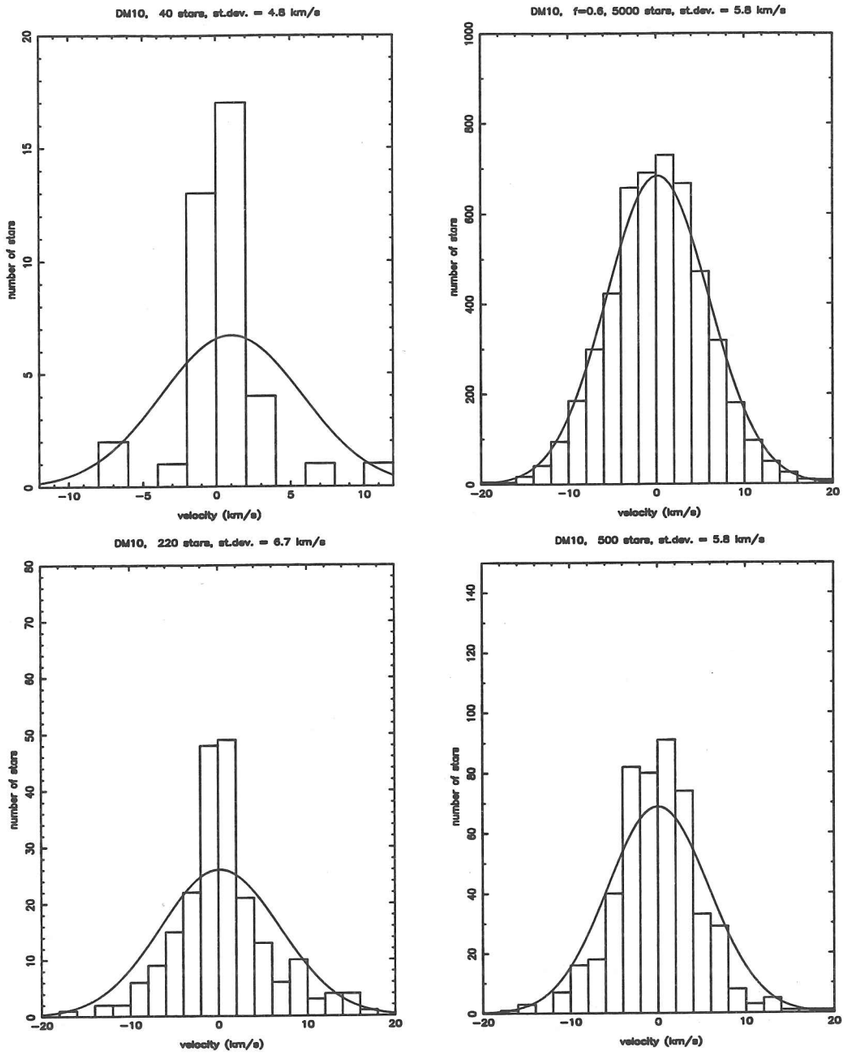

Figure 6.15: The plots on the left are the distributions for no intrinsic dispersion, and those on the right are for a binary fractions of 0.6. The upper plots show the standard DM10 model and the lower ones show the DM10 model with the periods restricted to below 3 years. The sample sizes are such that the K-S test would be very likely to reject the Gaussian hypothesis at the three sigma level. The Gaussians plotted have a one sigma width equal to the measured standard deviation (st. dev.) of the sample.

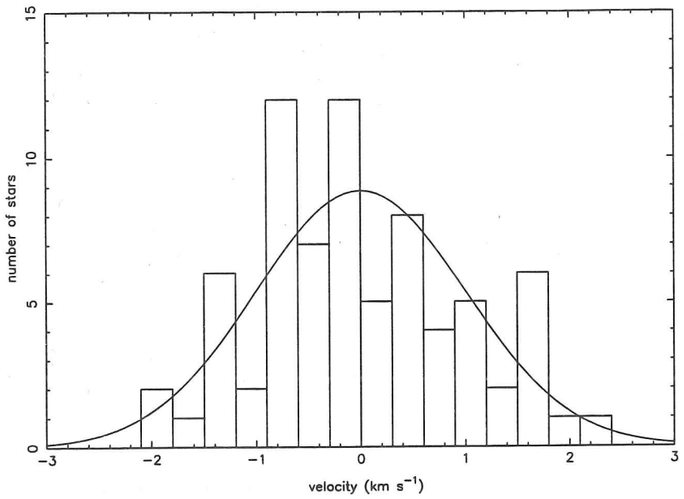

Figure 6.16: The combined sample of the Sextans, Ursa Minor and Draco data. The distribution from each sample has been normalised to a dispersion of 1 km s^{-1}. The probability from the K-S test for the Gaussian distribution shown was 0.8.

performed on the whole sample. This sample contained 74 stars and included the first epoch measurements from both suspected binary stars in Sextans. The probability from the K-S test was 0.8. Figure 6.16 shows the combined sample with the Gaussian function overlaid.

6.6 Conclusion

The velocity dispersion caused by binary stars with orbital parameters corresponding to the solar neighbourhood is small compared to the large velocity dispersions observed in dSph galaxies. The percentage of binary orbits that would be identified depends on the number of years of observation and on the precision of the velocity measurements. However, the simulations, which use orbital distributions derived from real observations, predict the identification of percentages of binary stars that are only slightly less than that actually observed.

To produce larger dispersions, more binary orbits with a mixture of lower periods, higher mass secondaries, or primaries with radii smaller than 10 $R_\odot$ are required. It is difficult to produce a velocity dispersion much above 6 km s^{-1} without requiring restriction of the orbits to periods below about 5 years. For

velocity dispersions from binary stars of the order of 6 $\mathrm{km\,s^{-1}}$ to be significantly modifying the overall observed dispersion a binary fraction of close to 1.0 would be required. From observations of such a population spanning ten years, around 30% of the binaries should be identified with such distributions. The observations are now slightly on the low side for this scenario, at 10%–20%, even accounting for the fact that not all these stars have been observed for ten years.

At present it seems likely that some of the stars which observers have assumed to be binaries are erroneous detections, as a consequence of an underestimate of their measurement errors. Continuing high precision observations, when analysed using the results of this work, will be able to quantify the contribution of the binary stars to the observed velocity dispersion. Samples of greater than about 500 stars with single epoch measurements would be required to define the kinematic distribution function, but precise data for a few stars over a long time interval should be able to quantify the true significance of binary stars in the dynamics of dSph galaxies.

References

Aaronson, M. & Olszewski, E., 1987, Kormendy, J., & Knapp, G.R., eds, in Dark Matter in the Universe, Proc. IAU Symp. 117, 153. Dordrecht, Reidel.

Beers, T.C., Flynn, K., Gebhardt, K., 1990, AJ, 100, 32.

Duquennoy, A, Mayor, M, 1991, A & A, 248, 485.

Kroupa, P., Tout, C.A. & Gilmore, G., 1990, MNRAS, 244, 76.

Kroupa, P., Tout, C.A. & Gilmore, G., 1993, MNRAS, 262, 545.

Mateo, M., Olszewski, E.W., Pryor, C., Welch, D.L., Fischer, P., 1993, AJ, 105, 510.

Mateo, M., 1994, Meylan, G., & Prugniel, P., eds, in Dwarf Galaxies, ESO/OHP Workshop No. 49, 309.

Mathieu, R.D., 1983, Ph.D. Thesis, University of California, Berkeley.

Pryor, C., Olszewski, E.W. & Armandroff, T.E., 1995, to appear in van der Kruit, P.C., Gilmore, G., eds, in Stellar Populations, Proc. IAU Symp. 164.

Suntzeff, N.B., Mateo, M., Terndrup, D.M., Olszewski, E.W., Geisler, D., Weller, W., 1993, ApJ, 418, 208.

Vogt, S.S., Mateo, M., Olszewski, E.W. & Keane, M.J., 1994, Preprint, submitted to AJ.